AWARD NUMBER: W81XWH-14-1-0286

TITLE: Mechanisms of Transendothelial Migration of Primary Human Invasive Ductal Carcinoma Cells from ER+, Her2+, and Triple-Negative Disease

PRINCIPAL INVESTIGATOR: Jeanine Pignatelli

CONTRACTING ORGANIZATION: Albert Einstein College of Medicine
Bronx, NY 10461

REPORT DATE: September 2016

TYPE OF REPORT: Final

PREPARED FOR: U.S. Army Medical Research and Materiel Command
Fort Detrick, Maryland 21702-5012

REPORT DOCUMENTATION PAGE

Form Approved
OMB No. 0704-0188

1. REPORT DATE	2. REPORT TYPE	3. DATES COVERED
September 2016	Final	1 Sep 2014 - 31 Aug 2016

4. TITLE AND SUBTITLE
Mechanisms of Transendothelial Migration of Primary Human Invasive Ductal Carcinoma Cells from ER+, Her2+, and Triple-Negative Disease

5a. CONTRACT NUMBER

5b. GRANT NUMBER
W81XWH-14-1-0286

5c. PROGRAM ELEMENT NUMBER

6. AUTHOR(S)
Jeanine Pignatelli

E-Mail: Jeanine.pignatelli@gmail.com

5d. PROJECT NUMBER

5e. TASK NUMBER

5f. WORK UNIT NUMBER

7. PERFORMING ORGANIZATION NAME(S) AND ADDRESS(ES)

Albert Einstein College of Medicine
1300 Morris Park Ave
Bronx, NY 10461

8. PERFORMING ORGANIZATION REPORT NUMBER

9. SPONSORING / MONITORING AGENCY NAME(S) AND ADDRESS(ES)

U.S. Army Medical Research and Materiel Command
Fort Detrick, Maryland 21702-5012

10. SPONSOR/MONITOR'S ACRONYM(S)

11. SPONSOR/MONITOR'S REPORT NUMBER(S)

12. DISTRIBUTION / AVAILABILITY STATEMENT

Approved for Public Release; Distribution Unlimited

13. SUPPLEMENTARY NOTES

14. ABSTRACT
The majority of breast cancer related deaths are not due to the primary tumor, but to the metastatic cancer spread to distant sites. The Condeelis lab has been successful in studying dissemination of breast cancer at single cell resolution using newly developed multiphoton imaging tools and mouse models. Their studies have led to the identification of the tumor microenvironment of metastasis or TMEM in mouse and human mammary tumors, sites where transendothelial migration (TEM) occur and therefore sites of intravasation. The constituent cells of TMEM are an endothelial cell, a perivascular macrophage and an invasive Menaexpressing tumor cell in direct contact. TMEMs are present in human invasive breast tumors and the density of TMEMs is positively associated with the risk of developing metastases. These studies also led to the identification of the Invasion Signature, revealing genes differentially expressed by tumor cells during macrophage dependent migration in the primary tumor. These studies indicate that many of the epigenetic changes observed in invasive mammary cancer cells are clustered in the motility pathways that control actin polymerization, directional cell movement, and the formation of invadopodia. The Mena family of actin binding proteins functions at the convergence of these pathways. Mena is a member of the Ena/VASP family of proteins that control F-actin network assembly and play a role in cell migration. The gene encoding Mena was identified as one of the key genes upregulated ininvasive mammary tumor cells in rats, mice and humans. Breast carcinoma cells express three Mena isoforms: Mena classic, MenaINV and Mena11a. Expression of Mena11a is associated with an epithelial, while MenaINV expression confers a potent pro-metastatic phenotype when expressed in breast cancer cells. Additionally, the expression of MenaINV correlates with TMEM score in human breast cancers. Thus, the expression of MenaINV may have clinical applications as a prognostic marker of metastatic risk. Our preliminary data indicate that cancer cell migration towards blood vessels and cancer cell intravasation at TMEM sites are regulated in a macrophage-dependent manner. We hypothesize that Mena isoform expression pattern as well as the physical contact between a tumor cell and a macrophage at sites of TMEM regulate cancer cell intravasation. We propose to delineate the mechanisms by which the tumor cellmacrophage interaction leads to invadopodium formation, TMEM assembly and TEM in 2 major breast cancer subtypes, estrogen positive (ER+/Her2-) and triple negative (TN), and understand a role of Mena11a and MenaINV in this process.

15. SUBJECT TERMS
Tumor microenvironment, macrophage, Mena, transendothelial migration, metastasis, Notch

16. SECURITY CLASSIFICATION OF:			17. LIMITATION OF ABSTRACT	18. NUMBER OF PAGES	19a. NAME OF RESPONSIBLE PERSON
a. REPORT	b. ABSTRACT	c. THIS PAGE			USAMRMC
Unclassified	Unclassified	Unclassified	Unclassified	96	19b. TELEPHONE NUMBER *(include area code)*

Table of Contents

Page

1. Introduction

The primary cause of morbidity and mortality in breast cancer is distant metastases (*1, 2*). The direct contact between a breast tumor cell, macrophage, and endothelial cell, termed the Tumor MicroEnvironment of Metastasis or TMEM, correlated with metastasis in breast cancer patients independently of other clinical prognostic indictors (*3-5*). Here we show, using both primary cells directly from patients and breast cancer cell lines, that TMEM counts positively correlate with Mena^{INV} mRNA expression regardless of breast cancer receptor subtype. Tumor cells and macrophages participate in a paracrine signaling loop involving EGF and CSF secretion and their respective receptors (*6-9*). This paracrine signaling is required for efficient transendothelial migration of the tumor cells, a necessary step in the intravasation process. In addition, Mena^{INV} expression also facilitates transendothelial migration of tumor cells (*10*). Furthermore, direct contact of a tumor cell and a macrophage drives the formation of mature invadopodia, protrusive structures that facilitate extracellular matrix degradation and have been shown to be necessary for transendothelial migration and thus intravasation (*11*). The direct contact between a macrophage and tumor cell results in the activation of Notch1 in the tumor cell. This Notch activity contributes to the invadopodia formation. These data considerably extend our understanding to the mechanisms of tumor cell transendothelial migration and thus intravasation into the blood, upon which cells can metastasize to secondary sites. It also further explores the mechanisms in which macrophages contribute to these processes. These results give us further insights into the prognostic value of TMEM as well as possible novel drug targets.

2. Keywords

Tumor microenvironment, macrophage, Mena, transendothelial migration, metastasis, Notch

3. Accomplishments

Aim 1: Define how macrophage-cancer cell contact and Mena isoform expression status affect invadopodium formation, TMEM assembly and TEM.

Task 1: *Using established breast cancer cell lines determine how Mena isoform expression affects the ability of cells to intravasate using the in vitro TEM assays.*

Utilizing MDA-MB-231 cells expressing GFP or GFP-Mena^{INV} (Fig. 1), it was determined that the over-expression of Mena^{INV} results in an increase in transendothelial migration (TEM) in the presence of macrophages utilizing an in vitro transendothelial migration assay (Fig. 1C).

Task 2: *Determine how Mena isoform expression affects TEM in the presence and absence of macrophages.*

I have developed three independent siRNAs specifically for Mena^{INV} (Fig 1A) that significantly reduce the expression of Mena^{INV} specifically, while having no effect on Mena11a expression. Knockdown of Mena^{INV} significantly reduces the macrophage – induced TEM activity of parental MDA-MB-231 tumor cells as well as cells over-expressing GFP-Mena Mena^{INV} (Figure 1B and C). There is a minimal effect on TEM activity with the knockdown of Mena^{INV} in the

absence of Mena^{INV}. Therefore, we conclude that Mena^{INV} is required for macrophage- induced tumor cell TEM activity.

I have recently developed siRNA tools for Mena11a that will be used to test to contribution of Mena11a to TEM and invadopodia activity in tumor cells. It is hypothesized that Mena11a expression will not be required for macrophage – induced TEM and invadopodia activity.

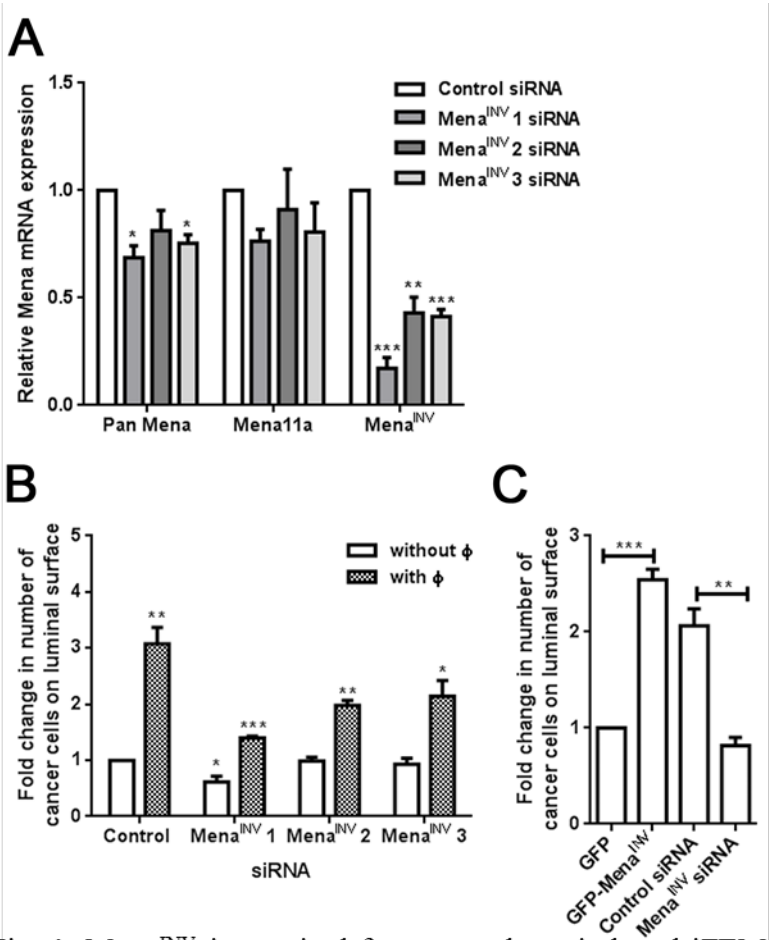

Fig. 1. Mena^{INV} is required for macrophage-induced iTEM in MDA-MB-231 TN breast cancer cells. (A) Transcript abundance for total Mena, Mena11a, and Mena^{INV} in parental MDA-MB-231 cells transfected with one of three MenaINV-targeted siRNAs. (B) iTEM of MDA-MB-231 cells after Mena^{INV} depletion in the presence or absence of macrophages (F). (C) iTEM of MDA-MB-231 cells expressing GFP-tagged MenaINV, alone or co-transfected with Mena^{INV}-targeted siRNA (1). iTEM was performed in the presence of macrophages. Data in (A) to (C) are means ± SEM from three experiments. *P < 0.05, **P < 0.005, ***P < 0.0005, by two-tailed Student's t tests assuming equal variances.

Task 3: *Determine the ability of Mena11a and* Mena^{INV} *expressing ER^{+}/Her2^{-} and TN cells to form TMEM and TEM in vivo.*

TMEM counts were performed from 100 patient samples across the different receptor subtypes, ER^{+}, Her2^{+} and TN. In addition, Mena11a and Mena^{INV} mRNA expression was measured by qPCR in the same patient population. Results from the entire cohort reveal that there is a positive correlation between TMEM count and Mena^{INV} expression, whereas there is a slightly negative correlation between TMEM and Mena11a in those same patient samples (Fig. 2 B).

When the patient samples are grouped according to receptor subtype, the same correlation holds true. This indicates that TMEM and Mena^{INV} positively correlate regardless of the receptor status of the breast tumor (Fig. 2 C). TMEM counts have been shown to be a predictive value for metastasis. These data indicate that in fact TMEM and Mena^{INV} correlation, or levels of Mena^{INV} will also have prognostic value in determining patients that are at risk of metastasis.

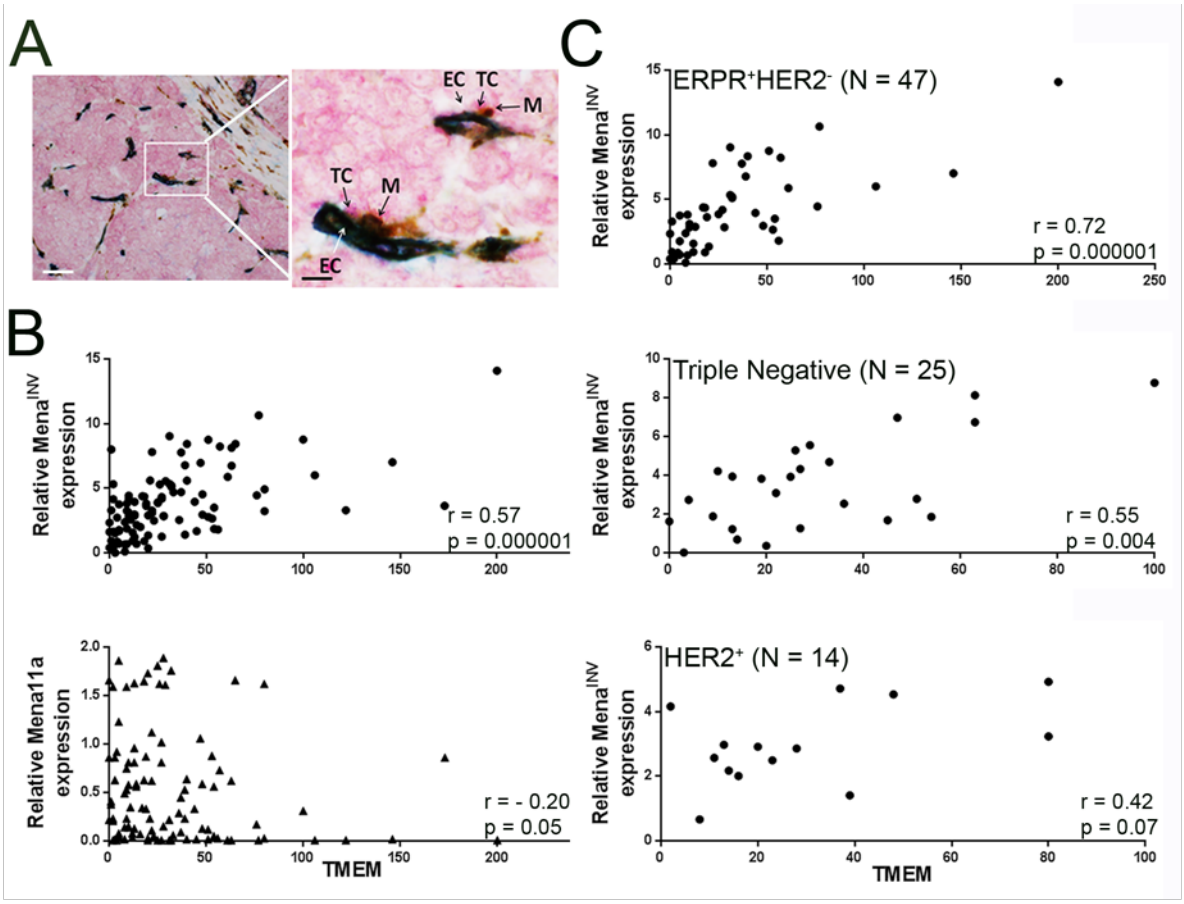

Fig. 2. Correlation of Mena isoform expression to TMEM score. (A) TMEM microanatomic cancer cell TEM sites visualized by IHC. TC, Mena expressing tumor cells; EC, CD31-expressing vascular endothelial cells; M, CD68-expressing macrophages. Scale bars, 300 mm (left) and 50 mm (right). (B and C) Scatter plots of relative Mena^{INV} transcript expression against TMEM score in the entire cohort of 100 IDCs (B) or by clinical subtype (C). Data were analyzed by rank-order correlation. The differences in slopes between subtypes were not statistically significant as shown by the regression model fit to the rank-transformed data. n, number of tumor cases.

Aim 2: Determine if breast cancer cell lines and primary tumor cells use the same mechanisms during TMEM assembly and transendothelial migration

Task 4: *Determine Mena isoform expression and invadopodia formation in primary FNA samples that have the ability to intravasate using TEM assay.*

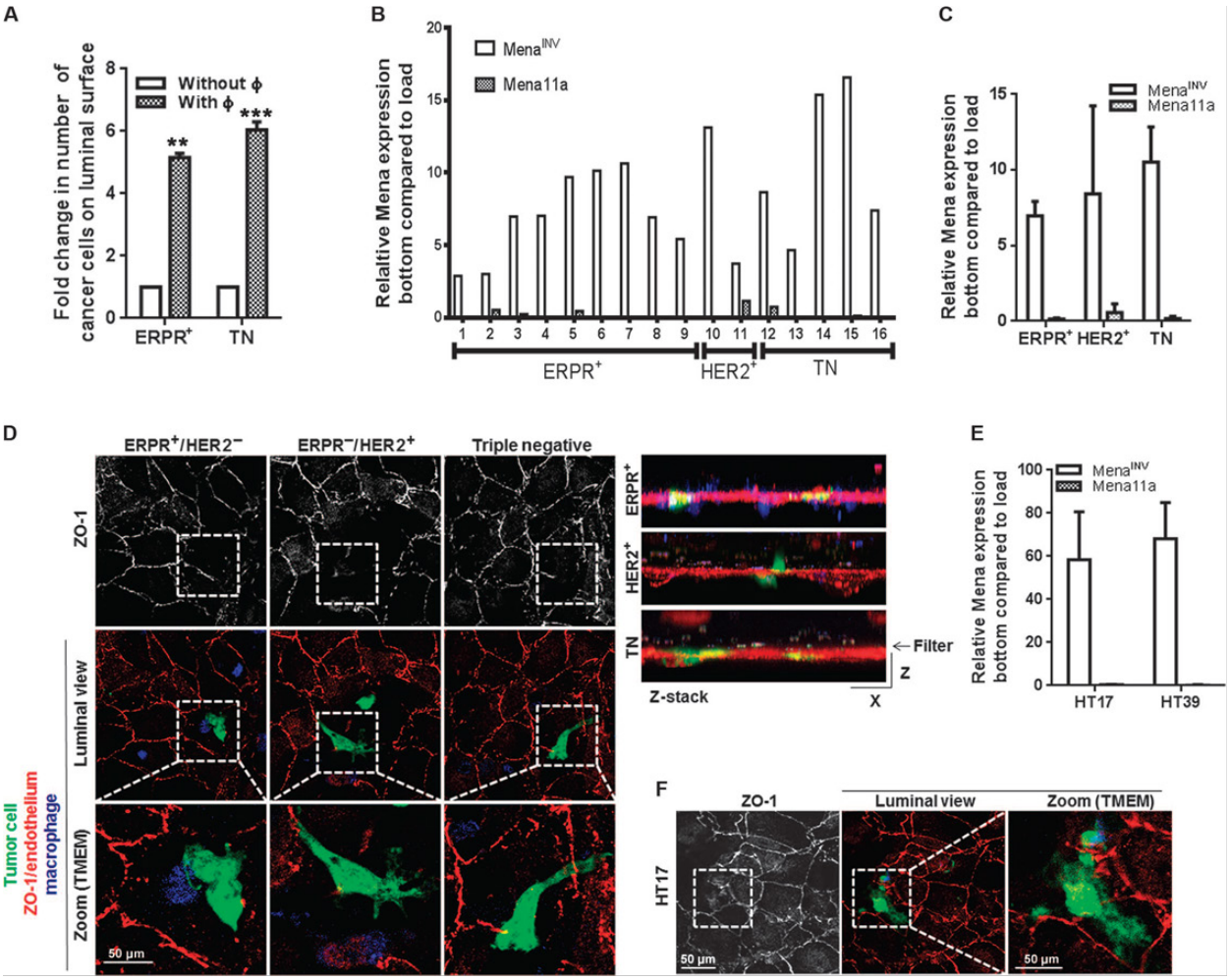

Fig. 3. iTEM assays using human patient IDC cells obtained from FNA biopsies. (A) Fold increase in the number of cells from ERPR$^+$ or TN cases that crossed a HUVEC monolayer in the presence of macrophages (F) relative to the number that crossed in the absence of macrophages. Data are means ± SEM from three experiments. **P < 0.005, ***P < 0.0005, by two-tailed Student's t tests assuming equal variances. (B) Mena^{INV} or Mena11a transcript expression in cells that crossed the HUVEC monolayer relative to that in the loaded cell population. Data are from 16 patient cases. (C) Average Mena^{INV} and Mena11a isoform expression in iTEM-competent cells from (B) grouped by clinical subtype. Data were not significantly different by a Student's t test. (D) Apical z-sections from the iTEM assay. Tumor cells, green; macrophages, blue; HUVEC junctions (ZO-1), red. Squares indicate dissociating HUVEC junctions, magnified below. Right: Representative z-stacks by clinical subtype. Data are representative of each from the 16 cases in (B). (E) Mena^{INV} and Mena11a transcript expression in iTEM-competent cells from TN human tissue transplants HT17 and HT39. Data are means ± SEM from three mice each. (F) Apical z-sections of the iTEM assay with HT17 tumor cells as in (D). Images are representative of three experiments.

Using an *in vitro* TEM assay, we have determined that cells from primary FNA samples have the ability to intravasate have significantly higher levels of Mena^{INV} compared with the starting sample (the load) (Fig. 3B). This is true for cells from the major different receptor subtype of invasive breast carcinoma, ER$^+$, Her2$^+$ and triple negative (TN). In all cases, cells with the ability to cross the endothelial layer have little to no detectable Mena11a.

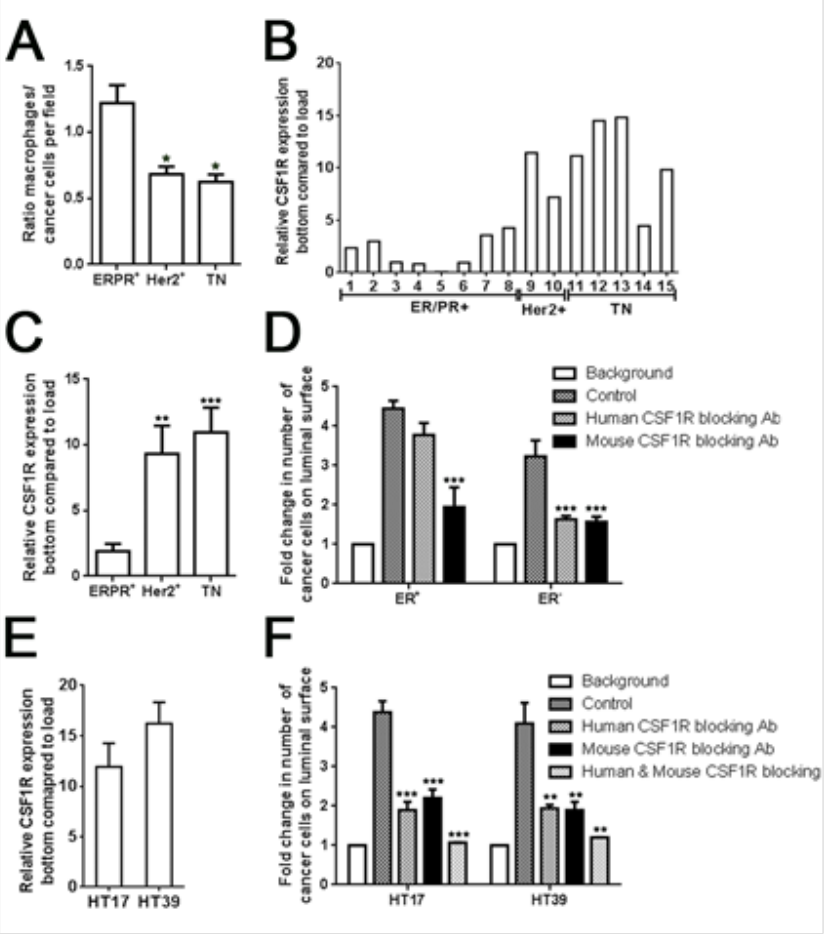

Fig. 4. CSF1R expression in iTEM-competent cells differs among breast cancer subtypes. (A) The number of macrophages associating with tumor cells during iTEM, presented as a ratio by clinical subtype. Data are means ± SEM from twelve 63× microscopic fields in two to three cases each. *P < 0.05 compared with that in ERPR+/HER2− cases. (B and C) CSF1R transcript abundance in iTEM-competent cells from each of 15 cases analyzed across clinical subtypes (B). Data in (C) are means ± SEM by clinical subtype shown in (B). (D) Effect of mouse-specific CSF-1R antibodies or human-specific CSF-1R antibodies on iTEM of ERPR+/HER2−, ERPR−/HER2+ (HER2+), and TN cancers. Data are means ± SEM from three cases per subtype relative to the background (tumor cells cross without the presence of macrophages). Control, tumor cells cross in the presence of macrophages. (E and F) CSF1R transcript abundance in iTEM competent cells from patient tumor transplants HT17 and HT39 (E), and the effect of mouse- or human specific CSF-1R functionally blocking antibodies on iTEM capacity. Data are means ± SEM from five mice per tumor sample. **P < 0.005, ***P < 0.0005. Statistical analyses in (A), (C), (D), and (F) used two-tailed Student's t tests assuming equal variances.

In addition, as detailed above, in the MDA-MB-231 cell line the knockdown of $Mena^{INV}$ inhibits macrophage-promoted tumor cell transendothelial migration. Conversely, the over-expression of $Mena^{INV}$ drives increased macrophage-mediated tumor cell transendothelial migration.

These data together indicate that primary tumor cells of different receptor subtypes as well as the breast tumor cell line MDA-MB-231 use the same $Mena^{INV}$ dependent mechanisms during transendothelial migration.

Task 5: *Determine the ability of primary human breast tumor cells from different cancer subtypes to form invadopodia.*

Although we have not yet looked at the ability of primary tumor cells from different cancer subtype to form invadopodia, we did determine that $Mena^{INV}$ expression is required for the formation of macrophage – induced invadopodia.

As detailed above in TASK X, $Mena^{INV}$ is upgulated in tumor cells when in contact with macrophages through a Notch dependent pathway. When the tumor cells are in

contact with macrophages we observe a significant increase in the number of invadopodia formed by tumor cells, as well as the associated matrix degradation.

If we knockdown total Mena expression of the Mena^{INV} isoform specifically, tumor cell lose the ability to form these invadopodia and degrade matrix.

This work was done in the triple negative breast cancer cell line MDA-MB-231. We were able to recapitulate some of these results with a limited panel of primary tumor cells from FNA's directly from patient samples or from patient derived xenographs (PDXs). Samples from patients and PDX models were triple negative or ER+.

Task 6: *Determine the influence of ER expression on TEM.*

The above data (Fig. 3A) indicate that in the presence of macrophages both ER+ and TN primary tumor cells show increased TEM activity, although TN cells are more efficient. Cells from ER+ and TN patients all show enhancement of Mena^{INV} expression in the TEM-competent cells (Fig. 3B), that are not significantly different from each other (Fig. 3C). It was noted while imaging the TEM assay that TN negative cells, which do not express ER, appeared to be less reliant on macrophage contact in order to cross the endothelial layer.

When quantified, cells from ER+ tumor transendothelial migrate at a higher ratio with macrophages than cells from Her2+ and TN tumors. This indicated that although the higher expression of Mena^{INV} was a common feature in all cells that transmigrate regardless of receptor status, there was also a difference in the mechanism of tumor cell transendothelial migration in ER+ an ER- tumor cells. It has previously been shown that TN cells can participate in an autocrine signaling loop by expressing the CSF-1 receptor. Indeed, I found that in cells lacking ER expression, there was increased CSF-1R expression in the TEM-capable cells (Fig. 4 B and C). Utilizing a mouse derived macrophage cell line and human primary tumor cells; I was able to selectively block the CSF-1R in macrophages or tumor cells using species specific blocking antibodies (Fig. 4 D and F). In cells from ER+ tumors, only inhibition of the macrophage CSF-1R reduced tumor cell TEM activity, whereas in cells from ER- tumors there was a contribution of both macrophage and tumor cell CSF-1R.

These data indicate that cells from ER- tumors have the ability to participate in both paracrine signaling with macrophages and autocrine signaling which allow them to intravasate whereas ER+ cells are more reliant on macrophages for intravasation. We speculate that the tumor cell expression of CSF-1R allows the cells to become more migratory. It will require further work to fully explore this difference in mechanism.

In evaluating the contribution of macrophages to tumor cell intravasation, we found that the direct contact of a tumor cell with a macrophage can induce the formation of invadopodia; invasive protrusions will the ability to degrade the extracellular matrix and basement membrane. These heterotypic cell-cell contact invadopodia are dependent on the expression of Notch1 in the tumor cell (Fig. 5).

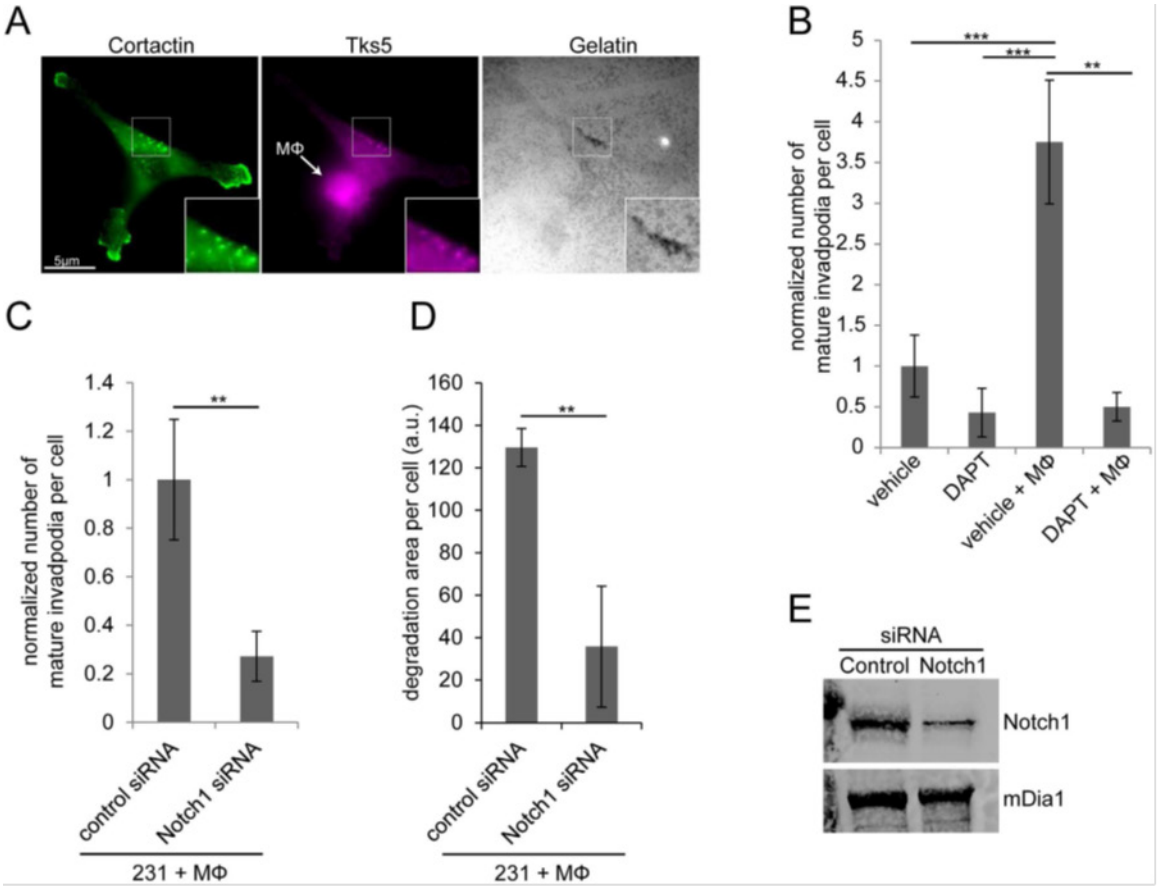

Fig. 5 Macrophage – induced tumor cell invadopodia require Notch1 signaling. (A) Immunofluorescence of MDA-MB-231 tumor cell in contact with BAC1.2F5 macrophage plated on 405-gelatin. Tumor cells were stained for Tks5 (purple) and cortactin (green) to identify invadopodium cores (insert is zoom of mature invadopodia). Position of the macrophage is indicated by the arrow. (B) Quantitation of the number of mature invadopodia per cell in MDA-MB-231 tumor cells plated alone or with BAC1.2F5 macrophages. Cells were treated with vehicle or DAPT γ - secretase inhibitor. (C) Quantitation of the number of mature invadopodia per cell in MDA-MB-231 tumor cells treated with control or Notch1 siRNA plated with BAC1.2F5 macrophages. (D) Quantitation of the area of matrix degradation in control and Notch1 siRNA treated MDA-MB-231 cells plated with BAC1.2F5 macrophages. (E) Western blot of MDA-MB-231 cells treated with control and Notch1 siRNA demonstrating knockdown efficiency. mDia1 (mammalian homolog of Drosophila diaphanous) was used as a loading control. $*P < 0.05$, $**P < 0.005$, $***P < 0.0005$.

This work expanded into a manuscript (Appendix B) that details the contribution of a macrophage – contact Notch1 signaling pathway in tumor cells that results in the upregulation of Mena^{INV}, resulting in increased formation of invadopodia and transendothelial migration.

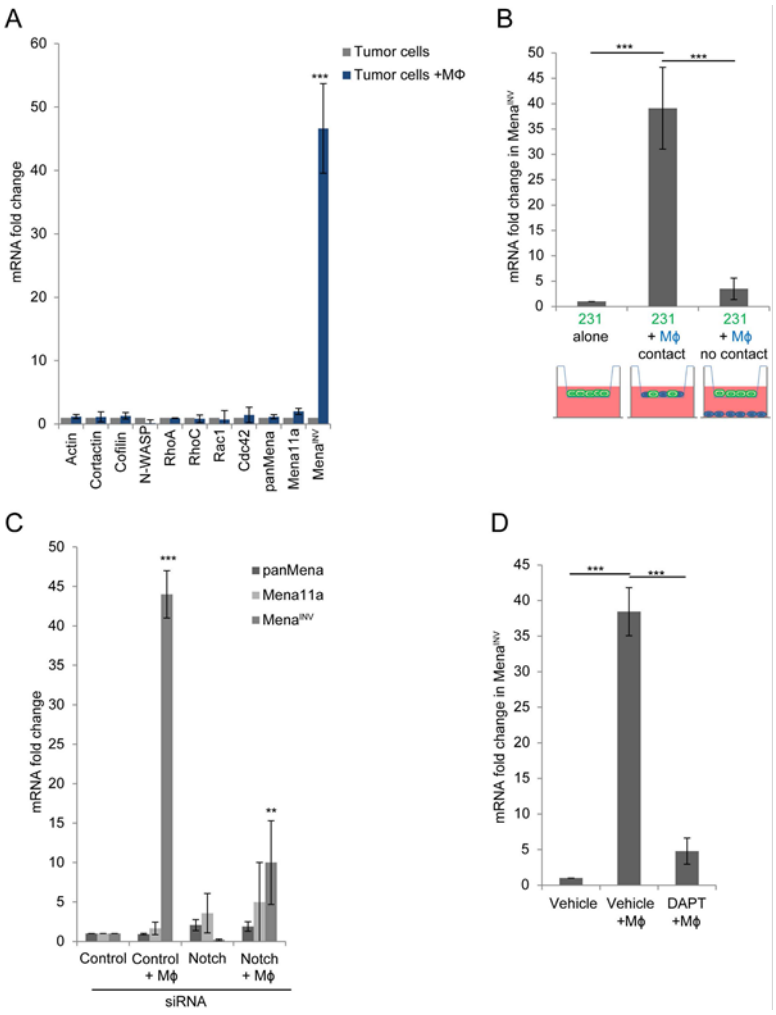

Fig. 6 Macrophage – tumor cell contact results in a Notch1 dependent upregulation in MenaINV mRNA expression in tumor cells. (A) qRT-PCR of invadopodia pathway components in MDA-MB-231 cells plated alone or with BAC1.2F5 macrophages (Mφ). (B) qRT-PCR of MenaINV in MDA-MB-231 cells plated in transwells alone, co-cultured in top well of transwells in contact with BAC1.2F5 macrophages (Mφ) or plated on opposite side of transwells (no contact). (C) qRT-PCR of MenaINV in MDA-MB-231 cells treated with control or Notch1 siRNA plated alone or with BAC1.2F5 macrophages. (D) qRT-PCR of MenaINV in MDA-MB-231 cells treated with vehicle or DAPT γ - secretase inhibitor plated alone or with BAC1.2F5 macrophages. *P < 0.05, **P < 0.005, ***P < 0.0005.

I found that when tumor cells are in direct contact with macrophages there is an upregulation of $Mena^{INV}$ mRNA, as measured by qPCR (Fig. 6 A and B). When the Notch1 pathway is inhibited in tumor cells, either by siRNA knockdown of Notch1 (Fig. 6C) or by chemical inhibition with DAPT (Fig. 6D), there is no longer an upregulation of $Mena^{INV}$, even with macrophage – tumor cell contact. These data show that upon macrophage – tumor cell contact there is an upregulation of $Mena^{INV}$ mRNA that occurs through a Notch1 mediated pathway. These results have also been shown using primary tumor cells from patients (see Appendix C).

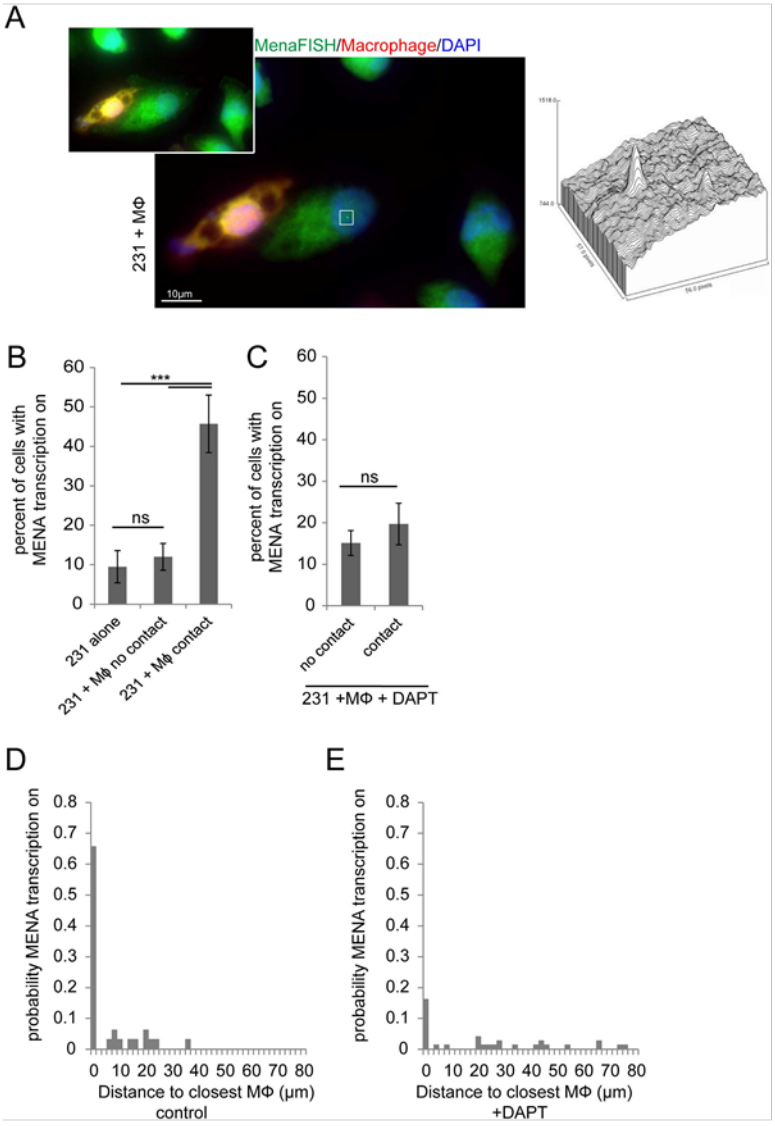

Fig. 7 Macrophage- tumor cell contact increases MENA transcription. (A) MDA-MB-231 cells plated with BAC1.2F5 macrophages for 60 min. Macrophages are labeled with cell tracker red. Cells were labeled with FISH probes that recognize all Mena isoforms (panMena) and DAPI. Inset shows z-section of direct contact of tumor cell with macrophage. White box is around the dot which is an active MENA transcription site. Histogram of FISH fluorescence intensity within white box showing signal to noise intensity of transcription site. (B) Quantitation of the percent of tumor cells with active MENA transcription when MDA-MB-231 cells are plated alone, with BAC1.2F5 macrophages (Mφ) not in contact and with Mφ in contact with tumor cells. (C) Quantitation of the percent of tumor cells with active MENA transcription when MDA-MB-231 cells with BAC1.2F5 macrophages (Mφ) not in contact and with Mφ in contact with tumor cells in the presence of DAPT γ - secretase inhibitor. (D) The distance of tumor cells from macrophages in the population of cells with MENA transcription sites being expressed (probability). (E) The distance of tumor cells from macrophages in the population of cells with MENA transcription sites being expressed in the presence of DAPT (normalized for the number of cells with MENA being expressed). *P < 0.05, **P < 0.005, ***P < 0.0005, ns = non-significant.

It is well known that Notch1 signaling is a regulator of gene transcription, so suing FISH probes to the MENA gene we measured active MENA gene transcription sites in tumors cells in contact with macrophages (Fig. 7). Tumor cells plated alone or with macrophages but with no macrophage-tumor cell contact deplay ~10% of cells with an active transcription site. When tumor cells are in contact with macrophages, there is a significant increase of active MENA transcription sites (~50% of cells). MENA transcription upon tumor cell contact with a macrophage can be block with the addition of the Notch inhibitor DAPT, demonstrating that macrophage – tumor cell contact results in Notch mediated MENA gene transcription.

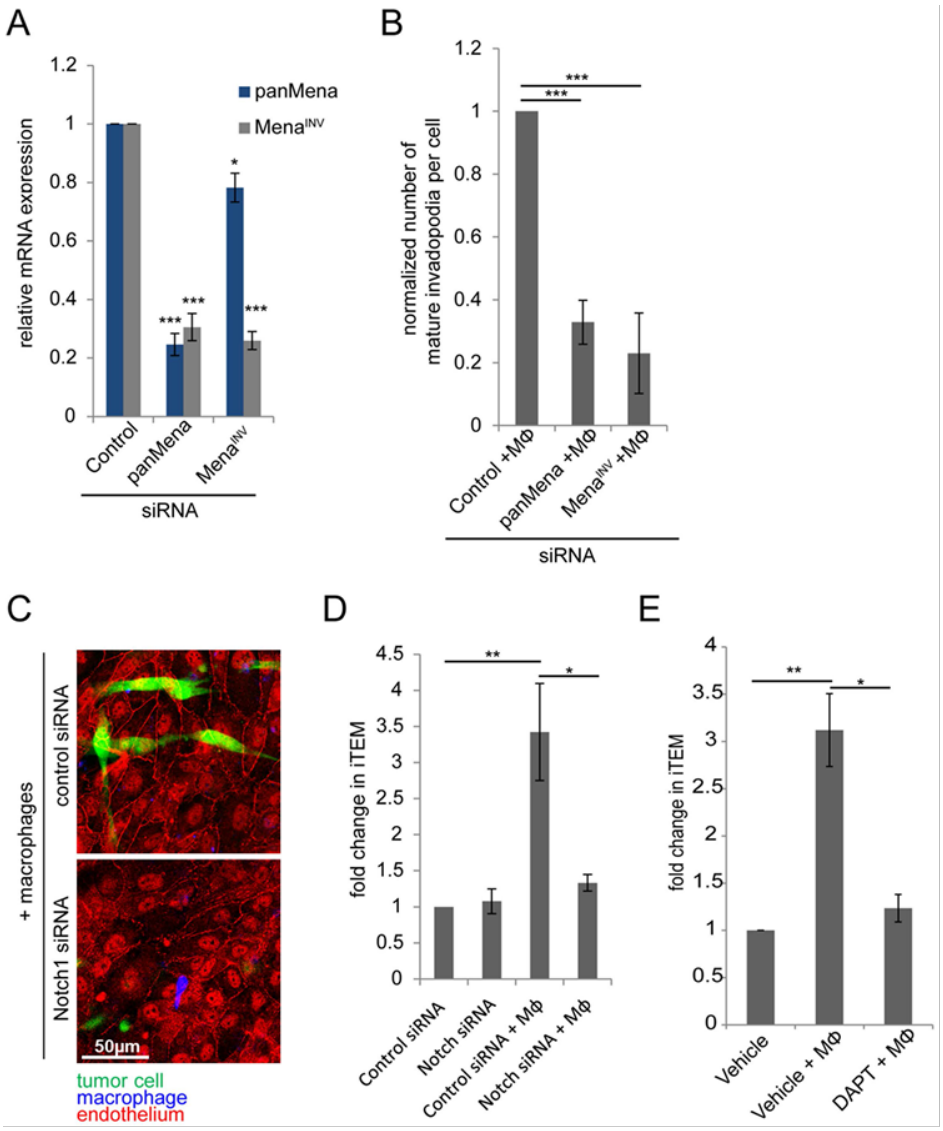

Fig. 8 MenaINV and Notch1 are required for macrophage – induced invadopodium assembly and transendothelial migration. (A) Quantitation of the relative mRNA expression in MDA-MB-231 cells treated with control, panMena or MenaINV siRNA in the absence of macrophages. (B) Quantitation of the relative number of invadopodia in MDA-MB-231 cells treated with control, panMena or MenaINV siRNA in the presence of macrophages. (C) Representative apical z-section of intravasation-directed transendothelial migration (iTEM) assay of tumor cells (green) and macrophages (blue, white arrows). Tumor cells were treated with control or Notch1 siRNA. Endothelial HUVEC cells were stained for ZO-1 (red). Shown is an "en face" view of the apicial side of the transwell, therefore the green-labeled tumor cells have crossed the endothelial monolayer and are on the 'bottom' or apical side of the transwell positioning them above the endothelial cells from this vantage point. (D) Quantitation of intravasation-directed is defined as subluminal to luminal transendothelial migration (iTEM) activity of MDA-MB-231 cells plated on the endothelium either alone or with BAC1.2F5 macrophages. Tumor cells were treated with control or Notch1 siRNA. (E) Quantitation of iTEM activity of MDA-MB-231 cells plated alone or with BAC1.2F5 macrophages with vehicle or DAPT treatment. *P < 0.05, **P < 0.005, ***P < 0.0005.

I then determined if Mena^{INV} expression is required for macrophage contact induced invadopodia in tumor cells. I depleted total Mena expression (panMena) or the Mena^{INV} isoform specifically in tumor cells (Fig. 8 A). When both panMena and Mena^{INV} knockdown cells were in contact with macrophages, the ability of the tumor cells to form invadopodia was significantly diminished (Fig. 8B). In addition, the inhibition of the Notch1 pathway through siRNA knockdown or DAPT treatment diminished the ability of tumor cells to undergo macrophage mediated transendothelial migration (Fig. 8 C-E). These data indicate that there is a Notch1 – Mena^{INV} pathway that is activated by macrophage – tumor cell contact. This pathway is required for the tumor cells to form invadopodia and transmigrate through and endothelial layer, steps required for tumor cell metastasis. These results are detailed and discussed in the published manuscript, Appendix C.

Milestone 2: *Preparation and submission of manuscript for publication.*

During Year 1 I completed a body of research that led to further insight on tumor cell transendothelial migration and the contribution of macrophages to this process. In addition, this work showed that the correlation between TMEM counts and Mena^{INV} expression could provide prognostic value to breast cancer patients presenting with different receptor subtypes of the disease. A manuscript detailing this work was published in Science Signaling during Year 1, attached as Appendix B.

Within Year 2, I have submitted and revised a manuscript detailing the macrophage – induced Notch1 signaling that occurs in tumor cells via direct cell contact. This signaling mechanism results in increased Mena^{INV} expression, formation of invadopodia, and subsequent tumor cell transendothelial migration. This manuscript was accepted and was published in November of 2016 in Scientific Reports (Appendix C).

In addition, I am second author on a manuscript in preparation for submission which details the use of a novel small molecule inhibitor to Tie2, rebastinib, in the blockade of TMEM function. Inhibition of Tie2 high macrophages in the iTEM assay significantly reduces the number of tumor cells that can effectivity transmigration across an endothelium (Appendix D, Figure 6).

Opportunities for training and professional development

Opportunities for professional development are outlined below.

Scientific conferences

In Year 1, I attended scientific conferences as outlined below. Poster or oral presentations are described.

- American Society for Cell Biology Annual Meeting, Philadelphia, PA. December 2014. Poster presentation.
- American Association for Cancer Research Annual Meeting, Philadelphia, PA. April 2015. Poster presentation.

Workshops and Symposia

- New York Symposium on Tumor Microenvironment, Cold Spring Harbor, NY. August 2015. Poster Presentation.
-

In Year 2, I attended scientific conferences as outlined below. Poster or oral presentations are described.

- American Society for Cell Biology Annual Meeting, San Diego, California. December 2015. Poster presentation and microsymposium talk.
- American Association for Cancer Research Annual Meeting, New Orleans, Louisiana. April 2015. Poster presentation.

4. Impact

Key Findings

- Discovery that TMEM counts and Mena^{INV} abundance positivity correlate.

- Discovery that Mena^{INV} expression drives and is required for tumor cell transendothelial migration.
- Finding that in primary breast tumor cells from different receptor subtype, the intravasation competent cells express high levels of Mena^{INV}.
- Finding that ER+ and ER- cells have differences in paracrine and autocrine signaling with macrophage that regulates intravasation.
- Discovery that there are macrophage-induced invadopodia that form in tumor cells in a Notch1 dependent manner.
- Macrophage – tumor cell contact also upregulates Mena^{INV} expression through a Notch1 signaling pathway that activates Mena gene transcription. The mechanisms of Mena^{INV} upregulation in tumor cells were previously undescribed.
- Notch1 signaling and Mena^{INV} expression are required for tumor cell transendothelial migration, a required step for tumor cell metastasis.

Conclusions
Findings from Year 1 and 2 of this study will have a significant impact on the understanding of tumor cell transendothelial migration, a process necessary for tumor cell intravasation and metastasis.

TMEM and Mena^{INV} *positive correlate in ER+, Her2+ and TN patient samples*
TMEM counts have been shown to be a prognostic indicator of metastasis in breast cancer (*4, 5*). Herein, it is shown that the expression level of Mena^{INV} positively correlates with TMEM counts, while Mena11a has a weak negative correlation among the same patients. Using primary tumor cells obtained by FNA biopsy and an in vitro assay for transendothelial migration (TEM) that mimics a necessary step for tumor cell intravasation, it is shown that intravasation-competent cells express high levels of Mena^{INV} compared with the total population of cells. Expression of Mena^{INV} is not only a mark for cells with this metastatic capability, but also has a functional role. Knockdown of the Mena^{INV} isoform specially inhibits TEM activity of tumor cells. These data indicate the importance of Mena^{INV} both as a clinical readout for risk of metastases and for therapeutic intervention.

Tumor associated macrophages contribute to tumor cell TEM activity
TMEM is defined as the direct contact of a Mena expressing tumor cell, macrophage, and endothelial cell of a blood vessel (*3, 4*). Thus far, in Year 1 of this project, I have determined that macrophages significantly enhance the intravasation capabilities of primary human tumor cells. This is in part due to the paracrine signaling loop between macrophages and tumor cells. In addition, macrophage – tumor cell contact results in Notch1 dependent invadopodia formation that will be further explored. These data further support the pro-metastatic role of tumor associated macrophages and the importance in dissecting the mechanisms.

5. Changes/Problems
Nothing to report.

6. Products
- Journal publications

- **Pignatelli, J**., S. Goswami, J. G. Jones, T. E. Rohan, E. Pieri, X. Chen, E. Adler, D. Cox, S. Maleki, A. Bresnick, F. B. Gertler, J. S. Condeelis and M. H. Oktay (2014). "Invasive breast carcinoma cells from patients exhibit Mena^{INV}- and macrophage-dependent transendothelial migration." Sci Signal **7**(353): ra112. (Federal support acknowledged)
- **Jeanine Pignatelli**, Jose Javier Bravo-Cordero, Minna Roh-Johnson, Saumil J. Gandhi, Yarong Wang, Xiaoming Chen, Robert J. Eddy, Alice Xue, Robert H. Singer, Louis Hodgson, Maja H. Oktay and John S. Condeelis (2016). "Macrophage-dependent tumorcell transendothelial migration ismediated by Notch1/MenaINV initiated invadopodium formation." Sci. Rep. 6, 37874. (Federal support acknowledged)

- Books or other non-periodical one-time publication
  - Nothing to report
- Website or other Internet site
  - Nothing to report
- Technologies or techniques
  - Nothing to report
- Inventions, patent applications and/or licenses
  - Nothing to report
- Other Products
  - Nothing to report

7. Participants

- Jeanine Pignatelli, PhD : no change

8. Special Reporting Requirements

Not Applicable

9. Appendices

- **Appendix A: References**
- **Appendix B: Manuscript** "Invasive breast carcinoma cells from patients exhibit Mena^{INV}- and macrophage-dependent transendothelial migration." By Pignatelli et al.
- **Appendix C: Manuscript "**Macrophage-dependent tumorcell transendothelial migration ismediated by Notch1/MenaINV initiated invadopodium formation." By Pignatelli et al.
- **Appendix D: Manuscript** "Rebastinib inhibits recruitment and function of TIE2+ macrophages in metastatic breast cancer." By Harney et al.

Appendix A: References

1. Weigelt, J. L. Peterse, L. J. van 't Veer, Breast cancer metastasis: markers and models. *Nature reviews. Cancer* 5, 591 (Aug, 2005).
2. R. Heimann, S. Hellman, Clinical progression of breast cancer malignant behavior: what to expect and when to expect it. *Journal of clinical oncology : official journal of the American Society of Clinical Oncology* 18, 591 (Feb, 2000).

3. B. D. Robinson, J. G. Jones, Tumor microenvironment of metastasis (TMEM): a novel tissue-based assay for metastatic risk in breast cancer. *Future oncology* 5, 919 (Sep, 2009).
4. B. D. Robinson *et al.*, Tumor microenvironment of metastasis in human breast carcinoma: a potential prognostic marker linked to hematogenous dissemination. *Clinical cancer research : an official journal of the American Association for Cancer Research* 15, 2433 (Apr 1, 2009).
5. T. E. Rohan *et al.*, Tumor microenvironment of metastasis and risk of distant metastasis of breast cancer. *Journal of the National Cancer Institute* 106, (Aug, 2014).
6. E. T. Roussos *et al.*, Mena invasive (MenaINV) promotes multicellular streaming motility and transendothelial migration in a mouse model of breast cancer. *Journal of cell science* 124, 2120 (Jul 1, 2011).
7. E. T. Roussos *et al.*, Mena invasive (Mena(INV)) and Mena11a isoforms play distinct roles in breast cancer cell cohesion and association with TMEM. *Clinical & experimental metastasis* 28, 515 (Aug, 2011).
8. A. Patsialou *et al.*, Selective gene-expression profiling of migratory tumor cells in vivo predicts clinical outcome in breast cancer patients. *Breast cancer research : BCR* 14, R139 (2012).
9. A. Patsialou *et al.*, Autocrine CSF1R signaling mediates switching between invasion and proliferation downstream of TGFbeta in claudin-low breast tumor cells. *Oncogene* 34, 2721 (May 21, 2015).
10. J. Pignatelli *et al.*, Invasive breast carcinoma cells from patients exhibit MenaINV- and macrophage-dependent transendothelial migration. *Science signaling* 7, ra112 (Nov 25, 2014).
11. M. Roh-Johnson *et al.*, Macrophage contact induces RhoA GTPase signaling to trigger tumor cell intravasation. *Oncogene* 33, 4203 (Aug 14, 2014).

CANCER IMMUNOLOGY

Invasive breast carcinoma cells from patients exhibit Mena^{INV}- and macrophage-dependent transendothelial migration

Jeanine Pignatelli,[1]* Sumanta Goswami,[1,2] Joan G. Jones,[1,3,4,5] Thomas E. Rohan,[3] Evan Pieri,[2] Xiaoming Chen,[1] Esther Adler,[4] Dianne Cox,[1] Sara Maleki,[4] Anne Bresnick,[6] Frank B. Gertler,[7] John S. Condeelis,[1,5,8]* Maja H. Oktay[4]*

Metastasis is a complex, multistep process of cancer progression that has few treatment options. A critical event is the invasion of cancer cells into blood vessels (intravasation), through which cancer cells disseminate to distant organs. Breast cancer cells with increased abundance of Mena [an epidermal growth factor (EGF)–responsive cell migration protein] are present with macrophages at sites of intravasation, called TMEM sites (for tumor microenvironment of metastasis), in patient tumor samples. Furthermore, the density of these intravasation sites correlates with metastatic risk in patients. We found that intravasation of breast cancer cells may be prevented by blocking the signaling between cancer cells and macrophages. We obtained invasive breast ductal carcinoma cells of various subtypes by fine-needle aspiration (FNA) biopsies from patients and found that, in an in vitro transendothelial migration assay, cells that migrated through a layer of human endothelial cells were enriched for the transcript encoding Mena^{INV}, an invasive isoform of Mena. This enhanced transendothelial migration required macrophages and occurred with all of the breast cancer subtypes. Using mouse macrophages and the human cancer cells from the FNAs, we identified paracrine and autocrine activation of colony-stimulating factor-1 receptor (CSF-1R). The paracrine or autocrine nature of the signal depended on the breast cancer cell subtype. Knocking down Mena^{INV} or adding an antibody that blocks CSF-1R function prevented transendothelial migration. Our findings indicate that Mena^{INV} and TMEM frequency are correlated prognostic markers and CSF-1 and Mena^{INV} may be therapeutic targets to prevent metastasis of multiple breast cancer subtypes.

INTRODUCTION

Metastasis is a complex multistep process that involves cancer cell dissemination and, ultimately, patient death (*1*). The outcome of breast cancer patients with metastatic disease has not improved in the past 30 years in spite of the development of targeted therapies (*2*). Thus, understanding the details of the metastatic process is of paramount importance for the development of new prognostic and therapeutic targets.

Intravital imaging in animal models has revealed many aspects of metastasis (*3*–*6*), including the essential roles that macrophages play in the microenvironments in which mammary tumor cells invade, migrate, and intravasate (*5*, *7*). In particular, intravital imaging of rodent mammary tumors shows that breast cancers contain a subpopulation of highly motile cancer cells that move alongside macrophages in streams toward blood vessels in response to paracrine chemotactic signaling (*6*, *8*, *9*). Upon reaching a blood vessel, cancer cells intravasate at sites enriched with perivascular macrophages (*5*).

Expression profiling of the invasive subpopulation of cancer cells obtained from primary tumors revealed changes in the expression of genes associated with motility pathways that control actin polymerization, epidermal growth factor (EGF)–directed cell movement, and invadopodium formation (*10*, *11*). Directed migration of various cells is typically initiated by chemotactic signaling, which induces cytoskeletal rearrangements involving cofilin (*12*–*14*). Mena, a member of Ena/VASP family of actin-binding proteins, is a key mediator of cytoskeletal arrangement and functions at the convergence of the cofilin-regulated motility pathways (*15*, *16*). Mena enhances tumor cell migration toward EGF in vivo in part by interfering with the activity of inhibitory capping proteins and increasing actin filament elongation rates, thereby promoting actin polymerization (*6*, *16*, *17*). These activities are essential for sustained directional cell movement in response to growth factors like EGF (*18*).

In patients, *MENA* expression is increased in precursor lesions of the cervix and colon, in breast lesions associated with high risk of cancer development, and in high-grade primary and metastatic breast tumors (*19*). Three Mena protein isoforms arising from alternative splicing are particularly important in human breast cancer: Mena^{classic}, Mena^{INV}, and Mena11a. Mena^{classic} contains only the constitutive exons, whereas the two splice variants Mena^{INV} and Mena11a contain alternatively included exons termed "INV" or "11a," respectively. The INV (also known as "+++") exon encodes a 19–amino acid residue inserted near the N terminus, whereas the 11a exon encodes a 21–amino acid residue inserted near the C terminus (*11*, *17*, *20*). Mena^{INV} abundance potentiates chemotactic and invasive responses of carcinoma cells to EGF (*6*, *16*). The observed increase in *MENA* expression in invasive and disseminating tumor cells reflects increased abundance of both Mena^{classic} and Mena^{INV}, and correlates with decreased Mena11a abundance relative to that observed in noninvasive, nonintravasating tumor cells within primary mammary tumors (*17*). Mena forms tetramers via a C-terminal coiled-coil sequence that is conserved in all Ena/VASP proteins, and Mena^{classic} and Mena^{INV} are thought to form Mena^{classic}/Mena^{INV} heterotetramers (*11*, *21*).

[1]Department of Anatomy and Structural Biology, Albert Einstein College of Medicine, Bronx, NY 10461, USA. [2]Department of Biology, Yeshiva University, New York, NY 10033, USA. [3]Department of Epidemiology and Population Health, Albert Einstein College of Medicine, Bronx, NY 10461, USA. [4]Department of Pathology, Albert Einstein College of Medicine/Montefiore Medical Center, Bronx, NY 10467, USA. [5]Integrated Imaging Program, Albert Einstein College of Medicine, Bronx, NY 10461, USA. [6]Department of Biochemistry, Albert Einstein College of Medicine, Bronx, NY 10461, USA. [7]David H. Koch Institute for Integrative Cancer Research, Massachusetts Institute of Technology, Cambridge, MA 02139, USA. [8]Gruss Lipper Biophotonics Center, Albert Einstein College of Medicine, Bronx, NY 10461, USA.
*Corresponding authors. E-mail: moktay@montefiore.org (M.H.O.); jeanine.pignatelli@einstein.yu.edu (J.P.); john.condeelis@einstein.yu.edu (J.S.C.)

MENA expression is found in cancer cells located at the microanatomical sites of cancer cell intravasation, called TMEM (tumor microenvironment of metastasis) sites (*22*, *23*). These sites, initially observed by intravital imaging of rodent mammary tumors, have also been detected in human invasive ductal carcinomas (IDCs) by triple immunohistochemistry (IHC) (*22*). A TMEM site is defined as a *MENA*-expressing tumor cell that is in direct contact with an endothelial cell and a perivascular macrophage. Case-control studies show that the number of TMEM sites is associated with increased risk of developing distant metastases in patients with IDC of the breast (*22*, *23*). IDC sampled by fine-needle aspiration (FNA) biopsies indicates that the relative abundance of Mena^{INV} correlates with TMEM frequency, stability, and/or function in patients (*14*). Increased Mena^{INV} abundance increases transendothelial migration (TEM) in cultured cells and promotes cell migration, streaming, intravasation, and formation of spontaneous lung metastases in orthotopic xenografts in mice (*6*). Other studies show that *Mena* knockout mice bred with PyMT (polyoma virus middle T antigen) transgenic mice develop tumors with reduced intravasation and metastasis and have prolonged survival (*24*). Thus, Mena^{classic} and/or Mena^{INV} may promote metastasis by inducing TEM activity during intravasation.

Here, we tested the hypothesis that the Mena^{INV} isoform in particular is linked to TMEM score and the associated TEM at these proposed sites of intravasation (*14*, *25*) by measuring the TEM activity of primary tumor cells from patients using new in vitro assays.

RESULTS

Mena^{INV} transcript expression positively correlates with the number of TMEM intravasation sites

Our previous study showed a positive correlation between Mena^{INV} and TMEM scores in a cohort of 40 IDCs of the breast obtained from patients, indicating that relative Mena^{INV} abundance correlates with epithelial discohesion and TMEM score in breast cancer patients (*14*). Here, we wanted to confirm this correlation in a larger patient cohort. We measured the abundance of transcripts encoding Mena^{INV} and Mena11a by quantitative real-time polymerase chain reaction (qRT-PCR) in FNA samples from IDCs in a cohort of 60 patients and determined TMEM scores in formalin-fixed, paraffin-embedded (FFPE) breast cancer tissue by triple IHC from the same cohort of 60 patients (Fig. 1A). We previously demonstrated that quantification of the Mena isoforms by immunoblotting is not precise enough for correlation analysis with the TMEM score because of the lack of antibodies capable of detecting Mena^{INV} protein present in FNA biopsies (*14*). Thus, the quantification of Mena isoform expression at the protein level was not performed in this study.

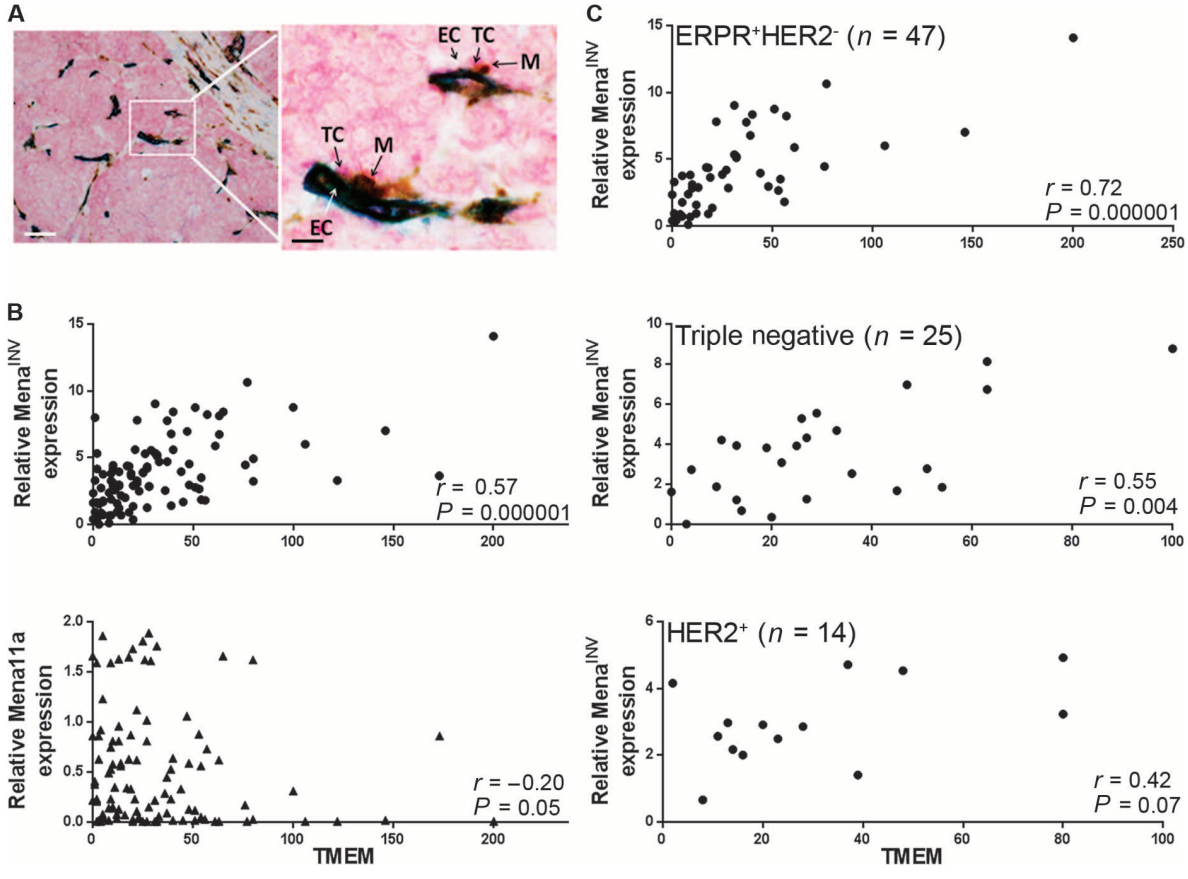

Fig. 1. Correlation of Mena isoform expression to TMEM score. (A) TMEM microanatomic cancer cell TEM sites visualized by IHC. TC, Mena-expressing tumor cells; EC, CD31-expressing vascular endothelial cells; M, CD68-expressing macrophages. Scale bars, 300 μm (left) and 50 μm (right). (B and C) Scatter plots of relative Mena^{INV} transcript expression against TMEM score in the entire cohort of 100 IDCs (B) or by clinical subtype (C). Data were analyzed by rank-order correlation. The differences in slopes between subtypes were not statistically significant as shown by the regression model fit to the rank-transformed data. *n*, number of tumor cases.

Similar to our previous study on samples from 40 patients (*14*), the new cohort of 60 patients showed a strong positive correlation between Mena^{INV} score and TMEM ($r = 0.62$, $P = 10^{-6}$) and a weak negative correlation between Mena11a score and TMEM ($r = –0.17$, $P = 0.19$), as did the combined cohort of 100 patients (*14*) (Fig. 1B). These data support the previous finding that Mena^{INV} may promote intravasation of human IDCs of the breast, whereas Mena11a may suppress intravasation.

Mena^{INV} and TMEM number correlate with each other regardless of clinical subtype and tumor grade

Because breast cancer is a heterogeneous disease, we investigated whether the Mena^{INV}-TMEM correlation is similar across the most common clinical subtypes and grades according to hormone receptor and *HER2* expression status. We observed a very strong correlation between TMEM and Mena^{INV} scores in the ERPR^{+}/HER2^{-} [estrogen receptor– and progesterone receptor–positive, EGF receptor 2 (also known as ErbB2 or neu)–negative] subtype (Fig. 1C). Triple-negative (TN) cases showed a strong correlation, whereas the Mena^{INV}-TMEM correlation in HER2^{+} cases was moderate. Using a regression model fit to the rank-transformed data, we observed that the differences in slopes between the tumor types were not statistically significant. Thus, although there were differences in the Spearman correlation coefficient among the clinical subtypes, this difference was not statistically significant and suggests that relative Mena^{INV} transcript expression correlates with intravasation-rich microenvironments in the most common clinical subtypes of breast cancer. We observed only weak correlation in 14 cases that were ER^{+}/HER2^{-} but lacked PR expression (table S2). This weak correlation may be due to an inadequate statistical power. However, both ER and PR signaling are very complex and involve various paracrine components. There is evidence that signaling through PR is important not only for cell proliferation and branching of breast ducts but also for extracellular matrix remodeling and angiogenesis (*26*). Thus, it is plausible that a lack of PR signaling affects either TMEM formation or Mena^{INV} transcript expression independently, resulting in observed lack of correlation.

In analyzing whether the Mena^{INV}-TMEM correlation was affected by tumor grade, we found that the correlation was strong in poorly and moderately differentiated tumors, and very strong in well-differentiated tumors (Fig. 2A). The regression model fit to the rank-transformed data again showed that the differences in slopes between tumor grades were not statistically significant; therefore, Mena^{INV}-TMEM correlation was not affected by tumor grade. Poorly differentiated IDCs grew in sheets transversed by blood vessels; moderately differentiated IDC grew in a combination

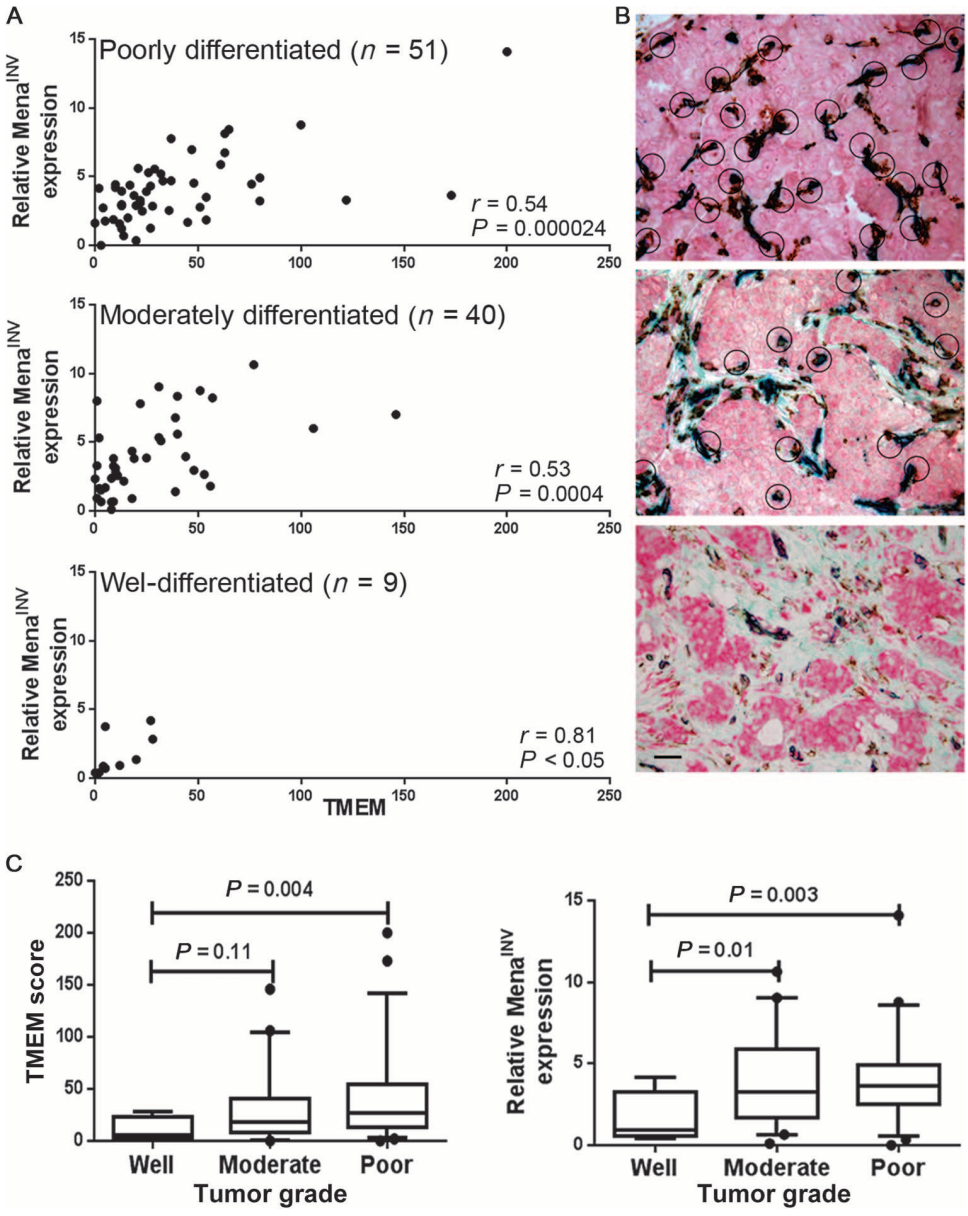

Fig. 2. Correlation of Mena^{INV}-TMEM scores in different grades of human IDCs. (**A**) Scatter plots of relative Mena^{INV} transcript expression against TMEM score in IDCs of different grades. Data were analyzed with Spearman's rank-order correlation. The differences in slopes between grades were not statistically significant as shown by the regression model fit to the rank-transformed data. (**B**) Representative microscopy of poorly differentiated (upper), moderately differentiated (lower), and well-differentiated (bottom) IDCs triple-stained for TMEM. TMEM sites are indicated by circles. Scale bar, 100 μm. (**C**) TMEM score (left panel) and relative Mena^{INV} transcript abundance (right panel) according to tumor grade. Median, 5th and 95th percentile for Mena^{INV} fold change, and TMEM score are presented for well-differentiated ($n = 9$), moderately differentiated ($n = 40$), and poorly differentiated ($n = 51$) tumors. Analyses were done using the Mann-Whitney *U* test at a statistical significance threshold of 0.008.

of glands and sheets; and well-differentiated IDC typically grew in glands and cords surrounded by stroma containing blood vessels (Fig. 2B). Because of the proliferative pattern, cancer cells in well-differentiated IDC were rarely found in direct contact with perivascular macrophages, thus explaining the low TMEM score (Fig. 2A). These "TMEM-low" microenvironments in well-differentiated cases also showed low Mena^{INV} scores, thus strongly correlating.

The data thus far indicate that relative Mena^{INV} transcript abundance in FNA samples positively correlates with the presence of TMEM-rich microenvironments in common clinical subtypes of IDCs and across all breast tumor grades.

Mena^{INV} and TMEM scores independently correlate with clinical and pathological parameters

Because high TMEM score correlates with metastatic outcome, and Mena^{INV} score correlates with TMEM score, we assessed whether Mena^{INV} and TMEM scores in our cohort independently correlate with known clinical and pathological parameters associated with prognosis. We quantified TMEM score and relative Mena^{INV} expression in tumors of different grade, size, lymph node (LN) status, as well as hormone receptor and HER2 status (table S3). We found significant differences in TMEM score and relative Mena^{INV} expression, independently, only between well-differentiated and poorly differentiated tumors (Fig. 2C). This is likely due to the differential cell proliferation pattern among the grades, as discussed above. There was no significant difference in either TMEM score or relative Mena isoform expression among tumors of different size, LN status, or hormone receptor and *HER2* expression. When we examined LN status within each clinical subtype, we observed a somewhat positive correlation of LN positivity with TMEM score and relative Mena^{INV} expression only in ERPR^{+}/HER2^{-} tumors, but this did not reach statistical significance (fig. S2). These data indicate that TMEM and Mena^{INV} scores measure aspects of tumor biology not addressed by the current clinical and pathological parameters other than tumor grade.

E-cadherin expression in tumors differs among samples according to Mena^{INV} and TMEM scores

Tumor grade reflects mitotic count, nuclear features, and cancer cell growth pattern. Because architectural tumor growth pattern was associated with TMEM formation (Fig. 2B), we investigated whether other aspects of tumor architecture would differ among cases with low and high TMEM and Mena^{INV} scores. Cell cohesion is one aspect of tumor biology that is not measured by current clinical and pathological parameters. The ability of tumor cells to migrate toward blood vessels, assemble TMEMs, and intravasate is believed to require the epithelial-to-mesenchymal transition (EMT) and the disruption of epithelial junctions. We previously found that discohesion of epithelial cell-cell contacts in mouse mammary tumors is associated with Mena^{INV} score, which is associated with increased TMEM score (*14*). We predicted that this was also true in samples of human breast cancer. We observed significantly more cells with strong staining of cell-cell junction protein E-cadherin in cases with low TMEM and Mena^{INV} scores than in the cases with high TMEM and Mena^{INV} scores (Fig. 3A). Conversely, there were more cells with low E-cadherin abundance in cases with high TMEM and Mena^{INV} scores (Fig. 3B), indicating a correlation between discohesion and the Mena^{INV}/TMEM phenotype, as predicted.

Mena^{INV} isoform expression is associated with TEM-competent breast carcinoma cells

On the basis of the above results and previous work indicating that Mena^{INV} potentiates breast cancer cell intravasation, dissemination, and lung metastases in vivo (*4*), we hypothesized in primary tumor cells from patients that Mena^{INV} expression is linked to TEM. Because human breast cancers with a high Mena^{INV}/high TMEM score have less E-cadherin abundance and are less cohesive, we anticipated that a population of discohesive, breast carcinoma cells with high Mena^{INV} scores could be obtained from patients by FNA biopsy to test this hypothesis. In addition, our previous study showed that the Mena isoform expression pattern in FNA samples reflects the cohesion or discohesion state of the cells in the tumor. In particular, smearing patterns of cells obtained by FNA from PyMT mice bearing late-stage tumors are significantly more discohesive (less aggregated) and expressed significantly more Mena^{INV} than those from cells from early-stage tumors (*14*). Therefore, we collected cancer cells by FNA from 32 patients with IDC of the breast of various clinical subtypes (*14*) and evaluated them in an in vitro subluminal-to-luminal TEM [intravasation-directed TEM (iTEM)] assay. The luminal side of the endothelium is defined as the cell surface facing the bottom well of the iTEM

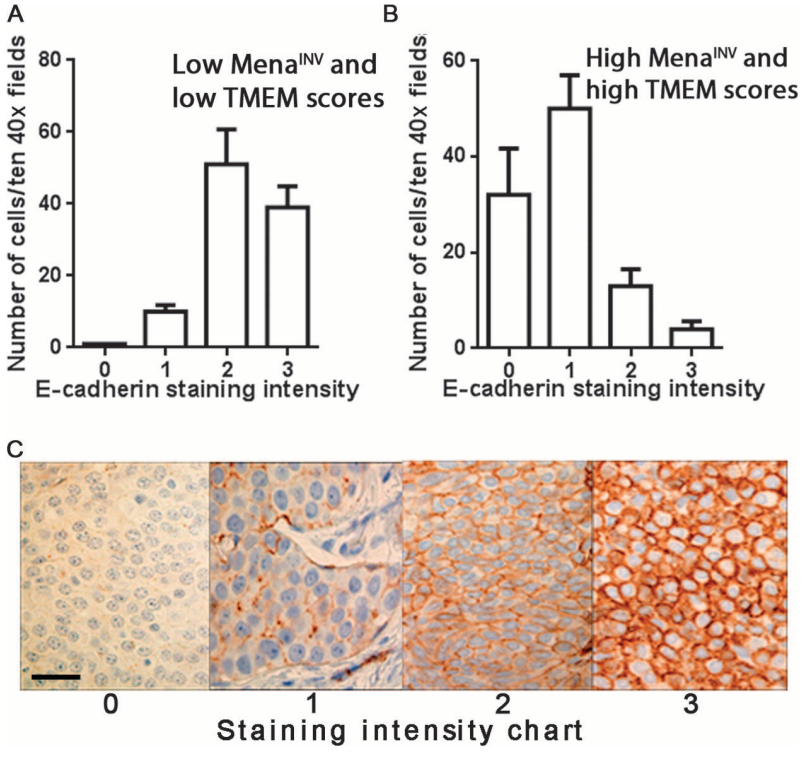

Fig. 3. Correlation of E-cadherin and TMEM and Mena^{INV} scores. (A and B) E-cadherin abundance in tumor tissues classified as either (A) low TMEM and low Mena^{INV} (scores <10 and <1, respectively) or high TMEM and high Mena^{INV} (scores >50 and >5, respectively). (C) Representative images showing staining scores of 0 (none) to 3 (strong). Data are means ± SEM from ten 40× fields scored from 10 cases in each group. $P <$ 0.001, number of cells in the low TMEM-Mena^{INV} group that had moderate to strong E-cadherin staining (2 and 3) compared with that in the high TMEM-Mena^{INV} group. $P < 0.0001$, number of cells in the high TMEM-Mena^{INV} group that had none to weak E-cadherin staining (0 and 1) compared with that in the low TMEM-Mena^{INV} group. Data were analyzed with unpaired, two-tailed Student's *t* tests assuming equal variances and an α level of 0.05.

chamber containing complete medium and colony-stimulating factor-1 (CSF-1) (fig. S1A). Clinical and pathological parameters from the 32 cases used in the iTEM assay are summarized in tables S4 and S5.

Sixteen cases were examined in assays using immortalized human microvascular endothelial cell line (HMEC-1) cells to form the endothelium (fig. S3A), and 16 cases were examined using an endothelium derived from primary human umbilical vein endothelial cells (HUVECs) (Fig. 4, A to D). Similar results were obtained with these two endothelial cell populations. Before performing the iTEM assay, FNA samples were analyzed for the presence of cancer cells and macrophages by IHC for keratin and CD68 abundance, respectively (fig. S3B). In each sample, about 97% of the cells were keratin-positive cancer cells. According to intravital imaging studies, only about 2.5% of breast cancer cells are migratory (*15*), and of these, only about 40% have an embryonic expression pattern, including high Mena^{INV} expression (*27*). Thus, we expected only about 1% of cells from the total aspirate to be iTEM-competent. The addition of macrophages significantly increased iTEM activity of tumor cells (Fig. 4A); therefore, unless otherwise noted, experiments were performed in the presence of

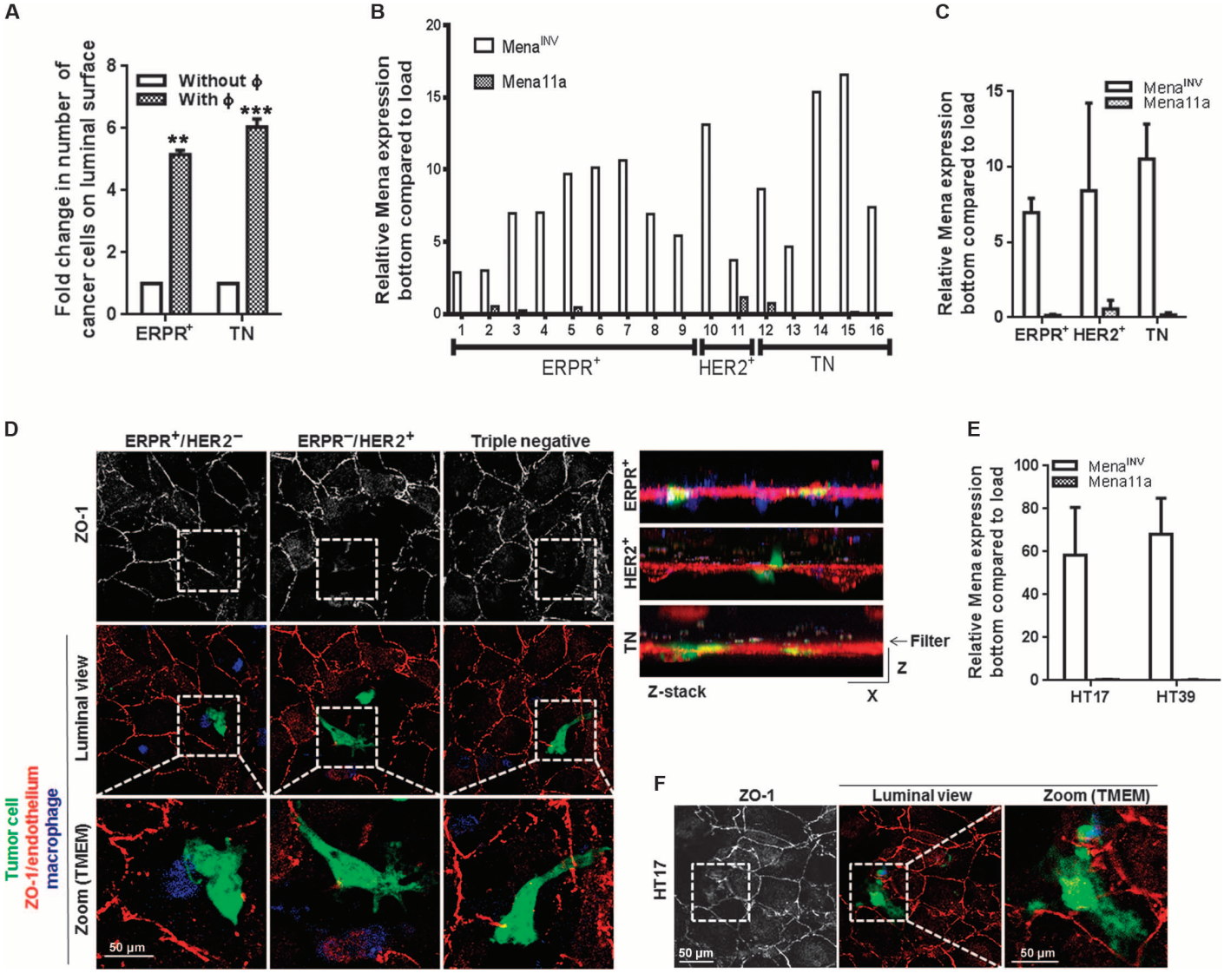

Fig. 4. iTEM assays using human patient IDC cells obtained from FNA biopsies. (**A**) Fold increase in the number of cells from ERPR$^+$ or TN cases that crossed a HUVEC monolayer in the presence of macrophages (**Φ**) relative to the number that crossed in the absence of macrophages. Data are means ± SEM from three experiments. $^{**}P < 0.005$, $^{***}P < 0.0005$, by two-tailed Student's *t* tests assuming equal variances. (**B**) Mena^{INV} or Mena11a transcript expression in cells that crossed the HUVEC monolayer relative to that in the loaded cell population. Data are from 16 patient cases. (**C**) Average Mena^{INV} and Mena11a isoform expression in iTEM-competent cells from (B) grouped by clinical subtype. Data were not significantly different by a Student's *t* test. (**D**) Apical z-sections from the iTEM assay. Tumor cells, green; macrophages, blue; HUVEC junctions (ZO-1), red. Squares indicate dissociating HUVEC junctions, magnified below. Right: Representative z-stacks by clinical subtype. Data are representative of each from the 16 cases in (B). (**E**) Mena^{INV} and Mena11a transcript expression in iTEM-competent cells from TN human tissue transplants HT17 and HT39. Data are means ± SEM from three mice each. (**F**) Apical z-sections of the iTEM assay with HT17 tumor cells as in (D). Images are representative of three experiments.

macrophages. This macrophage requirement for iTEM in vitro closely resembles cancer cell intravasation in vivo as observed by intravital imaging of mouse mammary tumors (*5*). In 5 of 32 cases, no cells crossed the endothelial barrier (fig. S3A). In the remaining 27 cases that showed iTEM activity, cells that crossed the endothelial layer exhibited a 3- to 15-fold greater Mena^{INV} abundance than that in the original population of cells loaded (fig. S3A and Fig. 4B). In cells that crossed the endothelium, there was no significant difference in relative Mena^{INV} expression between clinical subtypes (Fig. 4C).

The ability of cancer cells to cross the HUVEC endothelium was studied at single-cell resolution by imaging. We observed that cancer cells from all subtypes dissociated endothelial cell-cell junctions at the sites of transmigration and that they transmigrated in close proximity to macrophages (Fig. 4D). These data indicate that macrophage-mediated iTEM activity is present in all three clinical subtypes.

Similar results were obtained using FNA-collected cancer cells from xenografts derived from two human TN breast cancer tumor tissues (Fig. 4, E and F). The tumor grafts were described previously (*9*). The iTEM-competent cells from both human xenografts expressed 60- to 70-fold more Mena^{INV} abundance than did the original cell population (Fig. 4E). These data indicate that Mena^{INV} is associated with iTEM in human IDC tissue transplants in mice and primary human breast IDCs irrespective of clinical subtype.

Mena^{INV} promotes iTEM of tumor cells

To assess whether the expression of Mena^{INV} has a causal or promotional role in iTEM, or is instead an acquired trait in tumor cells after iTEM, Mena^{INV} was selectively knocked down in the TN human breast cancer cell line MDA-MB-231. The expression of the transcripts encoding Mena11a, Mena^{INV}, or total Mena (cumulative detection of all isoforms) was quantified using qPCR after transfection with control or one of three Mena^{INV}-targeted siRNAs (small interfering RNAs) (Fig. 5A). We observed a significant decrease in iTEM activity in cells depleted of Mena^{INV} compared to control cells (Fig. 5B). In addition, the overexpression of green fluorescent protein (GFP)–tagged Mena^{INV} in MDA-MB-231 cells caused a significant increase in macrophage-induced iTEM compared to cells expressing GFP alone, and this increased iTEM of GFP-Mena^{INV}–overexpressing cells was suppressed to baseline by Mena^{INV} knockdown (Fig. 5C). Together, these data indicate that Mena^{INV} is required for tumor cell iTEM.

iTEM-competent cells from TN and HER2$^+$ IDCs have increased abundance of the CSF-1 receptor

Increased CSF-1R (CSF-1 receptor) abundance in human TN mammary tumor cell lines results in a decreased reliance on macrophages for invasion and migration due to autocrine signaling (*28*, *29*). The transmigration of cancer cells from ERPR$^+$/HER2$^-$ cases was associated with a higher number of macrophages located in close proximity to tumor cells compared with those in TN and HER2$^+$ cases (Fig. 6A). Because clinical subtypes exhibit differences in the extent of tumor-associated macrophages during transmigration, and because CSF-1 is present in the bottom well of the iTEM assay, we investigated whether CSF-1R abundance in tumor cells differed among iTEM-competent cells from ERPR$^+$/HER2$^-$, TN, and ERPR$^-$/HER2$^+$ cancers. An examination of CSF-1R expression in iTEM-competent cells from these clinical subtypes as well as from TN tissue transplants revealed little or no enrichment of CSF-1R expression in iTEM-competent cells from ERPR$^+$/HER2$^-$ tumors; however, iTEM-competent cells from TN and ERPR$^-$/HER2$^+$ tumors had substantially more CSF-1R expression compared to the total FNA load (Fig. 6, B and C). These results suggest that CSF-1R–dependent autocrine signaling in TN and ERPR$^-$/HER2$^+$, but not in ERPR$^+$/HER2$^-$, accounts for the decreased numbers of macrophages associated with TN and ERPR$^-$/HER2$^+$ tumor cells during iTEM.

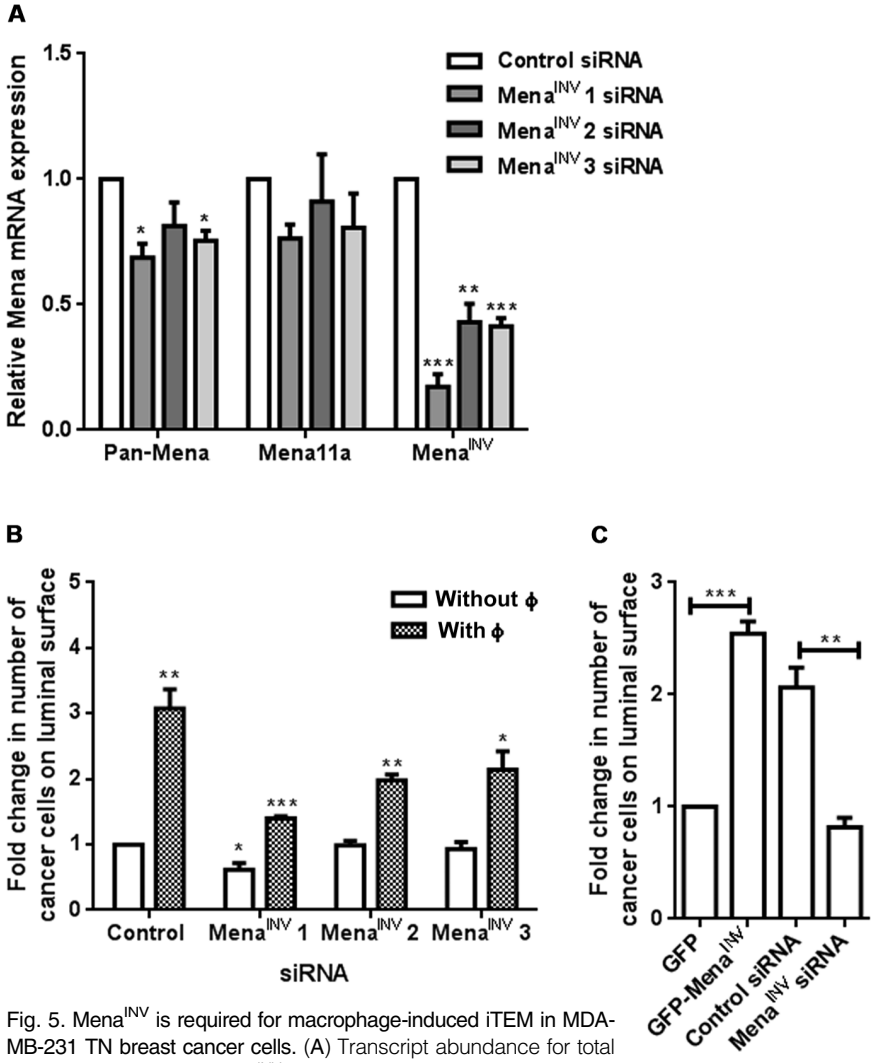

Fig. 5. Mena^{INV} is required for macrophage-induced iTEM in MDA-MB-231 TN breast cancer cells. (A) Transcript abundance for total Mena, Mena11a, and Mena^{INV} in parental MDA-MB-231 cells transfected with one of three Mena^{INV}-targeted siRNAs. (B) iTEM of MDA-MB-231 cells after Mena^{INV} depletion in the presence or absence of macrophages (Φ). (C) iTEM of MDA-MB-231 cells expressing GFP-tagged Mena^{INV}, alone or cotransfected with Mena^{INV}-targeted siRNA (1). iTEM was performed in the presence of macrophages. Data in (A) to (C) are means ± SEM from three experiments. *P < 0.05, **P < 0.005, ***P < 0.0005, by two-tailed Student's t tests assuming equal variances.

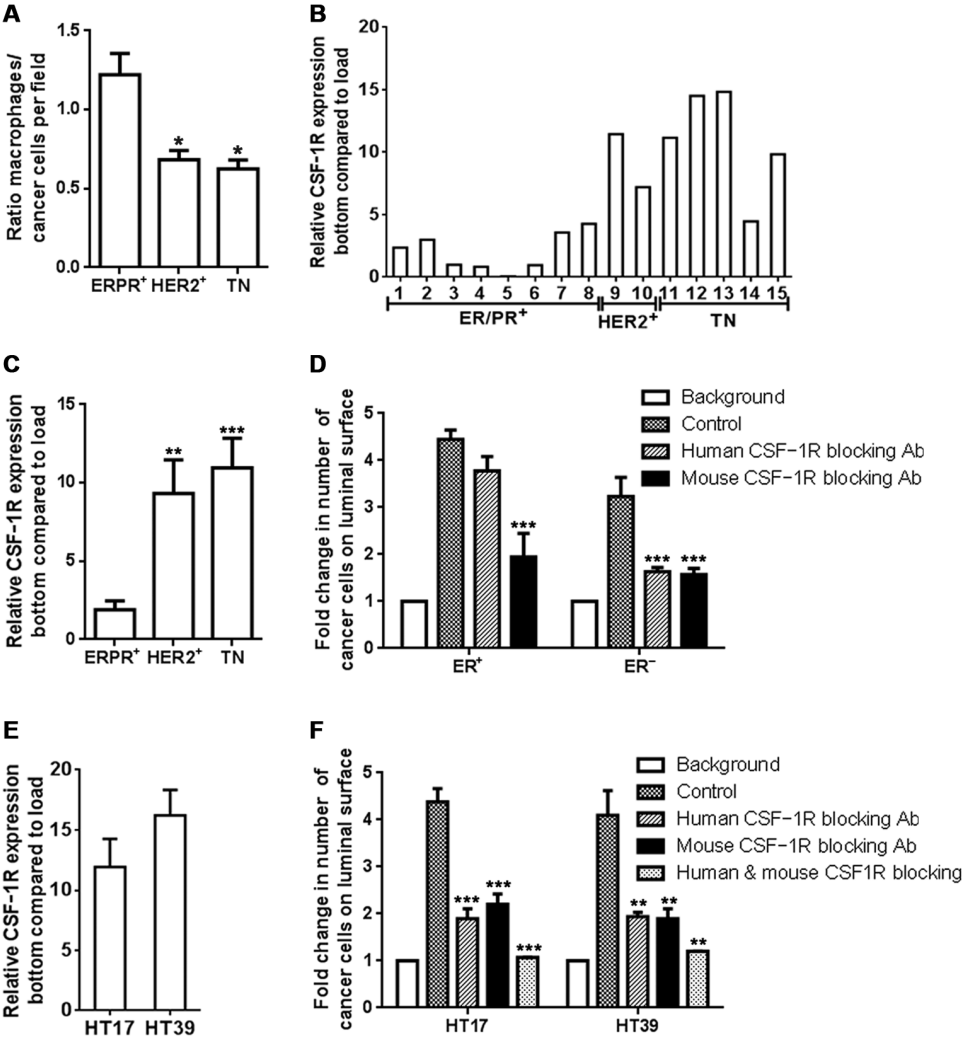

Fig. 6. *CSF1R* expression in iTEM-competent cells differs among breast cancer subtypes. (**A**) The number of macrophages associating with tumor cells during iTEM, presented as a ratio by clinical subtype. Data are means ± SEM from twelve 63× microscopic fields in two to three cases each. **P* < 0.05 compared with that in ERPR$^+$/HER2$^-$ cases. (**B** and **C**) *CSF1R* transcript abundance in iTEM-competent cells from each of 15 cases analyzed across clinical subtypes (B). Data in (C) are means ± SEM by clinical subtype shown in (B). (**D**) Effect of mouse-specific CSF-1R antibodies or human-specific CSF-1R antibodies on iTEM of ERPR$^+$/HER2$^-$, ERPR$^-$/HER2$^+$ (HER2$^+$), and TN cancers. Data are means ± SEM from three cases per subtype relative to the background (tumor cells cross without the presence of macrophages). Control, tumor cells cross in the presence of macrophages. (**E** and **F**) *CSF1R* transcript abundance in iTEM-competent cells from patient tumor transplants HT17 and HT39 (E), and the effect of mouse- or human-specific CSF-1R functionally blocking antibodies on iTEM capacity. Data are means ± SEM from five mice per tumor sample. ***P* < 0.005, ****P* < 0.0005. Statistical analyses in (A), (C), (D), and (F) used two-tailed Student's *t* tests assuming equal variances.

To investigate which signaling loops operate in IDC cells obtained from patients, we used an antibody specific for human CSF-1R (MAB3291) to block autocrine signaling specifically associated with the human CSF-1R present on human cancer cells, and an antibody specific for mouse CSF-1R (AFS98) to block paracrine signaling specifically associated with the mouse CSF-1R present on BAC1.2 mouse macrophages. Only inhibition of the mouse CSF-1R significantly reduced iTEM of ERPR$^+$/HER2$^-$ cells, indicating that only the paracrine signaling mediates the transmigration activity of this breast cancer subtype. However, blockade of both the mouse and human CSF-1Rs significantly inhibited iTEM in TN and ERPR$^-$/HER2$^+$ cancer cells (Fig. 6D). Similar results were obtained by blocking the mouse or human CSF-1R in the TN human tissue transplants HT17 and HT39 (Fig. 6, E and F). In addition, blocking both mouse and human CSF-1R brought iTEM to baseline levels (Fig. 6F). These data indicated that TN and ERPR$^-$/HER2$^+$ cells use both paracrine and autocrine signaling for transmigration activity.

Primary human macrophages enhance the iTEM activity of primary human breast cancer cells

Previous work demonstrated that several macrophage cell lines such as murine BAC1.2F5, immortalized bone marrow–derived macrophage cell line (iBMM), and RQW264.7 support iTEM in vitro (*30*). We wanted to assess whether primary human macrophages affected the iTEM of cancer cells in a similar fashion as do macrophage cell lines. Indeed, primary human macrophages substantially increased the iTEM activity of cells from human primary TN breast cancer xenografts HT17 and HT39 (Fig. 7A). Additionally, iTEM-competent cells showed greater Mena^{INV} expression (Fig. 7B) and greater CSF-1R expression (Fig. 7C) than the load. Furthermore, imaging at the single-cell resolution revealed transmigration of cancer cells in close proximity to macrophages as well as the dissociation of endothelial cell-cell junctions at the sites of transmigration (Fig. 7D). Thus, primary human macrophages affect iTEM of TN primary human breast cancer cells in the same manner as do macrophage cell lines.

DISCUSSION

Here, we tested the hypothesis that relative Mena^{INV} isoform expression is linked to TMEM number and the iTEM of tumor cells in human breast cancer by measuring the iTEM activity of primary tumor cells from patients. To our knowledge, this is the first study to use primary tumor cells obtained from patient breast cancers by FNA for functional iTEM assays in vitro.

We found that the abundance of Mena^{INV}, but not Mena11a, correlated positively with the number of TMEM intravasation sites in a cohort of 100 breast IDCs. Although human breast cancer is a heterogeneous disease consisting of several distinct subtypes with substantially different responses to therapy and clinical outcomes, we did not find statistically significant

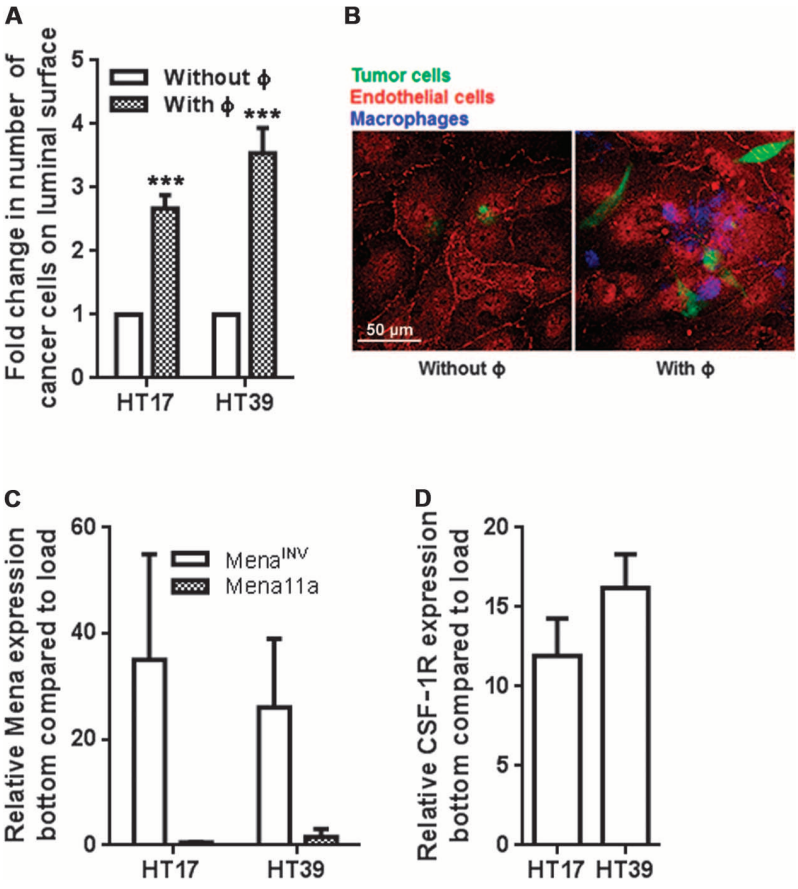

Fig. 7. Primary human macrophages increase iTEM of primary human breast cancer cells. (A) Number of iTEM-competent cells from TN human tissue transplants HT17 and HT39 in the presence or absence of primary human macrophages (Φ). (B) Representative apical z-sections of the iTEM assay demonstrating HT39 cells (green) and crossing the endothelial monolayer (red) in close proximity with macrophages (blue). (C and D) Relative Mena^{INV} and Mena11a (C) or CSF-1R (D) transcript abundance in iTEM-competent HT17 and HT39 cells in the presence of primary human macrophages. Data are means ± SEM from three mice for each tumor. ***$P < 0.0005$, two-tailed Student's *t* tests assuming equal variances.

differences in the correlation between relative Mena^{INV} abundance and TMEM counts among the three clinically distinct subtypes: ERPR^{+}/HER2^{-}, TN, and HER2^{+}. This suggests that a Mena^{INV}-TMEM–mediated mechanism of intravasation is present in all three disease subtypes; however, these conclusions need to be confirmed on a larger breast cancer cohort (*31*).

In accordance with previous work, we found that, due to their growth pattern, low-grade tumors have significantly lower TMEM score than poorly differentiated tumors (*14*, *22*). Unlike previous studies, most likely because of our larger cohort size, we found significantly higher relative Mena^{INV} abundance in poorly differentiated cases compared to well-differentiated cases. We did not find any correlations between relative Mena isoform expression or TMEM score and LN status, tumor size, ER, PR, or HER2 status, which is also in accordance with previous studies (*22*, *23*).

High abundance of Mena^{INV} and high TMEM counts were both correlated with reduced E-cadherin staining in human tumors. A recent study using a human mammary epithelial cell line that had been modified to mesenchymal phenotype by forced expression of the EMT transcription factor Twist (HMLE/pBP-Twist) supports a role for Mena11a in conferring epithelial, cohesive, noninvasive cell behavior (*32*). In particular, expression of splicing factor ESRP1 (epithelial-specific RNA binding protein 1) in HMLE/pBP-Twist cells induced Mena11a expression and promoted epithelial-like reorganization of peripheral actin, cell-cell junctions, and suppressed mesenchymal-like migration (*32*). Because overexpression of Mena^{INV} in rodent mammary tumors decreases cell cohesion, E-cadherin, and β-catenin expression (*14*), we anticipated that human breast cancer cases with high Mena^{INV}-TMEM scores would have less E-cadherin abundance than those with low Mena^{INV}-TMEM scores. Moreover, we documented previously that alternative splicing, a process that regulates Mena isoform expression, can induce EMT-like phenotypic changes, such as actin cytoskeleton remodeling, cell-cell junction formation, and cell migration (*32*). Similarly to the Mena^{INV} and TMEM scores, E-cadherin abundance did not correlate with clinically used prognostic parameters such as tumor size, grade, LN status, and hormonal or *HER2* expression (*33*). However, some studies indicate that reduced E-cadherin abundance in IDCs is associated with high histologic grade, loss of *ER* expression, and shorter disease-free survival (*34*). This suggests that high Mena^{INV} expression score, low E-cadherin abundance, and high TMEM score—associated with worse clinical outcome—reflect aspects of tumor biology that are not captured in currently used clinical and pathological parameters.

Using an iTEM assay with human primary tumor cells obtained by FNA, we demonstrated that the iTEM-competent subset of human IDC cells of all clinical subtypes has increased expression of Mena^{INV} but not Mena11a (Fig. 8). This result is also consistent with a recent study showing that loss of Mena11a relative to total Mena abundance in breast tumor tissue was a prognostic marker for poor outcome in two large breast cancer cohorts (*35*). These data indicate that the Mena^{INV} isoform is associated with iTEM in primary human IDCs of the breast irrespective of clinical subtype. Our data are in accordance with the results obtained with MTLn3 cells overexpressing various Mena isoforms (*6*). In that study, only MTLn3 cells overexpressing Mena^{INV} in the presence of macrophages showed significant iTEM (*6*). Here, using three different Mena^{INV}-targeted siRNAs or the overexpression of GFP-Mena^{INV}, we demonstrated that Mena^{INV} promotes iTEM in TN human breast cancer cell line MDA-MB-231. Thus, Mena^{INV} not only is associated with iTEM but also functionally promotes iTEM activity in tumor cells.

It is now well recognized that tumor-associated macrophages contribute to tumor progression and metastasis, as well as to the response to anticancer therapies (*30*, *36*, *37*). Macrophages facilitate cancer cell intravasation in at least two ways. First, they comigrate with cancer cells using a chemotactic paracrine signaling loop consisting of macrophage-secreted EGF [which activates EGFR (EGF receptor) on cancer cells] and cancer cell–secreted CSF-1 (which activates CSF-1R on macrophage). This paracrine loop results in migratory cell streams, which efficiently move toward perivascular macrophages (*8*, *10*, *38*). Second, the direct physical contact between perivascular macrophages and cancer cells induces RhoA activity and enhances the formation of invadopodia, actin-rich matrix-degrading protrusions that are required for iTEM (*7*, *8*, *39*). Both streaming and iTEM are macrophage-dependent tumor cell behaviors that are amplified by Mena^{INV} expression (*6*, *16*). The claudin-low subtype of

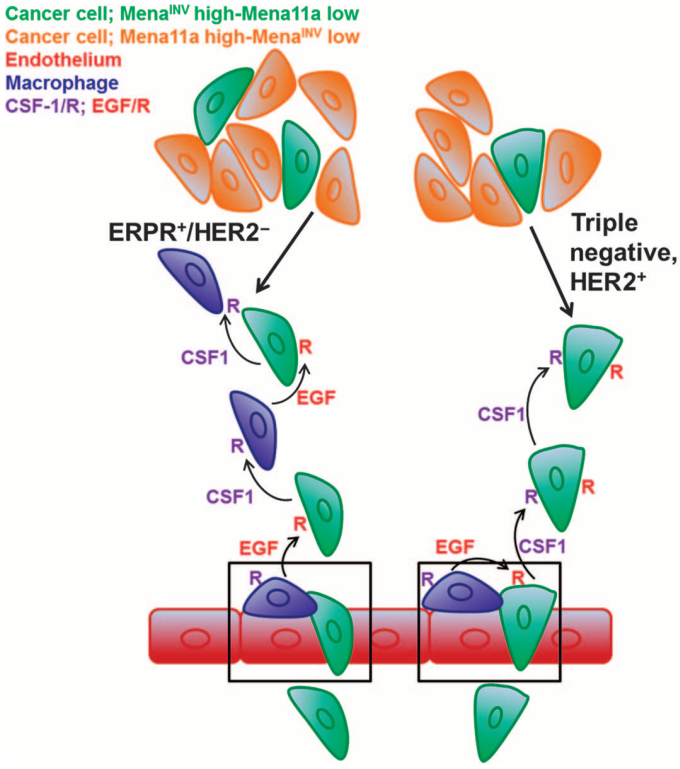

Fig. 8. Model of Mena^{INV}- and macrophage-mediated tumor cell invasion and TEM. ITEM-competent human breast cancer cells from all clinically relevant subtypes display Mena^{INV} high/Mena11a low isoform expression and perivascular macrophages promote endothelial transmigration at TMEM sites (outlined). iTEM in ERPR$^+$/HER2$^-$ cells is promoted by paracrine CSF-1–CSF-1R signaling, whereas iTEM in HER2$^+$ and TN cells is promoted by both paracrine and autocrine CSF-1–CSF-1R signaling. R, receptor.

TN human breast cancer cells also communicates through an autocrine CSF-1–CSF-1R loop (*28*, *29*). Human breast cancer cells express CSF-1R under the control of TGFβ (transforming growth factor–β) signaling, demonstrating a role of the tumor microenvironment in the induction of CSF-1R expression in human cancer cells (*28*, *29*). TGFβ also induces CSF-1R expression in cultured cells, and the presence of estradiol in ER$^+$ cells suppresses the expression of TGFβ-induced genes, possibly through ER-meditated degradation of the TGFβ effectors, SMADs (*40*). We demonstrated here that iTEM-competent TN and HER2$^+$ cells express more CSF-1R than iTEM-competent ER$^+$/HER2 cells. We also demonstrated that breast cancer cells from ER$^+$/HER2$^-$ disease primarily use a paracrine loop, whereas cancer cells from TN and HER2$^+$ disease use a tumor cell autocrine loop involving CSF-1 in addition to the paracrine loop for iTEM (Fig. 8). This may be advantageous for their ability to invade and intravasate. Thus, the higher likelihood of developing distant recurrence and worse clinical outcome in TN and HER2$^+$ disease (*41*) may be in part due to autocrine signaling involving CSF-1R expression on cancer cells. Indeed, human breast cancers that coexpress CSF-1 and its receptor have worse outcome, and high expression of CSF-1 promotes metastatic progression in mouse cancer models (*42*, *43*). Studies to thoroughly understand how CSF-1R, macrophages, and Mena^{INV} facilitate iTEM of human IDC cells are under way.

Overall, in addition to the potential for future clinical applications in prognosis and treatment of cancer, this study illustrates the value of using primary tumor cells from patients with different clinical subtypes to investigate the underlying biology behind tumor cell dissemination.

MATERIALS AND METHODS

Human tissue selection and FNA biopsy procedure

Lumpectomy and mastectomy specimens received at the Albert Einstein College of Medicine/Montefiore Medical Center, Moses and Weiler Divisions for pathological examination were used for FNA-based tissue collection under institutional review board approval. Four to five FNA aspiration biopsies per tumor were performed on grossly visible lesions using 25-gauge needles. The adequacy of the sample was assessed by the standard Diff-Quick protocol (*44*). Only samples composed of at least 90% malignant epithelial cells, as determined by standard pathologic characteristics (*44*), were used in the study. ER, PR, and HER2 receptor staining and scoring were done in accordance with United States and Canadian Academy of Pathology/American Society of Clinical Oncology (USCAP/ASCO) guidelines (*45*, *46*).

Intravasation TEM (iTEM)

The iTEM assay was performed as described previously (*6*) and briefly described here with modifications. The Transwell was prepared so that tumor cell TEM was in the intravasation direction [from subluminal side to luminal side of the endothelium (fig. S1A)]. We define this as the iTEM assay. To prepare the endothelial monolayer, the underside of each Transwell was coated with 50 μl of Matrigel (2.5 μg/ml; Invitrogen). About 100,000 HUVEC cells were plated on the Matrigel-coated underside of the Transwells. For HMEC-1 experiments, 200,000 human microvascular endothelial cells (HMEC-1) were plated. Transwells were then flipped onto a 24-well plate containing 200 μl of α-MEM (minimum essential medium) supplemented with 10% fetal bovine serum (FBS) + 3000 U of CSF-1 and incubated until the endothelium formed impermeable monolayers. Permeability of both monolayers was tested as described previously by diffusion of 70 kD of Texas Red dextran (fig. S1, C and D) (Molecular Devices SpectraMax M5 plate reader) and by electrical resistance (World Precision Instruments) (fig. S1, E and F) (*39*), which demonstrated that the monolayer was impermeable at 48 hours after plating of the HUVECs and HMECs; therefore, Transwells were used at this time point. HUVEC cells generated less permeable monolayers than HMECs; therefore, after the initial experiments, HUVECs were used exclusively. Once impermeable by these criteria, the Transwell assay was used for iTEM studies. All the assays were run in the presence of BAC1.2F5 murine macrophage cell line because it was demonstrated using cancer cell lines that iTEM of tumor cells is efficient only in the presence of macrophages (Fig. 4A) (*6*). Although it was shown previously that several other types of macrophages including immortalized bone marrow–derived macrophage cell line (iBMM) and the RQW264.7 support iTEM in vitro (*39*), we chose to do most of the work with BAC1.2F5 cell line, because it generated the most consistent and robust iTEM (*39*).

We confirmed major findings using primary human macrophages. Peripheral blood mononuclear cells (PBMCs) from anonymous donors were isolated from the Leuko Pak obtained from blood bank. To purify PBMCs, we used density gradient centrifugation, followed by clearance of the remaining red blood cells using hypotonic lysis. The PBMCs were then differentiated into macrophages by adherence in the presence of recombinant human CSF-1 and used a week after isolation.

Macrophages and FNA-obtained tumor cells were labeled with cell tracker dyes. Then, 15,000 macrophages and 37,500 tumor cells were

added to the upper chamber in 200 µl of Dulbecco's modified Eagle's medium (DMEM)/F12 supplemented with 0.5% FBS. After 18 hours of transmigration, the medium was removed from the top of the Transwell, and the migrated cells were scraped from the bottom of the plate and immediately subjected to qRT-PCR analysis.

For ZO-1 immunostaining, the Transwells were fixed in 4% paraformaldehyde, permeabilized with 1% Triton X-100, and stained with an anti–ZO-1 (Invitrogen). Transwells were imaged using a Leica SP5 confocal microscope using a 60× 1.4 numerical aperture objective and processed using ImageJ [National Institutes of Health (NIH)] and IMARIS programs. Quantitation was performed by counting the number of macrophages and tumor cells that had crossed the endothelium within the same field of view (60×, 10 random fields) and represented it as a ratio.

Human tissue transplants

The TN human tissue transplants HT17 and HT39 were previously described (*9*). Briefly, the tumor originated from human patient samples and have since only been propagated in SCID (severe combined immunodeficient) mice. Tumors were harvested once they reached 1- to 1.2-cm diameter. Cells were obtained by FNA from human tumors grown in mice, and experiments were carried out in the same manner as was done with direct patient samples. All procedures were conducted in accordance with the NIH regulations and approved by the Albert Einstein College of Medicine animal use committee.

CSF-1R blocking experiments

Inhibition of the mouse or human CSF-1R was done using the following species-specific blocking antibodies: monoclonal rat anti-mouse CSF-1R (AFS98) or monoclonal mouse anti-human CSF-1R (MAB3291; R&D Systems) (*47*) at final concentrations of 50 µg/ml. Transwells were prepared as described above, and blocking antibody or control immunoglobulin G (IgG) was added to the top well containing tumor cells and macrophages.

Quantitative real-time polymerase chain reaction

qRT-PCR for Mena splice variants was performed as described previously (*15*). Briefly, the data analysis was conducted using the $\Delta\Delta C_t$ method, in which all *MENA* C_t values in the carcinoma samples were first normalized to *GAPDH*. A subsequently generated Mena score indicated the relative amount of Mena isoforms in the IDCs compared to the average fold change of Mena isoforms detected in five fibroadenomas, using the $\Delta\Delta C_t$ values for each sample. The data are referred to as either the Mena score or the relative Mena expression. qRT-PCR for Mena splice variants in the iTEM assay was also conducted using the $\Delta\Delta C_t$ method, in which all *MENA* C_t values in TEM-competent cells were first normalized to *GAPDH*. Subsequently, relative isoform levels were estimated by comparing the normalized C_t values of Mena isoforms in the cells that crossed the endothelium to the *GAPDH*-normalized C_t values of Mena isoforms present in the starting sample. qRT-PCR analyses were performed with a SYBR Green kit (Qiagen) and analyzed with ABI 7300 sequence detector and associated software (Applied Biosystems). Primers detecting transcripts encoding $Mena^{INV}$ and Mena11a are described in table S1.

Tissue selection for TMEM staining and scoring

At the time of routine microscopic examination of the lesions on which FNA biopsies had been performed, an appropriate area containing invasive cancer suitable for TMEM analysis was identified by low-power scanning using the following criteria: high density of tumor, adequacy of tumor, lack of necrosis or inflammation, and lack of artifacts such as retraction or folds. TMEM stain is a triple immunostain for predicting metastatic risk in which three antibodies are applied sequentially and developed separately with different chromogens on a Bond Max autostainer (Leica Biosystems). The pan-Mena mouse monoclonal antibody (A351F7D9) was produced in the Gertler laboratory and is not commercially available. The assessment of TMEM scores was performed with Adobe Photoshop on 10 contiguous 400× digital images of the most representative areas of the tumor. The total TMEM for each image was tabulated, and the scores from all 10 images were summed to give a final TMEM density for each patient sample, expressed as the number of TMEM per total magnification (ten 400× fields) (*22*). Twenty-five randomly chosen cases were each independently scored by two pathologists. Because the correlation between the scores was excellent, with a correlation coefficient $r = 0.97$, the remaining 75 cases were scored by one pathologist.

Relationship of FNA sample to TMEM

FNA primarily collects loose tumor cells, with very few macrophages and no endothelial cells, and incurs minimal tissue damage (*48*). After the FNA procedure, the entire tumor was fixed in formalin and embedded in paraffin and sent for pathological examination. A representative block of FFPE tumor tissue was selected and triple immunostained for TMEMs. Therefore, each tumor was sampled by FNA for Mena isoform expression analysis and by FFPE for TMEM scoring (*14*).

IHC and scoring of E-cadherin

IHC for E-cadherin was done using commercially available monoclonal antibody against E-cadherin (Dako; 1:25 dilution). Antigen retrieval was performed in a steamer at 90°C for 30 min in Target Retrieval Solution (pH 6.0). The slides were incubated with the primary antibody for 30 min at room temperature and for 30 min with a secondary antibody. E-cadherin was visualized using horseradish peroxidase (HRP)–conjugated mouse-specific antibody (EnVision System, Dako) and DAB (diaminobenzidine) on an automated immunostainer (Autostainer, Dako) according to the manufacturer's instructions. The slides were counterstained with hematoxylin using standard techniques.

Similarly to TMEM scoring, 10 digital images were acquired at 400× total magnification for each tumor and scored by two pathologists as follows: 3, strong complete membranous staining; 2, moderate complete membranous staining; 1, weak incomplete membranous staining; 0, no staining. The cells within each scoring category were labeled with different Photoshop tools. Data were summed from all 10 images to give a final mean number (and percentage, with error) of cells per tumor with each score. Ten cases of low $Mena^{INV}$–low TMEM score ($Mena^{INV} < 1$, and TMEM < 10) and 10 cases of high $Mena^{INV}$–high TMEM score ($Mena^{INV} > 5$, and TMEM > 50) were analyzed for E-cadherin staining intensity. The cutoff levels for high and low scores were established on the basis of the scores above the top 85th and below the low 25th percentile

IHC and scoring of keratin and CD68-positive cells

Keratin staining was done on FNA samples prepared as cytospins. The staining was performed in an automatic slide stainer (Dako Autostainer Plus). The primary mouse monoclonal antibody AE13 (catalog no. M3515, Dako; 1:200) and mouse monoclonal antibody CD68 (catalog no. M0814, Dako; 1:2000) were applied for 30 min at room temperature, followed by 30 min in HRP-conjugated anti-mouse secondary antibody (DakoCytomation EnVision+ System, catalog no. K400111). Slides were incubated with DAB Substrate kit (Dako) for 5 min, counterstained with Surgipath Hematoxylin (Fisher HealthCare), dehydrated through graded alcohols, cleared in xylene, and cover-slipped with CytoSeal 60 (Richard-Allen Scientific). The whole cytospin area (314 mm^2) was scored for AE1:AE3 and CD68-positive cells; data are presented as a percentage of positive cells.

Small interfering RNA

Isoform-specific knockdown of Mena^{INV} in MDA-MB-231 cells was achieved using siRNA. Transfections were performed by resuspending 8×10^5 cells in a 100 μl of Lonza kit V transfection solution with 2 μM siRNA for 96 hours. Mena^{INV} siRNA was purchased from Ambion (Custom Select siRNA). Knockdown efficiency was measured by qPCR.

Statistical analysis

The strength of the association between *MENA* isoform expression and TMEM density was calculated using rank-order correlation and represented by Spearman's correlation coefficient. Wilcoxon-Mann-Whitney rank sum test was used to assess the differences between TMEM density and relative *MENA* expression in terms of their association with tumor grade, LN status, tumor size, ER, PR, and HER2/Neu status. A regression model fit was used to rank-transformed data and assess the differences in slopes among tumor types. Given that six comparisons were done for human samples, the P value for determining statistical significance was set at 0.008 by applying the Bonferroni correction to the standard assumption that $P < 0.05$ is statistically significant. Statistical significances in E-cadherin abundance as well as the difference in expression of genes encoding for Mena isoforms and CSF-1R in intravasation-competent cells between clinical subtypes were determined using unpaired, two-tailed Student's t tests assuming equal variances and an α level of 0.05. Differences were considered significant if $P < 0.05$. Actual P values are listed on the graphs or in the legends of each figure.

SUPPLEMENTARY MATERIALS

www.sciencesignaling.org/cgi/content/full/7/353/ra112/DC1

Fig. S1. The experimental setup of the iTEM assay and the permeability of HMEC endothelium.

Fig. S2. TMEM score and relative Mena^{INV} abundance in LN-positive or LN-negative cases.

Fig. S3. iTEM assays engineered with HMEC-1 endothelium performed with human IDC cells obtained by FNA.

Table S1. *MENA* and *GAPDH* primer sequences.

Table S2. Correlation coefficients for TMEM score and relative expression of *MENA* isoforms in IDCs, overall and by clinical subtype.

Table S3. TMEM scores and relative Mena isoform expression for tumors with different clinical and pathological variables.

Table S4. Clinical and pathological data pertaining to iTEM data in fig. S3A.

Table S5. Clinical and pathological data pertaining to iTEM data in Figs. 4 and 6.

REFERENCES AND NOTES

1. C. L. Chaffer, R. A. Weinberg, A perspective on cancer cell metastasis. *Science* **331**, 1559–1564 (2011).
2. A. J. Tevaarwerk, R. J. Gray, B. P. Schneider, M. L. Smith, L. I. Wagner, J. H. Fetting, N. Davidson, L. J. Goldstein, K. D. Miller, J. A. Sparano, Survival in patients with metastatic recurrent breast cancer after adjuvant chemotherapy: Little evidence of improvement over the past 30 years. *Cancer* **119**, 1140–1148 (2013).
3. W. Wang, J. B. Wyckoff, V. C. Frohlich, Y. Oleynikov, S. Huttelmaier, J. Zavadil, L. Cermak, E. P. Bottinger, R. H. Singer, J. G. White, J. E. Segall, J. S. Condeelis, Single cell behavior in metastatic primary mammary tumors correlated with gene expression patterns revealed by molecular profiling. *Cancer Res.* **62**, 6278–6288 (2002).
4. J. Wyckoff, B. Gligorijevic, D. Entenberg, J. Segall, J. Condeelis, High-resolution multiphoton imaging of tumors in vivo. *Cold Spring Harb. Protoc.* **2011**, 1167–1184 (2011).
5. J. B. Wyckoff, Y. Wang, E. Y. Lin, J. F. Li, S. Goswami, E. R. Stanley, J. E. Segall, J. W. Pollard, J. Condeelis, Direct visualization of macrophage-assisted tumor cell intravasation in mammary tumors. *Cancer Res.* **67**, 2649–2656 (2007).
6. D. Entenberg, J. Wyckoff, B. Gligorijevic, E. T. Roussos, V. V. Verkhusha, J. W. Pollard, J. Condeelis, Setup and use of a two-laser multiphoton microscope for multichannel intravital fluorescence imaging. *Nat. Protoc.* **6**, 1500–1520 (2011).
7. J. Wyckoff, W. Wang, E. Y. Lin, Y. Wang, F. Pixley, E. R. Stanley, T. Graf, J. W. Pollard, J. Segall, J. Condeelis, A paracrine loop between tumor cells and macrophages is required for tumor cell migration in mammary tumors. *Cancer Res.* **64**, 7022–7029 (2004).
8. S. Goswami, E. Sahai, J. B. Wyckoff, M. Cammer, D. Cox, F. J. Pixley, E. R. Stanley, J. E. Segall, J. S. Condeelis, Macrophages promote the invasion of breast carcinoma cells via a colony-stimulating factor-1/epidermal growth factor paracrine loop. *Cancer Res.* **65**, 5278–5283 (2005).
9. A. Patsialou, Y. Wang, J. Lin, K. Whitney, S. Goswami, P. A. Kenny, J. S. Condeelis, Selective gene-expression profiling of migratory tumor cells in vivo predicts clinical outcome in breast cancer patients. *Breast Cancer Res.* **14**, R139 (2012).
10. J. Condeelis, R. H. Singer, J. E. Segall, The great escape: When cancer cells hijack the genes for chemotaxis and motility. *Annu. Rev. Cell Dev. Biol.* **21**, 695–718 (2005).
11. F. Gertler, J. Condeelis, Metastasis: Tumor cells becoming MENAcing. *Trends Cell Biol.* **21**, 81–90 (2011).
12. A. Bagorda, V. A. Mihaylov, C. A. Parent, Chemotaxis: Moving forward and holding on to the past. *Throm. Haemost.* **95**, 12–21 (2006).
13. W. Wang, G. Mouneimne, M. Sidani, J. Wyckoff, X. Chen, A. Makris, S. Goswami, A. R. Bresnick, J. S. Condeelis, The activity status of cofilin is directly related to invasion, intravasation, and metastasis of mammary tumors. *J. Cell Biol.* **173**, 395–404 (2006).
14. E. T. Roussos, S. Goswami, M. Balsamo, Y. Wang, R. Stobezki, E. Adler, B. D. Robinson, J. G. Jones, F. B. Gertler, J. S. Condeelis, M. H. Oktay, Mena invasive (Mena^{INV}) and Mena11a isoforms play distinct roles in breast cancer cell cohesion and association with TMEM. *Clin. Exp. Metastasis* **28**, 515–527 (2011).
15. A. Patsialou, J. J. Bravo-Cordero, Y. Wang, D. Entenberg, H. Liu, M. Clarke, J. S. Condeelis, Intravital multiphoton imaging reveals multicelluar streaming as a crucial component of in vivo cell migration in human breast tumors. *Intravital* **2**, e25294 (2013).
16. U. Philippar, E. T. Roussos, M. Oser, H. Yamaguchi, H. D. Kim, S. Giampieri, Y. Wang, S. Goswami, J. B. Wyckoff, D. A. Lauffenburger, E. Sahai, J. S. Condeelis, F. B. Gertler, A Mena invasion isoform potentiates EGF-induced carcinoma cell invasion and metastasis. *Dev. Cell* **15**, 813–828 (2008).
17. S. Goswami, U. Philippar, D. Sun, A. Patsialou, J. Avraham, W. Wang, F. Di Modugno, P. Nistico, F. B. Gertler, J. S. Condeelis, Identification of invasion specific splice variants of the cytoskeletal protein Mena present in mammary tumor cells during invasion in vivo. *Clin. Exp. Metastasis* **26**, 153–159 (2009).
18. G. Mouneimne, V. DesMarais, M. Sidani, E. Scemes, W. Wang, X. Song, R. Eddy, J. Condeelis, Spatial and temporal control of cofilin activity is required for directional sensing during chemotaxis. *Curr. Biol.* **16**, 2193–2205 (2006).
19. F. Di Modugno, M. Mottolese, A. Di Benedetto, A. Conidi, F. Novelli, L. Perracchio, I. Venturo, C. Botti, E. Jager, A. Santoni, P. G. Natali, P. Nisticò, The cytoskeleton regulatory protein hMena (ENAH) is overexpressed in human benign breast lesions with high risk of transformation and human epidermal growth factor receptor-2–positive/hormonal receptor–negative tumors. *Clin. Cancer Res.* **12**, 1470–1478 (2006).
20. M. S. Pino, M. Balsamo, F. Di Modugno, M. Mottolese, M. Alessio, E. Melucci, M. Milella, D. J. McConkey, U. Philippar, F. B. Gertler, P. G. Natali, P. Nisticò, Human Mena^{+11a} isoform serves as a marker of epithelial phenotype and sensitivity to epidermal growth factor receptor inhibition in human pancreatic cancer cell lines. *Clin. Cancer Res.* **14**, 4943–4950 (2008).
21. K. Kühnel, T. Jarchau, E. Wolf, I. Schlichting, U. Walter, A. Wittinghofer, S. V. Strelkov, The VASP tetramerization domain is a right-handed coiled coil based on a 15-residue repeat. *Proc. Natl. Acad. Sci. U.S.A.* **101**, 17027–17032 (2004).
22. B. D. Robinson, G. L. Sica, Y. F. Liu, T. E. Rohan, F. B. Gertler, J. S. Condeelis, J. G. Jones, Tumor microenvironment of metastasis in human breast carcinoma: A potential prognostic marker linked to hematogenous dissemination. *Clin. Cancer Res.* **15**, 2433–2441 (2009).
23. T. E. Rohan, X. Xue, H. M. Lin, T. M. D'Alfonso, P. S. Ginter, M. H. Oktay, B. D. Robinson, M. Ginsberg, F. B. Gertler, A. G. Glass, J. A. Sparano, J. S. Condeelis, J. G. Jones, Tumor microenvironment of metastasis and risk of distant metastasis of breast cancer. *J. Natl. Cancer Inst.* **106**, dju136 (2014).
24. E. T. Roussos, Y. Wang, J. B. Wyckoff, R. S. Sellers, W. Wang, J. Li, J. W. Pollard, F. B. Gertler, J. S. Condeelis, Mena deficiency delays tumor progression and decreases metastasis in polyoma middle-T transgenic mouse mammary tumors. *Breast Cancer Res.* **12**, R101 (2010).
25. E. T. Roussos, J. S. Condeelis, A. Patsialou, Chemotaxis in cancer. *Nat. Rev. Cancer* **11**, 573–587 (2011).
26. C. Brisken, Progesterone signalling in breast cancer: A neglected hormone coming into the limelight. *Nat. Rev. Cancer* **13**, 385–396 (2013).
27. H. Liu, M. R. Patel, J. A. Prescher, A. Patsialou, D. Qian, J. Lin, S. Wen, Y. F. Chang, M. H. Bachmann, Y. Shimono, P. Dalerba, M. Adorno, N. Lobo, J. Bueno, F. M. Dirbas, S. Goswami, G. Somlo, J. Condeelis, C. H. Contag, S. S. Gambhir, M. F. Clarke, Cancer stem cells from human breast tumors are involved in spontaneous metastases in orthotopic mouse models. *Proc. Natl. Acad. Sci. U.S.A.* **107**, 18115–18120 (2010).
28. A. Patsialou, J. Wyckoff, Y. Wang, S. Goswami, E. R. Stanley, J. S. Condeelis, Invasion of human breast cancer cells in vivo requires both paracrine and autocrine loops involving the colony-stimulating factor-1 receptor. *Cancer Res.* **69**, 9498–9506 (2009).
29. A. Patsialou, Y. Wang, J. Pignatelli, X. Chen, D. Entenberg, M. Oktay, J. S. Condeelis, Autocrine CSF1R signaling mediates switching between invasion and proliferation downstream of TGFβ in claudin-low breast tumor cells. *Oncogene* 10.1038/onc.2014.226 (2014).
30. M. De Palma, C. E. Lewis, Macrophage regulation of tumor responses to anticancer therapies. *Cancer Cell* **23**, 277–286 (2013).

31. N. R. Bertos, M. Park, Breast cancer—One term, many entities? *J. Clin. Invest.* **121**, 3789–3796 (2011).
32. I. M. Shapiro, A. W. Cheng, N. C. Flytzanis, M. Balsamo, J. S. Condeelis, M. H. Oktay, C. B. Burge, F. B. Gertler, An EMT-driven alternative splicing program occurs in human breast cancer and modulates cellular phenotype. *PLOS Genet.* **7**, e1002218 (2011).
33. R. Singhai, V. W. Patil, S. R. Jaiswal, S. D. Patil, M. B. Tayade, A. V. Patil, E-cadherin as a diagnostic biomarker in breast cancer. *N. Am. J. Med. Sci.* **3**, 227–233 (2011).
34. S. M. Siitonen, J. T. Kononen, H. J. Helin, I. S. Rantala, K. A. Holli, J. J. Isola, Reduced E-cadherin expression is associated with invasiveness and unfavorable prognosis in breast cancer. *Am. J. Clin. Pathol.* **105**, 394–402 (1996).
35. S. Agarwal, F. B. Gertler, M. Balsamo, J. S. Condeelis, R. L. Camp, X. Xue, J. Lin, T. E. Rohan, D. L. Rimm, Quantitative assessment of invasive mena isoforms (Mena^{calc}) as an independent prognostic marker in breast cancer. *Breast Cancer Res.* **14**, R124 (2012).
36. V. Cortez-Retamozo, C. Engblom, M. J. Pittet, Remote control of macrophage production by cancer. *Oncoimmunology* **2**, e24183 (2013).
37. H. Fang, Y. A. Declerck, Targeting the tumor microenvironment: From understanding pathways to effective clinical trials. *Cancer Res.* **73**, 4965–4977 (2013).
38. A. Dovas, B. Gligorijevic, X. Chen, D. Entenberg, J. Condeelis, D. Cox, Visualization of actin polymerization in invasive structures of macrophages and carcinoma cells using photoconvertible β-actin—Dendra2 fusion proteins. *PLOS One* **6**, e16485 (2011).
39. M. Roh-Johnson, J. J. Bravo-Cordero, A. Patsialou, V. P. Sharma, P. Guo, H. Liu, L. Hodgson, J. Condeelis, Macrophage contact induces RhoA GTPase signaling to trigger tumor cell intravasation. *Oncogene* **33**, 4203–4212 (2014).
40. N. Goto, H. Hiyoshi, I. Ito, M. Tsuchiya, Y. Nakajima, J. Yanagisawa, Estrogen and antiestrogens alter breast cancer invasiveness by modulating the transforming growth factor-β signaling pathway. *Cancer Sci.* **102**, 1501–1508 (2011).
41. E. A. Rakha, S. Chan, Metastatic triple-negative breast cancer. *Clin. Oncol. (R. Coll. Radiol.)* **23**, 587–600 (2011).
42. B. M. Kacinski, CSF-1 and its receptor in ovarian, endometrial and breast cancer. *Ann. Med.* **27**, 79–85 (1995).
43. E. Y. Lin, A. V. Nguyen, R. G. Russell, J. W. Pollard, Colony-stimulating factor 1 promotes progression of mammary tumors to malignancy. *J. Exp. Med.* **193**, 727–740 (2001).
44. P. K. Gupta, Z. W. Baloch, Intraoperative and on-site cytopathology consultation: Utilization, limitations, and value. *Semin. Diagn. Pathol.* **19**, 227–236 (2002).
45. M. E. Hammond, D. F. Hayes, M. Dowsett, D. C. Allred, K. L. Hagerty, S. Badve, P. L. Fitzgibbons, G. Francis, N. S. Goldstein, M. Hayes, D. G. Hicks, S. Lester, R. Love, P. B. Mangu, L. McShane, K. Miller, C. K. Osborne, S. Paik, J. Perlmutter, A. Rhodes, H. Sasano, J. N. Schwartz, F. C. Sweep, S. Taube, E. E. Torlakovic, P. Valenstein, G. Viale, D. Visscher, T. Wheeler, R. B. Williams, J. L. Wittliff, A. C. Wolff; American Society of Clinical Oncology; College of American Pathologists, American Society of Clinical Oncology/College of American Pathologists guideline recommendations for immunohistochemical testing of estrogen and progesterone receptors in breast cancer (unabridged version). *Arch. Pathol. Lab. Med.* **134**, e48–e72 (2010).
46. M. E. Hammond, D. F. Hayes, M. Dowsett, D. C. Allred, K. L. Hagerty, S. Badve, P. L. Fitzgibbons, G. Francis, N. S. Goldstein, M. Hayes, D. G. Hicks, S. Lester, R. Love, P. B. Mangu, L. McShane, K. Miller, C. K. Osborne, S. Paik, J. Perlmutter, A. Rhodes, H. Sasano, J. N. Schwartz, F. C. Sweep, S. Taube, E. E. Torlakovic, P. Valenstein, G. Viale, D. Visscher, T. Wheeler, R. B. Williams, J. L. Wittliff, A. C. Wolff, American Society of Clinical Oncology/College of American Pathologists guideline recommendations for immunohistochemical testing of estrogen and progesterone receptors in breast cancer. *J. Clin. Oncol.* **28**, 2784–2795 (2010).
47. H. Pang, R. Flinn, A. Patsialou, J. Wyckoff, E. T. Roussos, H. Wu, M. Pozzuto, S. Goswami, J. S. Condeelis, A. R. Bresnick, J. E. Segall, J. M. Backer, Differential enhancement of breast cancer cell motility and metastasis by helical and kinase domain mutations of class IA phosphoinositide 3-kinase. *Cancer Res.* **69**, 8868–8876 (2009).
48. W. F. Symmans, M. Ayers, E. A. Clark, J. Stec, K. R. Hess, N. Sneige, T. A. Buchholz, S. Krishnamurthy, N. K. Ibrahim, A. U. Buzdar, R. L. Theriault, M. F. Rosales, E. S. Thomas, K. M. Gwyn, M. C. Green, A. R. Syed, G. N. Hortobagyi, L. Pusztai, Total RNA yield and microarray gene expression profiles from fine-needle aspiration biopsy and core-needle biopsy samples of breast carcinoma. *Cancer* **97**, 2960–2971 (2003).

Acknowledgments: We would like to acknowledge M. Kim's help in assessing the differences in slopes among tumor types and Y. Wang and A. Patsialou for assistance with human tissue transplants. **Funding:** This work was supported by grants from the NIH (CA170507-01 to J.P., X.C., J.S.C., E.A., M.H.O., and S.G.; CA100324 to S.G., T.E.R., and A.B.), the Breast Cancer Alliance (S.G.), the Department of Defense Breast Cancer Research Program (W81XWH-14-1-0286 to J.P.), and the Albert Einstein College of Medicine Integrated Imaging Program (J.G.J.). **Author contributions:** J.P. performed qPCR analysis, developed and performed the iTEM assay, immunofluorescence, xenographs, mouse FNA, siRNA, data analysis, and statistics, and contributed to the experimental design and wrote the manuscript. S.G. performed qPCR and data analyses, and contributed to the experimental design and manuscript editing. J.G.J. performed IHC and TMEM scoring. T.E.R. performed the statistical analysis of patient samples. E.P. performed qPCR analysis. X.C. and E.A. collected patient FNA samples. D.C. differentiated the primary macrophages. S.M. performed E-cadherin scoring. A.B. developed the iTEM assay. F.B.G. developed the Mena antibody. J.S.C. contributed to the experimental design, data analysis, and wrote the manuscript. M.H.O. performed IHC, TMEM, and E-cadherin scoring, statistics, and data analysis, and contributed to the experimental design and wrote the manuscript. **Competing interests:** T.E.R., J.G.J., J.S.C., and F.B.G. hold stock and/or equity in MetaStat Inc. T.E.R. and J.G.J. have received consulting fees from MetaStat Inc. J.G.J. was a member of MetaStat's Clinical Advisory Board. All other authors declare that they have no competing interests. **Data and materials availability:** J.S.C., S.G., and F.B.G. hold a patent pertaining to the use of Mena^{INV} in cancer diagnosis, prognosis, and treatment (U.S. Patent 8603738). J.S.C., T.E.R., F.B.G., and J.G.J. hold a patent for the TMEM-based MetaSite Breast diagnostic assay (8642277).

Submitted 31 March 2014
Accepted 6 November 2014
Final Publication 25 November 2014
10.1126/scisignal.2005329
Citation: J. Pignatelli, S. Goswami, J. G. Jones, T. E. Rohan, E. Pieri, X. Chen, E. Adler, D. Cox, S. Maleki, A. Bresnick, F. B. Gertler, J. S. Condeelis, M. H. Oktay, Invasive breast carcinoma cells from patients exhibit Mena^{INV}- and macrophage-dependent transendothelial migration. *Sci. Signal.* **7**, ra112 (2014).

Invasive breast carcinoma cells from patients exhibit Mena^{INV}- and macrophage-dependent transendothelial migration

Jeanine Pignatelli, Sumanta Goswami, Joan G. Jones, Thomas E. Rohan, Evan Pieri, Xiaoming Chen, Esther Adler, Dianne Cox, Sara Maleki, Anne Bresnick, Frank B. Gertler, John S. Condeelis and Maja H. Oktay (November 25, 2014)

Science Signaling **7** (353), ra112. [doi: 10.1126/scisignal.2005329]

Science Signaling
AAAS

www.sciencesignaling.org/cgi/content/full/7/353/ra112/DC1

Supplementary Materials for

Invasive breast carcinoma cells from patients exhibit Mena^{INV}- and macrophage-dependent transendothelial migration

Jeanine Pignatelli,* Sumanta Goswami, Joan G. Jones, Thomas E. Rohan, Evan Pieri, Xiaoming Chen, Esther Adler, Dianne Cox, Sara Maleki, Anne Bresnick, Frank B. Gertler, John S. Condeelis,* Maja H. Oktay*

*Corresponding author. E-mail: moktay@montefiore.org (M.H.O.); jeanine.pignatelli@einstein.yu.edu (J.P.); john.condeelis@einstein.yu.edu (J.S.C.)

Published 25 November 2014, *Sci. Signal.* **7**, ra112 (2014)
DOI: 10.1126/scisignal.2005329

The PDF file includes:

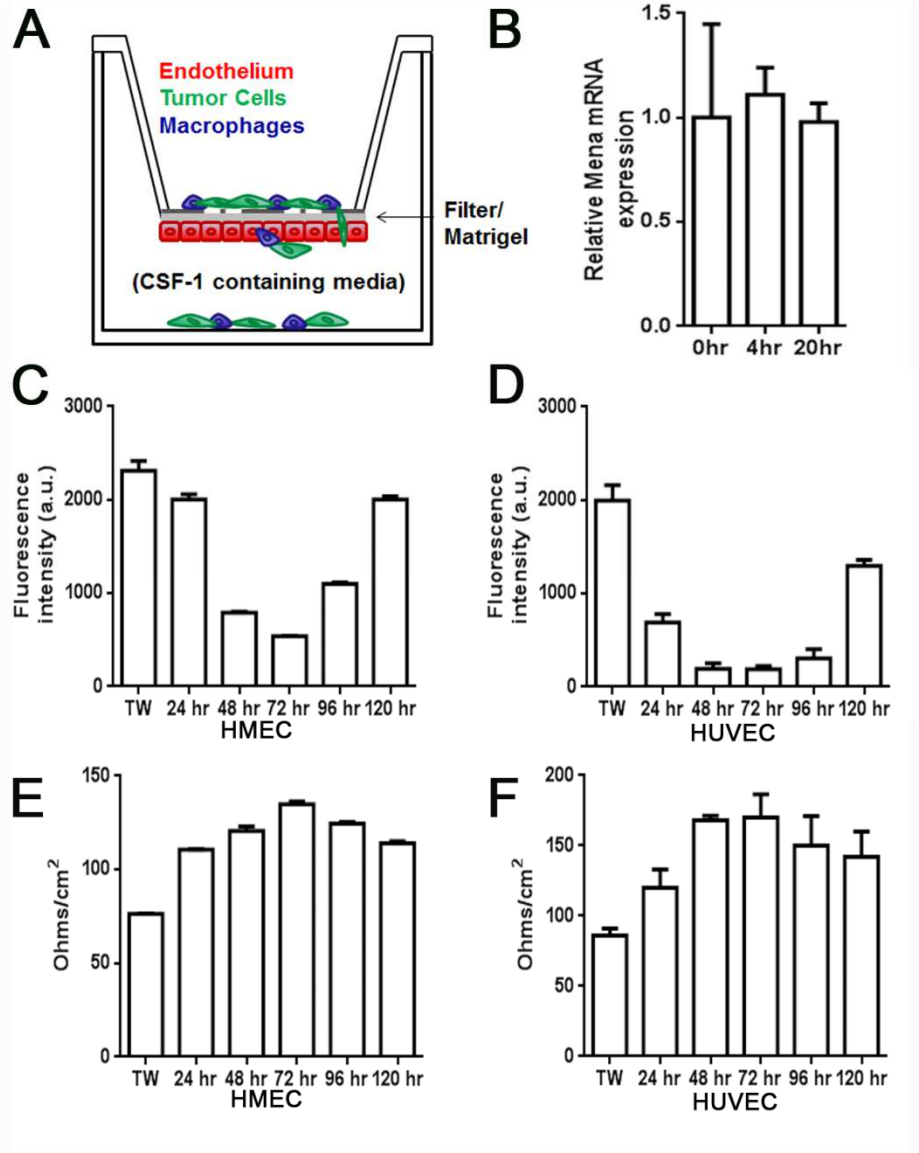

Figure S1. The experimental setup of the iTEM assay and the permeability of HMEC endothelium. (A) For in vitro iTEM assay, the bottom of a transwell is coated with Matrigel and an endothelial monolayer. Tumor cells and macrophages are added to the top of the transwell in serum-free medium, and medium containing CSF-1 is placed in the bottom well (the luminal side). **(B)** The effect of time in culture (hr: hours) on Mena^{INV} expression in FNA-obtained primary human breast cancer cells. **(C & D)** Fluorescence intensity measurements in bottom well 30 min after addition of 70 kD Texas Red dextran to upper well of HMEC and HUVEC monolayers. **(E & F)** Transendothelial electrical resistance measurements of HMEC (E) and HUVEC (F) monolayers. Data are means ±SEM for 3 independent experiments. TW; uncoated transwell control.

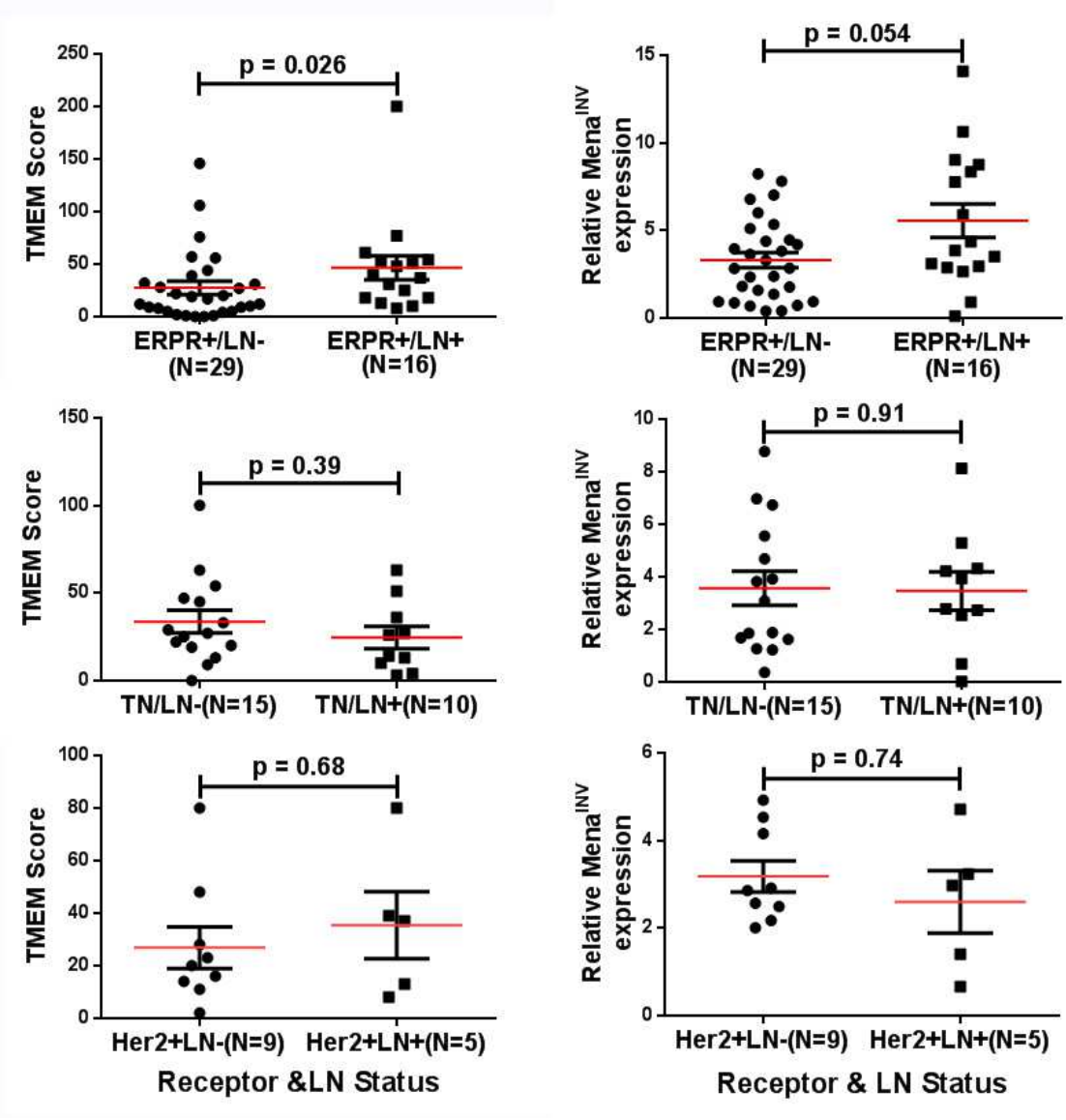

Figure S2. TMEM score and relative Mena^{INV} expression in LN-positive or LN-negative cases. TMEM score and relative Mena^{INV} expression are greater in lymph node-positive (LN+) compared with lymph node-negative (LN-) cases only in ERPR^{+}/Her^{-} clinical subtype, (*P*=0.026 and 0.054, respectively). However, this difference does not reach statistical significance (set at 0.008; see Materials and Methods). Data was analyzed with the Wilcoxon Mann-Whitney rank-sum test.

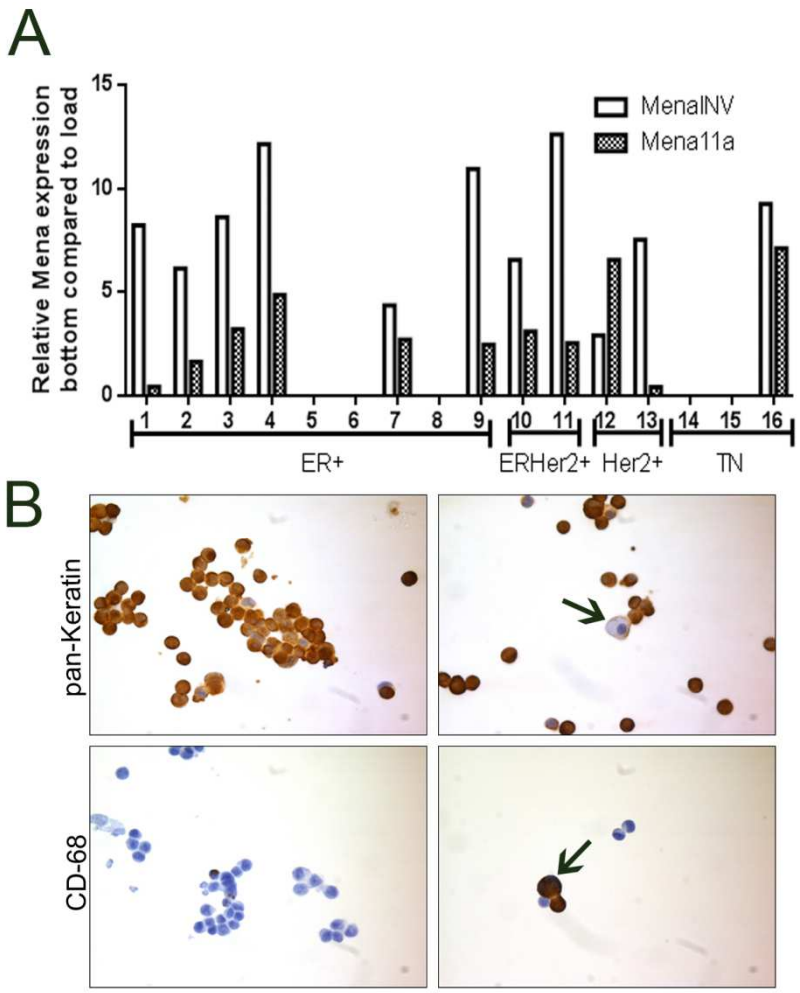

Figure S3. iTEM assays engineered with HMEC-1 endothelium performed with human IDC cells obtained by FNA. (**A**) RT-PCR for *MENA* isoform expression Cells from 11 out of 16 cases obtained from patient breast cancer FNA biopsies were capable of crossing an in vitro engineered endothelium. In 10 out of the 11 FNA samples that showed crossing ability, the cells in the bottom well of the intravasation assay were enriched for Mena^{INV}-expressing cells. (**B**) Representative images of immunochemically stained human IDC cells used in iTEM assays. The cells in the upper panels are stained with pan-keratin antibody AE1:3, while the cells in the lower panels are stained with CD68 antibody. The % of tumor cells and macrophages was assessed on the whole cytospin filed (314 µm). About 97% of the cells present in FNA sample are keratin-positive, CD68-negative. Macrophages represent about 3% of the cells in FNA samples and they were keratin-negative (arrow in upper right) and CD68-positive (arrow in bottom right).

Primers:
GAPDH F: CAT GAG AAG TAT GAC AAC AGC CT
GAPDH R: AGT CCT TCC ACG ATA CCA AAG T
Mena 11a F: CAA CCT GTT GTC AAA AAC AAT CT
Mena 11a R: GGA CCT GTT GTC AAA AAC AAT CT
Mena INV F: AGA GGA TGC CAA TGT CTT CG
Mena INV R: TTA GTG CTG TCC TGC GTA GC

Table S1. *MENA* and *GAPDH* primer sequences. F, forward sequence 5'–3'; R, reverse sequence 5'–3'.

Clinical Subtype	**N**	**Mena^{INV}**		**Mena11a**	
All	100	r = 0.57	p = 10^{-6}	r = -0.20	p = 0.04
ERPR^{+}/Her2^{-}	47	r = 0.72	p = 10^{-6}	r = -0.34	p = 0.02
Triple Negative	25	r = 0.55	p = 4^{-3}	r = -0.20	p = 0.34
ER^{+}/PR^{-}/HER2^{-}	14	r = 0.28	p = 0.34	r = -0.22	p = 0.44
Her2^{+}	14	r = 0.42	p = 0.07	r = 0.04	p = 0.90

Table S2. Correlation coefficients for TMEM score and relative expression of *MENA* isoforms in IDCs, overall and by clinical subtype. The values represented in the table are based on TMEM score and Mena isoform analyses form the 100 IDCs used to generate data in Figures 1 and 2. The statistically significant correlations indicated in red were calculated using Pearson's correlation coefficient.

	Mena^{INV}	Mena 11a	TMEM
Tumor Characteristics	Median *(5th, 95th percentile)*	Median *(5th, 95th percentile)*	Median *(5th, 95th percentile)*
BR 3, 4 & 5 N = 9	0.93 *(0.39, 4.02)*	0.15 *(0.02, 1.11)*	5.00 *(0.80, 27.60)*
BR 6 & 7 N = 40	3.28 *(0.67, 8.78)*	0.37 *(0.01, 1.65)*	18 *(1.00, 78.45)*
BR 8 & 9 N = 51	3.63 *(0.96, 8.28)*	0.31 *(0.01, 1.75)*	27 *(3.05, 111.00)*
< 2 cm N = 59	3.30 *(0.67, 7.83)*	0.51 *(0.01, 1.62)*	10.50 *(1.00, 107.60)*
> 2 < 5 cm N = 35	2.95 *(0.59, 8.76)*	0.21 *(0.01, 1.75)*	13.50 *(1.70, 76.30)*
> 5 cm N = 6	4.19 *(0.59, 12.83)*	0.02 *(0.01, 0.22)*	31.00 *(10.00, 162.75)*
LN+ N = 34	3.32 *(0.47, 9.59)*	0.19 *(0.01, 1.64)*	33.5 *(3.65, 78.05)*
LN- N = 64	2.91 *(0.67, 7.98)*	0.34 *(0.01, 1.66)*	22.00 *(1.00, 105.1)*
ER+ N = 70	3.63 *(0.67, 8.61)*	0.23 *(0.01, 1.68)*	25.00 *(1.00, 114.80)*
ER- N = 30	2.49 *(0.50, 7.60)*	0.56 *(0.01, 1.68)*	25.00 *(3.45, 63.00)*
PR+ N = 55	3.70 *(0.58, 8.85)*	0.22 *(0.01, 1.66)*	28.50 *(1.1, 89.10)*
PR- N = 46	2.78 *(0.66, 8.10)*	0.53 *(0.01, 1.65)*	22 *(2.00, 91.25)*
HER2/Neu+ N = 14	2.91 *(1.50, 4.78)*	0.42 *(0.02, 1.72)*	23 *(5.90, 80.00)*
HER2/Neu- N = 86	3.30 *(0.47, 8.68)*	0.32 *(0.01, 1.66)*	25 *(1.00, 104.50)*
Triple Negative N = 25	2.78 *(0.43, 7.90)*	0.59 *(0.01, 1.62)*	27 *(3.2, 63.00)*

Table S3. TMEM scores and relative Mena isoform expression for tumors with different clinical and pathological variables. Median, 5th and 95th percentile of relative expression of Mena^{INV} or Mena11a and TMEM counts for (i) well-differentiated

[Bloom-Richardson score (BR) 3-5], moderately differentiated (BR 6 & 7), or poorly differentiated (BR 8 & 9) IDCs; (ii) tumors that were < 2cm, between 2 and 5 cm, or > 5 cm in diameter; (iii) tumors with positive (+) or negative (–) expression of the genes encoding estrogen (ER), progesterone (PR), or HER2/Neu receptor. The only statistically different values (by Mann-Whitney test) were those observed for the fold change in $Mena^{INV}$ and TMEM scores between well-differentiated and poorly differentiated IDCs (indicated in red).

Case#	Mena^{INV}	Mena11a	Size	Grade	LN	LVI	ER %	PR %	Her2/Neu	Age
1	8.22	0.43	1.3	7	0/4	+	99	99	-	78
2	6.13	1.65	4	6	3/10	-	90	60	-	45
3	8.61	3.21	0.9	6	0/5	-	90	30	-	57
4	12.14	4.86	1.2	6	0/11	-	95	95	-	77
5	0.00	0.00	2.6	9	1/11	-	100	99	-	86
6	0.00	0.00	1.1	6	0/11	-	90	5	-	48
7	4.36	2.71	1.3	8	0/2	-	90	90	-	82
8	10.93	2.45	1.9	5	0/1	-	90	80	-	58
9	6.55	3.09	1.5	5	0/5	-	90	80	-	60
10	12.61	2.53	1.5	9	0/7	-	98	2	+	58
11	0.00	0.00	4	8	0/15	+	80	70	+	45
12	2.91	6.54	2.4	7	0/11	-	<1	<1	+	62
13	7.53	0.42	2.3	9	0/6	-	<1	<1	+	57
14	0.00	0.00	1.6	8	0/2	-	<1	<1	-	48
15	0.00	0.00	3.5	9	0/4	-	<1	<1	-	55
16	9.24	7.12	1	7	0/5	-	<1	<1	-	53

Table S4. Clinical and pathological data pertaining to iTEM data in fig. S3A. Mena values represent relative expression of Mena isoforms in the cells collected from the bottom well of iTEM assay compared to that in cells loaded in the top well. Tumor size is represented as the largest diameter in centimeters. Tumor grade is expressed as Bloom-Richardson score. LN: lymph node status, represented as the number that were positive out of the total number examined. LVI: lymphovascular invasion, represented as present (+) or absent (-). ER and PR expression is represented as percentage of positive cells. Her2/Neu abundance was examined by IHC and was considered positive if the score was 3+; any 2+ score was analyzed for copy number change by FISH and considered positive if the copy number was > 2.2 per nucleus.

Case#	Mena^{INV}	Mena11a	CSF-1R	Size	Grade	LN	LVI	ER (%)	PR (%)	Her2/Neu	Age
1	2.88	0.04	2.36	3.5	6	0/2	-	90	95	-	54
2	3.01	0.53	2.99	1.5	6	0/5	-	100	60	-	62
3	6.96	0.23	1.00	2	7	1/6	+	90	90	-	58
4	7.01	0.004	0.83	2.3	6	0/7	-	100	100	-	70
5	9.7	0.45	0.05	1.8	6	0/4	-	80	<1	-	70
6	10.13	ND	0.95	1.2	5	0/6	-	90	<1	-	70
7	10.63	ND	3.58	2.2	6	0/3	-	100	90	-	73
8	6.931	0	-	5.2	6	17/2	-	90	30	-	87
9	5.42	ND	4.29	1.9	9	1/2	-	90	90	-	67
10	13.11	ND	11.45	6	8	0/4	-	70	55	+	49
11	3.73	1.49	7.2	1.8	8	0/3	-	30	<1	+	52
12	8.65	0.74	11.16	8	9	0/6	-	<1	<1	-	95
13	4.66	ND	14.51	1	8	0/6	-	<1	<1	-	69
14	15.37	ND	14.83	1.6	9	0/1	-	<1	<1	-	79
15	16.56	0.11	4.46	2.5	9	1/7	-	<1	<1	-	40
16	7.39	ND	9.82	2.2	9	0/6	-	<1	<1	-	53

Table S5. Clinical and pathological date pertaining to iTEM data in Figs. 4 and 6. Mena and CSF-1R values represent relative expression of Mena isoforms and CSF-1R in the cells collected from the bottom well of iTEM assays compared to that from cells loaded in the top well. Details and abbreviations as described for table S4.

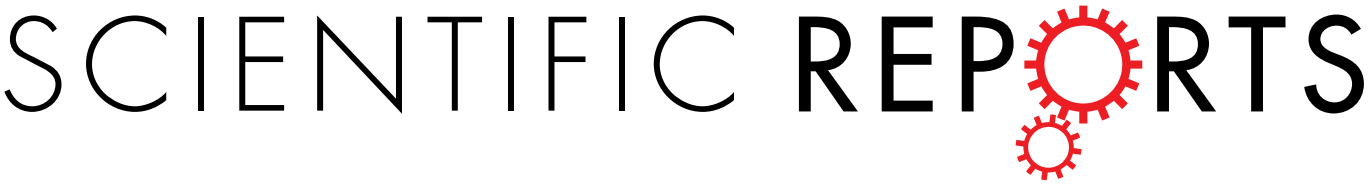

OPEN

Received: 15 June 2016
Accepted: 02 November 2016
Published: 30 November 2016

Macrophage-dependent tumor cell transendothelial migration is mediated by Notch1/Mena^{INV}-initiated invadopodium formation

Jeanine Pignatelli[1,2,*,†], Jose Javier Bravo-Cordero[1,2,*,‡], Minna Roh-Johnson[1,2,#], Saumil J. Gandhi[1], Yarong Wang[1,2], Xiaoming Chen[1], Robert J. Eddy[1], Alice Xue[1], Robert H. Singer[1], Louis Hodgson[1,2], Maja H. Oktay[1,3] & John S. Condeelis[1,2]

The process of intravasation involving transendothelial migration is a key step in metastatic spread. How the triple cell complex composed of a macrophage, Mena over-expressing tumor cell and endothelial cell, called the tumor microenvironment of metastasis (TMEM), facilitates tumor cell transendothelial migration is not completely understood. Previous work has shown that the physical contact between a macrophage and tumor cell results in the formation of invadopodia, actin-rich matrix degrading protrusions, important for tumor cell invasion and transendothelial migration and tumor cell dissemination. Herein, we show that the macrophage-induced invadopodium is formed through a Notch1/Mena^{INV} signaling pathway in the tumor cell upon macrophage contact. This heterotypic tumor cell – macrophage interaction results in the upregulation of Mena^{INV} through the activation of MENA transcription. Notch1 and Mena^{INV} expression are required for tumor cell transendothelial migration, a necessary step during intravasation. Inhibition of the Notch signaling pathway blocked macrophage-induced invadopodium formation *in vitro* and the dissemination of tumor cells from the primary tumor *in vivo*. Our findings indicate a novel role for Notch1 signaling in the regulation of Mena^{INV} expression and transendothelial migration and provide mechanistic information essential to the use of therapeutic inhibitors of metastasis.

Metastasis is the primary cause of morbidity and mortality of breast cancer patients. The process of breast cancer metastasis requires tumor cells to migrate towards blood vessels where they intravasate. Intravasation of tumor cells during metastasis remains poorly understood, although it has become increasingly apparent that components of the tumor microenvironment such as macrophages, contribute to the efficacy of this process. Within invasive breast carcinoma we have identified multicellular microanatomical structures called the tumor microenvironment of metastasis (TMEM) that serve as the functional sites of tumor cell intravasation, and have been validated as a prognostic marker of metastatic outcome in patients[1–5]. Each TMEM site is comprised of a Mena over-expressing tumor cell, a peri-vascular macrophage and an endothelial cell of a blood vessel in direct contact with each other. It is at these sites that transient vascular- permeability events and intravasation of breast tumor cells uniquely occur in breast tumors[2]. The importance of the direct contact of these three cell types and signaling between these cells during the function of TMEM in intravasation has not yet been explored.

[1]Department of Anatomy and Structural Biology Albert Einstein College of Medicine of Yeshiva University, Bronx, NY 10461, United States. [2]Gruss Lipper Biophotonics Center Albert Einstein College of Medicine of Yeshiva University, Bronx, NY 10461, United States. [3]Department of Pathology Albert Einstein College of Medicine of Yeshiva University, Bronx, NY 10461, United States. [†]Present address: Pfizer Oncology Targeted Therapeutics Division, 401 N Middletown Rd, Pearl River, NY 10965, United States. [‡]Present address: Division of Hematology and Oncology, Department of Medicine, Mount Sinai School of Medicine, Tisch Cancer Institute, New York, NY, United States. [#]Present address: Fred Hutchinson Cancer Research Center, Basic Sciences Division, 1100 Fairview Ave N, Seattle, WA 98109, United States. [*]These authors contributed equally to this work. Correspondence and requests for materials should be addressed to J.P. (email: jeanine.pignatelli@pfizer.com) or M.H.O. (email: maja.oktay@einstein.yu.edu) or J.S.C. (email: john.condeelis@einstein.yu.edu)

Migratory and disseminating breast tumor cells at TMEM over-express the ENA/Vasp family member Mena (mammalian-ENA) when compared to normal breast epithelium[4,6]. Overexpression of Mena, an actin regulatory protein, is also seen in other cancers of epithelial origin including pancreatic, lung, cervical and colon cancers[7]. Mena is alternatively spliced during tumor progression resulting in the expression of multiple isoforms encoded by the same gene[7]. The expression of the different isoforms is associated with various cell phenotypes. Predominate expression of the Mena11a isoform confers an epithelial, cohesive, non-invasive cell behavior; while the over-expression of Mena^{INV} results in a highly motile, invasive phenotype[8–10].

The number of TMEM sites in patient samples positively correlates with the abundance of Mena^{INV} mRNA, whereas Mena11a demonstrates a negative correlation in the same patient cohort[1]. Previous work has demonstrated that the expression of the Mena11a isoform is regulated by Twist signaling[11], but despite the numerous studies indicating the over-expression of Mena^{INV} in invasive-intravasation-competent tumor cells *in vivo*, the signals regulating the expression of the Mena^{INV} isoform have remained unknown.

In addition to the macrophage-regulated vascular permeability events that contribute to tumor cell intravasation and metastasis, tumor cells form an invasive actin-rich invadopodium that enables the tumor cell to degrade extra-cellular matrix proteins and migrate, invading across barriers like blood vessel walls and intravasate[12–14]. Invadopodia are required for tumor cell transendothelial migration, a necessary step for intravasation[13]. Although it has been generally appreciated that invadopodia are important for tumor cell migration and intravasation it is not completely understood how[15,16]. There is evidence in multiple *in vivo* models such as chicken chorioallantoic membrane (CAM) models, tumor xenographs in mice and zebrafish and transgenic mouse models that invadopodia can be observed in mammalian cells *in vivo* and that these structures play a critical role in the cells ability to breech the basement membrane for invasion[17–20]. In addition, the depletion of critical invadopodial components *in vivo* reduces the numbers of circulating tumor cells and metastasis[12]. Interestingly, we have previously shown that the direct interaction of a tumor cell and macrophage results in the formation of the tumor cell invadopodium that is required for transendothelial migration of tumor cells and this cannot be mimicked with macrophage-conditioned medium[13]. Therefore, a direct contact event between tumor cells and macrophages results in a signal inducing the formation of invadopodia.

A major signaling pathway that is involved in cell contact-mediated communication is the Notch signaling pathway. In addition to critical roles in development, Notch signaling has been implicated in cancers such as breast, lung and pancreatic cancers and leukemia, where activation of Notch pathways can promote proliferation, prevent differentiation, and promote metastasis[21–24]. Disruption of the Notch signaling pathways can affect cell growth, cell fate, angiogenesis and apoptosis. In tumor cells, activation of Notch upon homotypic cell contact triggers invadopodium formation under hypoxia conditions[25].

Herein, we explore the contribution of the Notch signaling pathway to TMEM function; in particular macrophage-dependent tumor cell invadopodium formation and its relationship to Mena expression during transendothelial migration and tumor cell dissemination.

Results

Notch1 signaling is required for macrophage-induced formation of invadopodia in tumor cells. To evaluate if Notch signaling is required for macrophage – induced invadopodium formation (Fig. 1A), cells were treated with DAPT, a γ-secretase inhibitor, which inhibits intracellular Notch signaling by preventing its cleavage into the active NICD[26]. A mature invadopodium is defined herein as having cortactin and Tks5 positive staining as well as being co-localized with a discreet area of matrix degradation. Tks5 is required for anchoring the invadopodium core to the plasma membrane via its binding to PI (3, 4) P2[27] and its association with these other two markers is a definitive identifier of mature invadopodia. In the absence of macrophages and in serum-starved conditions, DAPT treatment has no significant effect on invadopodium assembly by MDA-MB-231 human breast tumor cells (Fig. 1B). When BAC1.2F5 macrophages are added to the MDA-MB-231 culture there is a significant increase in the number of mature invadopodia per tumor cell but the addition of DAPT to these co-cultures prevents the macrophage-mediated induction of invadopodia (Fig. 1B).

Increased Notch1 signaling is associated with a greater chance of metastasis and poor prognosis[23]. Therefore, to determine if Notch1 receptor is important in macrophage–induced invadopodium formation we used siRNA mediated knockdown of Notch1. Knockdown of Notch1 receptor in MDA-MB-231 cells resulted in a significant reduction in macrophage-induced invadopodia as well as a significant reduction in invadopodium-associated matrix degradation to baseline levels seen in the absence of macrophages (Fig. 1C–E). Notch1 inhibition had no significant effect on steady sate invadopodium formation in the absence of macrophages (Supplemental Figure 1A and B). Thus, we conclude that Notch1 is required for macrophage-induced invadopodium assembly and function. These data indicate a novel signaling pathway involving heterotypic cell-cell communication of Notch1 in macrophage-induced invadopodium formation in tumor cells.

Notch1 signaling is required for macrophage – tumor cell contact-induced Mena^{INV} expression. Notch1 has well defined roles in the regulation of gene and protein expression at the transcriptional level, although a role for Notch1 in the regulation of the macrophage-induced invadopodium pathway is unknown. We sought to determine if macrophage – induced Notch1 signaling in tumor cells results in expression changes in genes with known roles in invadopodium formation and function. We performed a qRT-PCR analysis to determine changes in mRNA levels of the known invadopodium pathway regulatory proteins (Fig. 2A). The co-culture of MDA-MB-231 tumor cells with macrophages resulted in no significant mRNA changes in actin, cortactin, cofilin, N-WASp or the RhoGTPases Rac1, Cdc42, RhoA and RhoC, which all have well defined roles in invadopodia regulation[12,28–33]. There was no significant change in the level of total (pan) Mena mRNA levels which are very abundant compared to Mena^{INV} (Supplemental Figure 2B), but the Mena^{INV} isoform was highly upregulated (~45x) while Mena11a isoform levels remain unchanged. This finding is of great interest because high expression

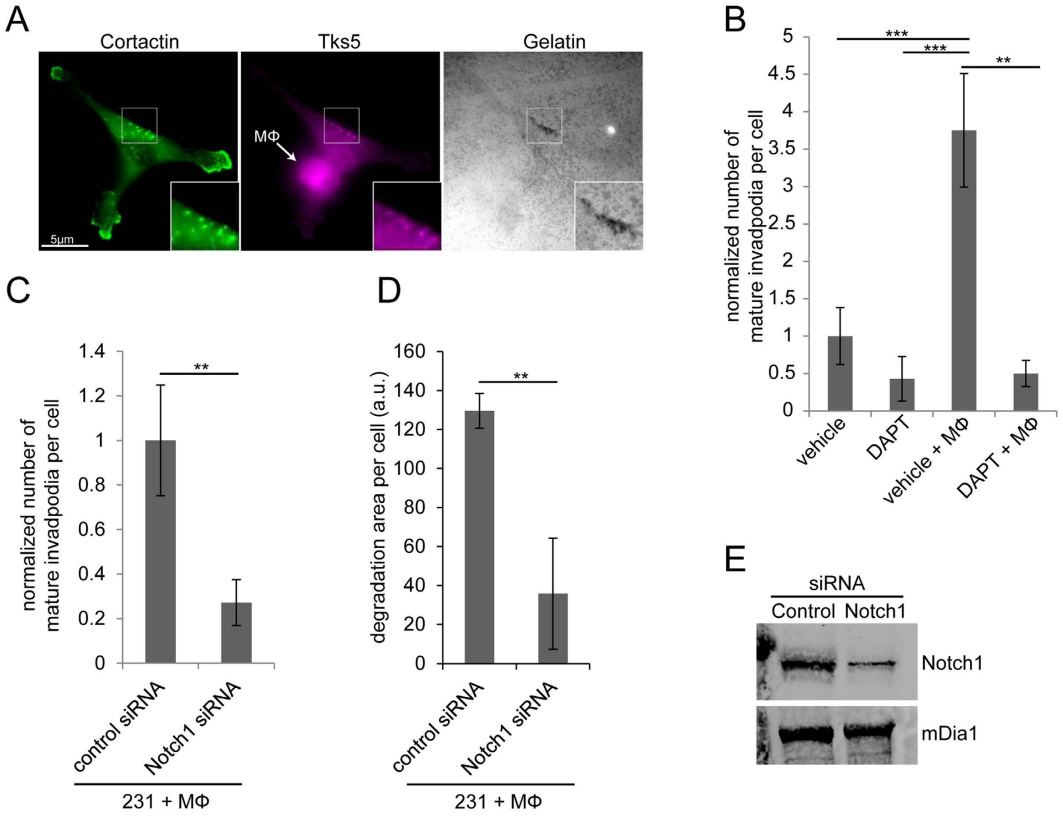

Figure 1. Macrophage – induced tumor cell invadopodia require Notch1 signaling. (**A**) Immunofluorescence of MDA-MB-231 tumor cell in contact with BAC1.2F5 macrophage plated on 405-gelatin. Tumor cells were stained for Tks5 (purple) and cortactin (green) to identify invadopodium cores (insert is zoom of mature invadopodia). Position of the macrophage is indicated by the arrow. (**B**) Quantitation of the number of mature invadopodia per cell in MDA-MB-231 tumor cells plated alone or with BAC1.2F5 macrophages. Cells were treated with vehicle or DAPT γ- secretase inhibitor. (**C**) Quantitation of the number of mature invadopodia per cell in MDA-MB-231 tumor cells treated with control or Notch1 siRNA plated with BAC1.2F5 macrophages. (**D**) Quantitation of the area of matrix degradation in control and Notch1 siRNA treated MDA-MB-231 cells plated with BAC1.2F5 macrophages. (**E**) Western blot of MDA-MB-231 cells treated with control and Notch1 siRNA demonstrating knockdown efficiency. mDia1 (mammalian homolog of Drosophila diaphanous) was used as a loading control. $^{*}P < 0.05$, $^{**}P < 0.005$, $^{***}P < 0.0005$.

of the Mena^{INV} isoform has been implicated in the increased motility, invadopodium assembly and invasion by tumor cells[1,8,34,35].

There is a well described paracrine signaling loop between human breast or mouse mammary tumor cells and macrophages[1,35,36]. Due to this well-defined soluble signaling pathway between tumor cells and macrophages, we wanted to confirm that the increase in Mena^{INV} upon co-culture with macrophages was a result of cell-cell contact and not soluble signaling factors. We performed co-culture experiments utilizing 3 μm pore transwells, which allow for the passage of soluble factors but not the tumor cells. Tumor cells were either plated in the transwell alone, with the two cell types mixed in the top of the well, or with macrophages added to the bottom of the well to prevent tumor cell – macrophage contact (Fig. 2B). When the cell types were mixed together in the top of the transwell, allowing cell-cell contact, we observed the increase in Mena^{INV} mRNA whereas when the cells were plated on opposite sides of the transwell, allowing for the exchange of soluble factors but not direct contact, no significant change in Mena^{INV} mRNA was observed.

To confirm that the increase in Mena^{INV} mRNA is regulated by the macrophage-tumor cell contact initiated Notch1 signaling, we treated the tumor cells with Notch1 siRNA or DAPT. We found that both had the ability to abrogate the increase in Mena^{INV} mRNA during co-culture of the two cell types (Fig. 2C and D).

To determine if these events are macrophage-contact specific, we co-cultured tumor cells at high density to induce tumor cell-tumor cell contact, tumor cell and macrophage contact or tumor cells and endothelial cell contact. These are the three different cell types that comprise TMEM sites. The only contact that was able to induce an increase in Mena^{INV} expression was the tumor cell and macrophage co-culture (Supplemental Figure 2A). In addition, the contact between tumor cells and HUVEC endothelial cells did not result in an increase in mature invadopodia or matrix degradation (Supplemental Figure 2B and C).

In addition to the MDA-MB-231 cells, we confirmed the macrophage-induced expression of Mena^{INV} in primary tumor cells. Tumor cells were obtained by fine needle aspiration biopsy (FNA), which yields ~97% pure

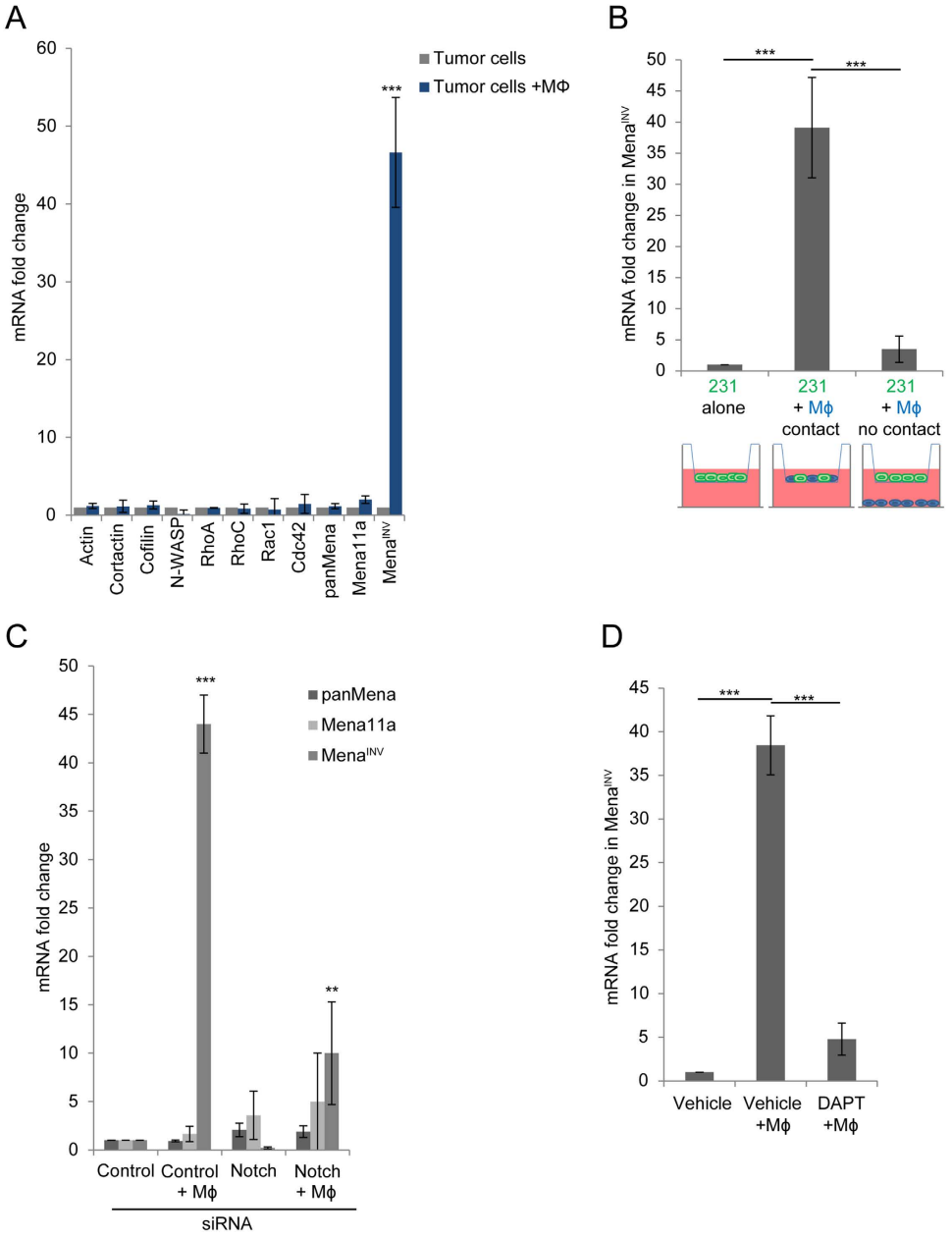

Figure 2. Macrophage – tumor cell contact results in a Notch1 dependent upregulation in Mena^{INV} mRNA expression in tumor cells. (**A**) qRT-PCR of invadopodia pathway components in MDA-MB-231 cells plated alone or with BAC1.2F5 macrophages (Mϕ). (**B**) qRT-PCR of Mena^{INV} in MDA-MB-231 cells plated in transwells alone, co-cultured in top well of transwells in contact with BAC1.2F5 macrophages (Mϕ) or plated on opposite side of transwells (no contact). (**C**) qRT-PCR of Mena^{INV} in MDA-MB-231 cells treated with control or Notch1 siRNA plated alone or with BAC1.2F5 macrophages. (**D**) qRT-PCR of Mena^{INV} in MDA-MB-231 cells treated with vehicle or DAPT γ- secretase inhibitor plated alone or with BAC1.2F5 macrophages. *$P < 0.05$, **$P < 0.005$, ***$P < 0.0005$.

tumor cell samples[1]. Cells obtained by FNA from triple negative human tumor tissue transplants (HT17)[1,37] were plated with or without macrophages for 6 hours. Although a subset of tumor cells *in vivo* express elevated Mena^{INV}, when cells were cultured with macrophages there is a significant increase in Mena^{INV} mRNA (Fig. 3A). When cells are plated with macrophages in the presence of DAPT there was an inhibition of Mena^{INV} expression (Fig. 3A), indicating a requirment for Notch signaling in primary tumor cells.

Primary cancer cells were also obtained by FNA from two human invasive ductal carcinomas immediately after surgical resection (Fig. 3B, patient #1 had ER+ disease and patient #2 had ER- disease). In cells from these 2 patient samples we also observed a dramatic increase in Mena^{INV} mRNA when co-cultured with macrophages (Fig. 3B). These data indicate a novel pathway for the upregulation of the pro-migratory/invasive Mena^{INV} isoform of Mena that is common to breast cancer cells with different ER expression status.

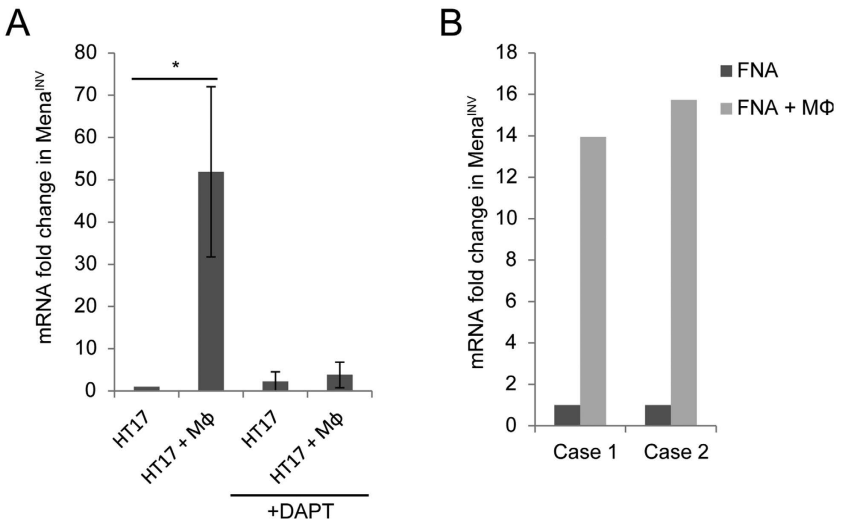

Figure 3. Macrophage contact induces a Notch dependent upregulation of Mena^{INV} in primary human breast tumor cells. (**A**) qRT-PCR of Mena^{INV} of primary FNA tumor cells from HT17 triple negative human tissue transplants in SCID mice cultured alone or with BAC1.2F5 macrophages (n = 3 mice) in the presence of absence of DAPT. (**B**) qRT-PCR of Mena^{INV} from primary FNA tumor cells from two independent patients cultured alone or with BAC1.2F5 macrophages. Case 1 was an ER+ tumor and case 2 was an ER − tumor.

Macrophage – tumor cell contact turns on Notch-dependent MENA gene transcription and Mena^{INV} protein expression. The above results indicate that a Mena isoform switch is taking place upon macrophage contact because the panMena and Mena11a mRNA levels remained unchanged while Mena^{INV} levels increase dramatically. This expression switch of isoforms presumably requires the transcription of the MENA gene, where the newly transcribed RNA would be spliced to include the Mena^{INV} exon.

To test the hypothesis that the increase in Mena^{INV} mRNA seen in tumor cells in contact with macrophages is associated with increased Mena gene transcription, we designed fluorescent *in-situ* hybridization (FISH) probes to MENA. The different Mena isoforms are splice variants transcribed by the same gene[6,11]; therefore the probes designed recognize the full length MENA gene transcript (Supplemental Figure 3). Macrophages were labeled with cell tracker red and co-cultured with tumor cells for 60 minutes (Fig. 4A). When MDA-MB-231 tumor cells are cultured alone, only ~10% have an active MENA transcription site, as seen by FISH (Fig. 4B). When tumor cells and macrophages are plated in co-culture for 1 hour, tumor cells that are not in contact with macrophages still only display ~10% of cells actively transcribing MENA, while tumor cells touching a macrophage have over 45% of cells with active transcription sites (Fig. 4A and B). Figure 4A shows a tumor cell in direct contact with a macrophage displaying active MENA transcription, and a tumor cell not in contact with a macrophage displaying no active MENA transcription site. The addition of DAPT to the tumor cell-macrophage co-culture prevented the macrophage induction of MENA transcription, even when the tumor cells were in direct contact with macrophages (Fig. 4C).

In addition, we measured the probability of active MENA transcription as a function of the distance of a tumor cell to the nearest macrophage in control conditions or in the presence of DAPT (Fig. 4D and E). When tumor cells are touching macrophages (0 μm distance), the probability of active MENA transcription is ~0.65, a high probability of transcription. As the distance becomes greater than 35 μm away, there is zero probability that the tumor cell has an active MENA transcription site. In the presence of DAPT treatment, tumor cells show a scattered pattern of low level transcription versus distance from a macrophage indicating that by blocking Notch signaling we have inhibited the macrophage contact induced MENA transcription.

These FISH data and the qPCR data above indicate that when tumor cells come into direct contact with a macrophage there is a rapid Notch-dependent induction of MENA transcription.

To determine if the macrophage activation of MENA transcription and the increased accumulation of Mena^{INV} mRNA results in increased Mena^{INV} protein in the tumor cells, we developed a polyclonal anti- Mena^{INV} specific antibody (Supplemental Figure 4). MDA-MB-231 cells plated alone or in co-culture with macrophages for 16 hours were stained using the newly developed Mena^{INV}-specific antibody (Fig. 5A). The average intensity was measured with Mena^{INV} staining in tumor cells alone or those cultured with macrophages. When cultured with macrophages, tumor cells show a significant increase in Mena^{INV} protein staining intensity (Fig. 5). This data indicates that the Notch-mediated increase in Mena^{INV} mRNA observed in tumor cells in contact with macrophages is translated into an increase in Mena^{INV} protein levels in the tumor cells.

Mena^{INV} and Notch1 are required for invadopodium-driven transendothelial migration. The above results demonstrate that macrophage – induced tumor cell invadopodium formation requires Notch1 signaling. We also know from previous work that macrophages induce transendothelial migration of tumor cells both *in vitro*[13] and *in vivo*[2], and that Mena^{INV} is required for transendothelial migration[1]. Therefore, we hypothesized

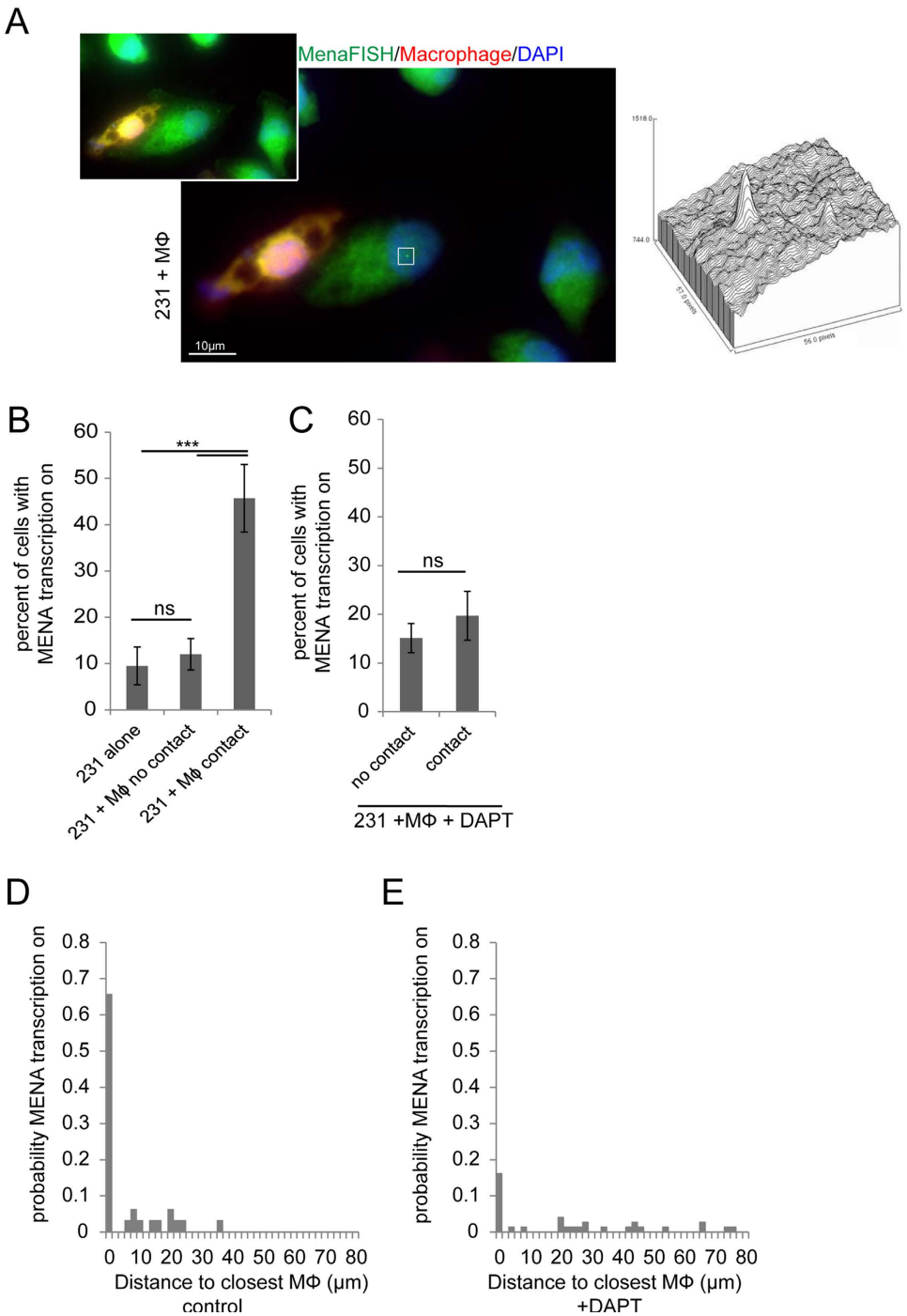

Figure 4. Macrophage- tumor cell contact increases MENA transcription. (**A**) MDA-MB-231 cells plated with BAC1.2F5 macrophages for 60 min. Macrophages are labeled with cell tracker red. Cells were labeled with FISH probes that recognize all Mena isoforms (panMena) and DAPI. Inset shows z-section of direct contact of tumor cell with macrophage. White box is around the dot which is an active MENA transcription site. Histogram of FISH fluorescence intensity within white box showing signal to noise intensity of transcription site. (**B**) Quantitation of the percent of tumor cells with active MENA transcription when MDA-MB-231 cells are plated alone, with BAC1.2F5 macrophages (Mϕ) not in contact and with Mϕ in contact with tumor cells. (**C**) Quantitation of the percent of tumor cells with active MENA transcription when MDA-MB-231 cells with BAC1.2F5 macrophages (Mϕ) not in contact and with Mϕ in contact with tumor cells in the presence of DAPT γ- secretase inhibitor. (**D**) The distance of tumor cells from macrophages in the population of cells with MENA transcription sites being expressed (probability). (**E**) The distance of tumor cells from macrophages in the population of cells with MENA transcription sites being expressed in the presence of DAPT (normalized for the number of cells with MENA being expressed). $^{*}P < 0.05$, $^{**}P < 0.005$, $^{***}P < 0.0005$, *ns* = non-significant.

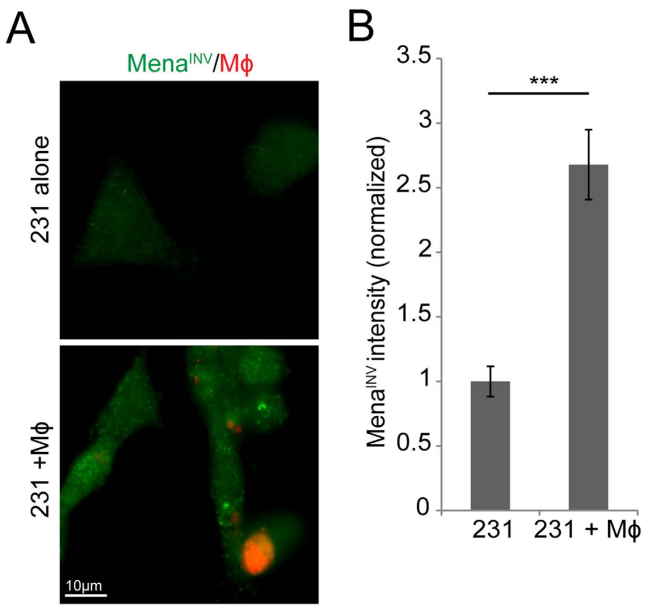

Figure 5. Macrophage-tumor cell contact increases Mena^{INV} protein expression in tumor cells. (**A**) Immunofluorescence of MDA-MB-231 cells plated alone or with BAC1.2F5 macrophages (cell tracker red) stained with a Mena^{INV} specific antibody. (**B**) Quantitation of the average pixel intensity of Mena^{INV} staining in MDA-MB-231 cells plated alone or with BAC1.2F5 macrophages.

that Notch1 and Mena^{INV} are both required for the formation of the invadopodia necessary for tumor cells to undergo transendothelial migration.

Specific knockdown of Mena^{INV} significantly reduces the number of mature invadopodia formed upon macrophage-tumor cell contact (Fig. 6A and B). Knockdown of panMena results in the knockdown off all Mena isoforms, therefore also depleting Mena^{INV}. Interestingly, depletion of total Mena has no additive effect over the Mena^{INV} knockdown (Fig. 6A and B). Therefore, Mena^{INV} is the key isoform that regulates macrophage-induced invadopodia.

To determine the role of Notch1 in tumor cell intravasation-directed transendothelial migration (iTEM) activity, we either depleted Notch1 in tumor cells with siRNA or inhibited Notch signaling with DAPT and quantified the tumor cell iTEM activity in the presence and absence of macrophages. Notch1 depletion had no effect on the iTEM activity of tumor cells alone, but either depletion of Notch1 with siRNA or its inhibition with DAPT inhibited macrophage-induced tumor cell iTEM activity (Fig. 6C–E).

Notch1 inhibition decreases macrophage-dependent invadopodium formation *in vitro* and the dissemination of photo-converted tumor cells *in vivo*. Formation of invadopodia *in vitro* as well as invasion *in vivo* has been well characterized using the rat mammary adencocarcoma MTLn3 cells. Like MDA-MB-231 cells, MTLn3 cells can form invadopodia and undergo migration *in vivo* when they upregulate Mena^{INV} expression[6,35]. Here, we tested their ability to form macrophage-induced invadopodia. When MTLn3 cells are co-cultured with macrophages, we observed a highly significant increase in formation of invadopodia (Fig. 7A and B). As an additional method of inhibiting Notch1 signaling applicable to the MTLn3 cells, we treated MTLn3 cells with a Notch1 specific blocking antibody or control isotype IgG. Cells co-cultured with macrophages and treated with the Notch1 blocking antibody demonstrate significantly fewer invadopodia (Fig. 7A and B). These data demonstrate that the macrophage-induced invadopodia can be stimulated in a different well-characterized invasive and metastatic tumor cell line and this is Notch1 dependent.

We utilized MTLn3 cells expressing photo-convertible Dendra2 to measure the effects of Notch1 inhibition on loss of tumor cells from the primary tumor *in vivo* as described previously[12,38]. Peri-vascular regions within the MTLn3 – Dendra2 tumors were photo-converted and were tracked every 24 hours over a 72 hour period to measure intravasation as described previously[10,14,38] (Fig. 7 C and D). Mice were treated daily with 1 mg/kg control IgG or Notch1 blocking IgG. In control treated mice, there was a significant decrease every 24 hour period in the percent of photo-converted-Dendra2 cells remaining in the region[10,14,38]. In mice treated with the Notch1 blocking antibody there was a significant reduction in the percent of cells that were leaving the photo-converted regions of the tumor, indicating these tumor cells were less efficient at leaving the primary tumor.

To find out if cells leaving the tumor site were correlated with circulating tumor cells, mice with MTLn3 xenographs were treated with control or Notch1 blocking IgG for 6 hours and the circulating tumor cells were measured after treatment. There was a significant decrease in the number of circulating tumor cells in mice that were treated with the Notch1 blocking antibody compared to control treated mice (Fig. 7E), consistent with the idea that transendothelial migration is involved in CTC (Circulating Tumor Cells) number. These data indicate a role for Notch1 signaling in tumor cells leaving the primary tumor.

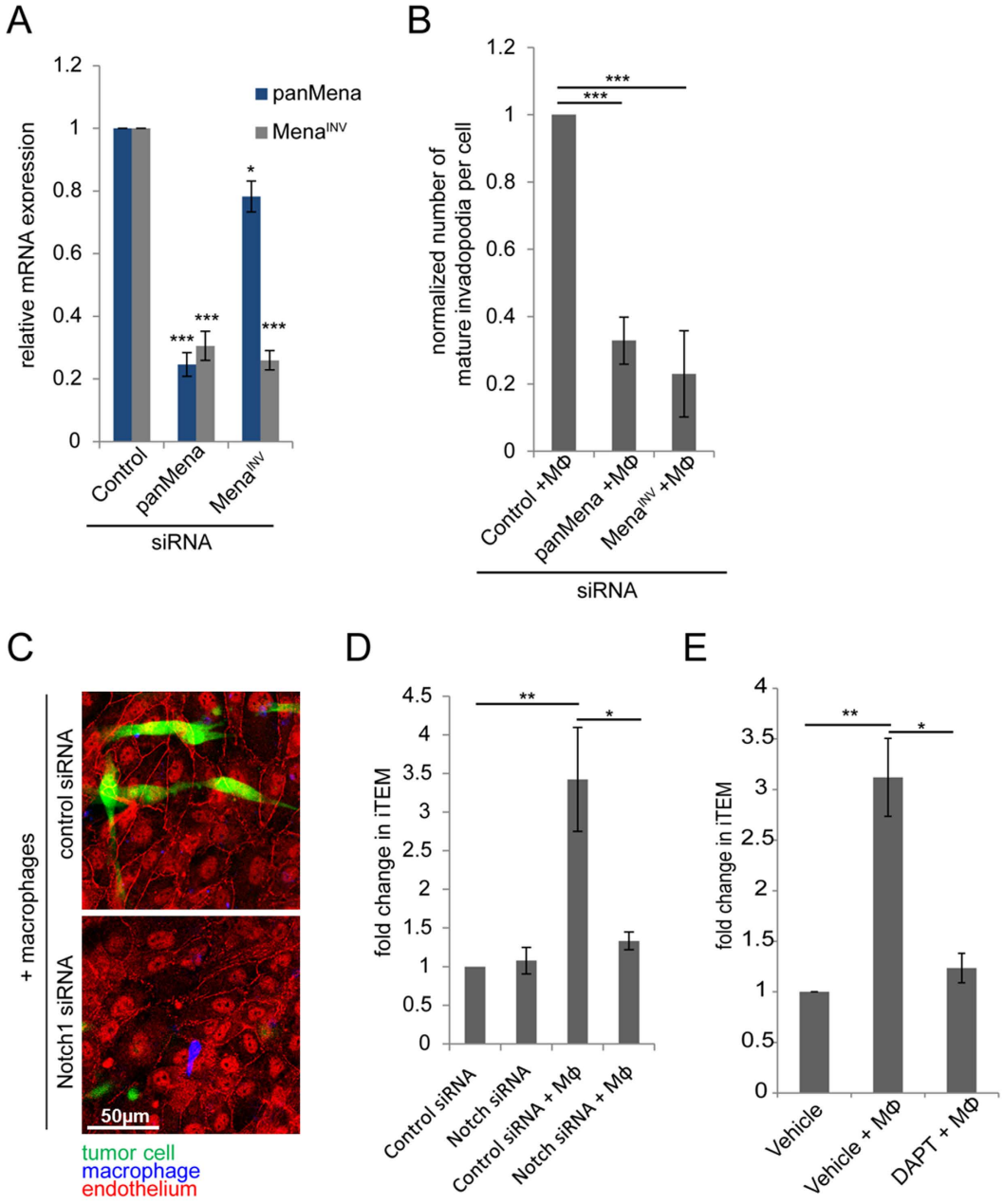

Figure 6. Mena^{INV} and Notch1 are required for macrophage – induced invadopodium assembly and transendothelial migration. (**A**) Quantitation of the relative mRNA expression in MDA-MB-231 cells treated with control, panMena or MenaI^{NV} siRNA in the absence of macrophages. (**B**) Quantitation of the relative number of invadopodia in MDA-MB-231 cells treated with control, panMena or Mena^{INV} siRNA in the presence of macrophages. (**C**) Representative apical z-section of intravasation-directed transendothelial migration (iTEM) assay of tumor cells (green) and macrophages (blue, white arrows). Tumor cells were treated with control or Notch1 siRNA. Endothelial HUVEC cells were stained for ZO-1 (red). Shown is an "en face" view of the apicial side of the transwell, therefore the green-labeled tumor cells have crossed the endothelial monolayer and are on the 'bottom' or apical side of the transwell positioning them above the endothelial cells from this vantage point. (**D**) Quantitation of intravasation-directed is defined as subluminal to luminal transendothelial migration (iTEM) activity of MDA-MB-231 cells plated on the endothelium either alone or with BAC1.2F5 macrophages. Tumor cells were treated with control or Notch1 siRNA. (**E**) Quantitation of iTEM activity of MDA-MB-231 cells plated alone or with BAC1.2F5 macrophages with vehicle or DAPT treatment. $^{*}P < 0.05$, $^{**}P < 0.005$, $^{***}P < 0.0005$.

Discussion

Tumor cell dissemination via blood vessels in breast tumors requires tumor cells to undergo transendothelial migration. This occurs uniquely at TMEM sites where macrophages are in direct contact with tumor cells and

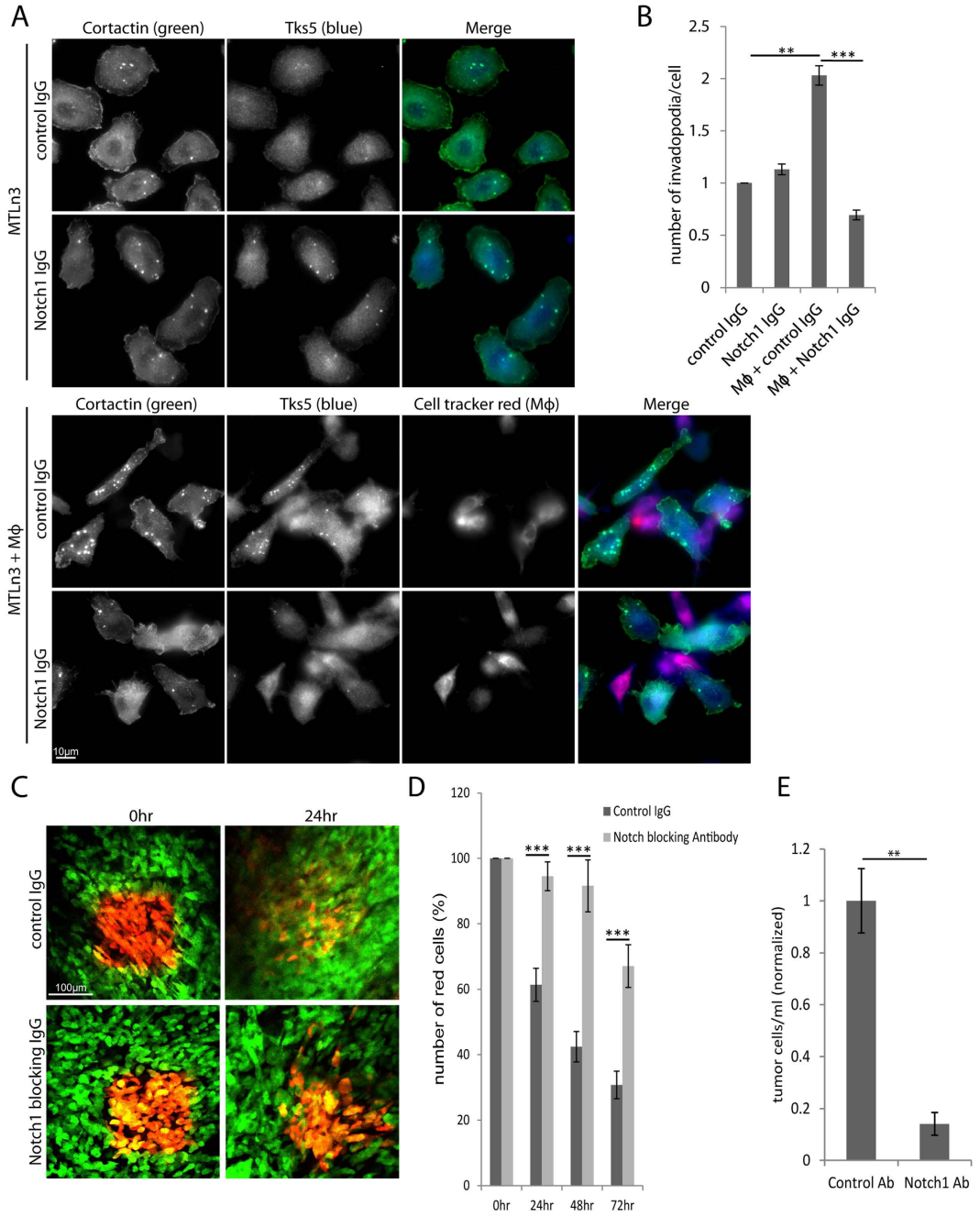

Figure 7. Notch1 inhibition decreases macrophage-dependent invadopodium formation *in vitro* and the dissemination of tumor cells *in vivo*. (**A**) Immunofluorescence images of MTLn3 tumor cells plated in the presence or absence of BAC1.2F5 macrophages (Mϕ) and treated with control IgG or Notch1 blocking IgG. Macrophages were labeled with cell tracker red and cells were stained for cortactin and Tks5. (**B**) Quantitation of the relative number of invadopodia per cell in MTLn3 cells plated alone or with Mϕ and treated with control IgG or Notch1 blocking IgG. (**C**) Dendra2-MTLn3 xenograph mammary tumors in SCID nice were imaged using a mammary imaging window. Regions in vascularized areas were photo-converted in mice treated with control IgG or Notch1 blocking IgG. Photo-converted cells were tracked at 0 and 24 hours. (**D**) Quantitation of the percent of red photo-converted cells remaining in the photo-converted region at 24 hours measures amount of intravasation. (**E**) Quantitation of the circulating tumor cells from SCID mice with MTLn3 xenographs. Mice were treated with control IgG or Notch1 blocking IgG. $^{*}P < 0.05$, $^{**}P < 0.005$, $^{***}P < 0.0005$.

endothelial cells[2]. In this study we define the molecular mechanism by which the direct contact between macrophages and tumor cells leads to invadopodium formation and transendothelial migration. We show that these events require the Notch1 receptor on the tumor cell and that Notch1 signaling induces Mena^{INV} expression via activation of transcription. We found that Notch1 is required for transendothelial migration of tumor cells and

dissemination of tumor cells from the primary tumor. These results are consistent with previous work showing that Mena^{INV} expression is required for transendothelial migration by tumor cells[1], that the knockdown of Mena^{INV} inhibits macrophage-mediated transendothelial migration of tumor cells[1] and, conversely, that Mena^{INV} over-expression drives invadopodium assembly and function, and transendothelial migration[10].

The relative expression of Mena^{INV} to that of Mena11a is associated with TMEM assembly, metastatic recurrence and death of breast cancer patients[1,39,40]. This is significant because TMEM is the doorway for intravasation of tumor cells into the blood vessels in breast tumors and the number of TMEM sites in a breast tumor is highly predictive of risk of distant recurrence in patients[3,4]. Previous work demonstrated the signals that lead to decreased expression of Mena11a[11]. However, until now the signals responsible for the induction of Mena^{INV} were not known. Here we show that the expression of the Mena^{INV} isoform is induced by activation of Notch1 signaling in tumor cells. In this regard our findings indicate a novel role for Notch1 signaling in the regulation of Mena^{INV} expression and transendothelial migration at TMEM sites.

The induction of invadopodia in tumor cells by macrophages identifies an important step in tumor cell dissemination. Invadopodia are F-actin-rich protrusions on tumor cells capable of degrading extracellular matrix and assisting in tumor cell chemotaxis and migration[41]. Invadopodium initiation has been described during tumor hypoxia emphasizing the importance of the tumor microenvironment in the regulation of invasive protrusion initiation and function[25]. While tumor cells form invadopodia in response to both growth factor and integrin signaling[29,42,43] our studies described herein show, for the first time, that macrophages can initiate invadopodium assembly and this requires Notch signaling uniquely. These results emphasize selectivity differences in how invadopodia are initiated, and the importance of the tumor microenvironment in determining the different invadopodium functions that result from differences in how invadopodia are initiated; chemotaxis during invasive migration involving invadopodium initiation in response to growth factors[44], fibronectin directed invasion involving invadopodium initiation by integrin beta-1[43], and transendothelial migration as described here involving invadopodium initiation via Notch signaling in response to heterotypic cancer cell-macrophage contact.

The analysis of the gene expression pattern of migratory and disseminating tumor cells in breast tumors revealed an "invasion signature" that is associated with distant recurrence in breast cancer patients[5,35,37]. A prominent pathway in the invasion signature is the Mena–Cofilin pathway that regulates actin polymerization during chemotaxis and invasion of tumor cells[9,34,45] and which is associated with poor outcome in breast cancer patients[39,40,46]. Investigation of the gene expression pathways of the invasion signature revealed that differentially spliced Mena^{INV} is upregulated, while the invasion-suppressing Mena11a isoform is downregulated in migratory/disseminating tumor cells[6,8–10,35,37,47]. This isoform splicing pattern of Mena (Mena$^{INV\text{-}high}$/Mena11a^{low}) is associated with directional cell migration towards chemotactic factors such as EGF and HGF, matrix degradation, TMEM assembly and transendothelial migration[8,10,34,35,37,48], as well as poor outcome in breast cancer patients[5,39,40]. In addition, Mena^{INV} dramatically increases the sensitivity of receptor tyrosine kinases to their ligands EGF, IGF1 and HGF to increase cell protrusion and locomotion of tumor cells toward blood vessels[9,10,49].

Previous studies have shown that heterotypic interactions among cells surrounding intratumoral vasculature can promote cancer cell dissemination. For example, fibroblast-derived lysly oxidase, a matrix cross-linking enzyme that stiffens collage fibers, driven by myeloid cell-derived TGFβ, promotes cancer metastasis[50]. Another study demonstrated involvement of endosialin-expressing pericytes in cancer cell transendothelial migration and dissemination[51]. Endothelial cells are also actively involved in regulation of cancer cell dissemination. The interaction of CXCR12 (SDF-1), secreted by endothelial cells, with tumor cell expressed CXCR4 is sufficient to stimulate transendothelial migration of the tumor cells[52]. Interestingly, the induction of SDF-1 in endothelial cells seems to be mediated by hypoxia. CXCL12 (SDF-1) can also be expressed by tumor cells and it results in increased macrophage and microvessel density and *in vivo* invasiveness[53]. Increased macrophage density has been shown to contribute to cancer cell invasiveness and metastasis as shown by several laboratories including ours[1,2,13,54]. The presence of macrophages greatly enhances the ability of both tumor cell lines and primary breast tumor cells to undergo intravasation-directed transendothelial migration (iTEM) and that iTEM requires Mena^{INV} expression and invadopodium formation[1,10,13]. Our study here has added the mechanistic insight into how Mena^{INV} upregulation is achieved in tumor cells and opens the future exploration of how different macrophage ligands might activate Notch signaling on tumor cells to lead to phenotypes associated with tumor metastasis.

Our results are directly relevant to how Mena isoform expression and TMEM number can predict distant recurrence in breast cancer patients[3–5,39,40]. The molecular characterization of the Notch1 - dependent Mena^{INV} expression shown here opens the possibility of developing additional markers that might be used in combination with TMEM sites to better predict the risk of distant metastatic recurrence of breast cancer patients and their response to treatment. We think that combining measures of Mena^{INV} expression with the presence of TMEM sites could be useful in determining the relative activity of TMEM sites in transendothelial migration and the response to inhibitors designed to suppress either Mena^{INV} expression and/or TMEM activity. Further work will be required to explore this possibility in patient cohorts of known outcome.

The spatial heterogeneity of expression of Mena^{INV} in primary mammary tumor cells and its consequences has been well described in previous studies[8,10,34,55]. However, the mechanisms regulating Mena^{INV} have remained unknown until now. Our finding of the increased expression of Mena^{INV} in response to Notch1 signaling between tumor cells and macrophages, but not between tumor cells and endothelial cells, restricts the origin of Mena^{INV} expression in the TMEM tumor cell, and therefore invadopodium assembly[34], to the macrophage-tumor cell interaction. This leaves open the question about the myeloid cell type specificity of the induction of Mena^{INV} expression and invadopodia in tumor cells. In this regard neutrophils have been tested for their ability to induce invadopodia and transendothelial migration in a previous study and fail to do either[13]. Of relevance to the macrophage subtypes involved in tumor cell invasion and intravasation, the myeloid cells associated with tumor cells in mammary tumors during invasive migration resulting in intravasation[56] are CD11b positive (a classical myeloid lineage marker) and GR1 negative (neutrophil marker) further excluding neutrophils from association

with these particular tumor cells[57]. Furthermore, the CD11b positive tumor cell associated myeloid cells have been expression profiled to determine their identity as invasive macrophages[57]. High resolution intravital imaging has shown that transendothelial migration of tumor cells resulting in intravasation in mammary tumors occurs only in association with these invasive macrophages at TMEM. Furthermore, conditional depletion of the macrophages and/or knock out of the macrophage specific VEGF gene completely blocks intravasation *in vivo*[2] further implicating macrophages in intravasation.

There is significant interest in targeting Notch1 signaling for the treatment of a number of cancers but previous studies have shown chronic Notch inhibition can lead to detrimental secondary effects and in some cases increased vascular tumor development[21,58]. Therefore, further study of the mechanisms of Notch1 signaling in breast cancer progression, as we show here, might lead to the identification of novel therapeutic targets within the Notch1 signaling cascade that might be better tolerated in patients.

Methods

Cell Lines and Reagents. MDA-MB-231 cells were cultured in DMEM supplemented with 10% FBS and antibiotics. MDA-MB-231 cells were serum-starved in DMEM supplemented with 0.5% FBS/0.8% BSA 16 h before macrophage induction studies. MTLn3 cells, derived from the 13762NF rat mammary adenocarcinoma, were cultured in α-MEM supplemented with 5% FBS and antibiotics. MTLn3 cells were serum-starved in α-MEM supplemented with 0.5% FBS/0.8% BSA 4 h before macrophage induction studies. BAC1.2F5 cells were cultured in MEM supplemented with 10% FBS, 2 mm l-glutamine, 22 μg/ml l-asparagine and 3000 U/ml of purified human recombinant CSF-1 (generously provided by Richard Stanley, Albert Einstein College of Medicine). Human umbilical vein endothelial cells (HUVECs, Lonza, Allendale, NJ, USA) were cultured in EGM-2 (Lonza, Allendale, NJ, USA) and only used between passage 1–4. DAPT (Sigma 10 μM) was used for gamma-secretase inhibition experiments as indicated in the results. When used, the DAPT or vehicle was added at the beginning of the experiments. Notch1 function blocking antibody (R&D Systems) was used *in vitro* at 5 μg/mL and *in vivo* via intraperitoneal injection at 1 mg/kg.

siRNA. Control non-silencing siRNA was from Qiagen. Human-specific Notch1 siRNA pool was from Dharmacon and panMena and Mena^{INV} siRNA from Ambion[1]. A total of 1 × 106 MDA-MB-231 cells were transfected with 2 μm siRNA using the Lonza Nucleofection Kit V 72 h before each experiment. Immunoblot analysis and/or qPCR were performed to confirm knockdown for each experiment.

Assay for Detection of Invadopodia. The 405 gelatin-labeled Mattek dishes were prepared as previously described[43,59]. Tumor cells were plated in complete media for 6 h on the Alexa 405-labeled gelatin dishes. Dishes were fixed and immunostained for cortactin and Tks5 as previously described. Cells were imaged on a wide-field microscope (Inverted Olympus IX70) and images were acquired with a cooled CCD camera (Sensicam QE cooled CCD camera) with a 60 × NA = 1.4 oil immersion objective using IP Laboratory 4.0 software. Invadopodia were detected as punctate structures that were positive for both cortactin and tks5 and capable of degrading Alexa 405-gelatin.

To detect macrophage-induced invadopodia, MDA-MB-231 cells were serum-starved for 16 h. BAC1.2F5 cells were cell tracker-labeled (CMPTX, Invitrogen). A total of 25 K MDA-MB-231 cells were incubated with 125 K BAC1.2F5 cells in serum-starvation media on 405-labeled gelatin-coated dishes for 6 h, fixed and immunostained for invadopodium markers as described above. For MTLn3 experiments, tumor cells were serum starved for 4 hrs before being plated with BAC1.2F5 cells for 6 hrs as described above.

qPCR. qRT-PCR for Mena splice variants was performed as described previously[35]. Briefly, the data analysis was conducted using the ΔΔCt method in which all *MENA* Ct values in the carcinoma samples were first normalized to *GAPDH*. qRT-PCR analyses were performed using a SyBR Green kit (Qiagen) and analyzed with a Qiagene Rotor Gene-Q detector and associated software.

Fine Needle Aspiration Biopsy. For primary cancer cells from two human invasive ductal carcinomas fine needle aspiration (FNA) was completed as previously described[1]. Briefly, lumpectomy and mastectomy specimens received at the Albert Einstein College of Medicine/Montefiore Medical Center, Moses and Weiler Divisions for pathological examination were used for FNA-based tissue collection under institutional review board approval. Four to five FNA aspiration biopsies per tumor were performed on grossly visible lesions using 25-gauge needles.

The TN human tissue transplant HT17 was previously described[1,37]. Briefly, the tumor originated from human patient samples and have since only been propagated in SCID mice. Tumors were harvested once they reached 1- to 1.2-cm diameter. Cells were obtained by FNA from human tumors grown in mice. All procedures were conducted in accordance with the NIH regulations and approved by the Albert Einstein College of Medicine animal use committee.

FISH. *In Situ Probes.* 48 oligodeoxynucleotide probes for MENA were designed with online Stellaris RNA FISH probe designer (Biosearch Tehchnologies). Each probe was 20 nt long and contained a 5′ amino-modified nucleotide that was chemically coupled to CAL Fluor 610 fluorescent dye. The sequences for probes used to detect MENA mRNA are provided in Supplementary Information.

In Situ Hybridization. For FISH experiments, MDA-MB-231 cells we starved overnight as described above. Tumor cells were plated in the presence or absence of BAC1.2F5 macrophages that were labeled with cell-tracker red on glass coverslips for 1 h then fixed with 4% paraformaldehyde for 20 minutes at room temperature. After washing away the fixative, the cells were stored in 70% (v/v) ethanol at 4 °C. Prior to hybridiazation, stored coverslips were washed with 1 × PBS and pretreated with 10% formamide/2 × SSC at room temperature for 5 minutes.

The converslips were then inverted onto 20 μl of hybridization solution containing MENA FISH probes (0.125 μM), dextran sulfate (10%), 2xSSC, 10% formamide, *E. Coli* tRNA (1 mg/ml), vanadyl ribonucleoside complex (0.2 mg/ml), and bovine serum albumin (0.2 mg/ml). The cells were hybridized for 3 hours at 37 °C and washed with 10% formamide/2xSSC. The nuclei were stained with DAPI and the coverslips were then mounted with ProLong Gold antifade reagent (Invitrogen).

Image Acquisition and Analysis. Images were acquired on an Olympus BX61 epi-fluorescence microscope with an UPlanApo 60x, 1.35 numerical aperture oil immersion objective (Olympus). X-Cite 120 PC (EXFO) light source was used for illumination with filter sets 31000 (DAPI), 41001 (Cell-tracker Green), and SP-103v1 (CAL Fluor 610) (Chroma Technology). Vertical stacks of 30 images with a Z step size of 0.2 μm were acquired using a CoolSNAP HQ camera (Photometrics) with 6.4 μm pixel size CCD. IPLab (BD Biosciences) software platform was used for instrument control as well as image acquisition. Automated detection and counting of mRNAs was performed by fitting Gaussians to fluorescent spots with FISH-quant as described previously[60,61].

Production of Mena^{INV} antibody. Chicken poly-clonal antibodies were generated by Covance. Animals were immunized with a peptide containing the unique Mena^{INV} INV exon sequence.

Western blots of cell lysates from MDA-MB-231 cells expressing either GFP or GFP- Mena^{INV}, when stained with the affinity purified anti-Mena^{INV} IgY, contain a single faint endogenous Mena^{INV} band in both cell types as described previously[55] and a more intense band for GFP- Mena^{INV} in the over-expressing cells consistent with the specificity of this antibody (Supplemental Figure 4A). In addition, *in situ* immunofluorescent staining of mammary tumor tissue from WT and Mena Null PyMT mice demonstrate specificity of the antibody, where the WT tissue shows the presence of Mena^{INV} positive tumor cells while there is no staining above background in the Mena Null tissue[62] (Supplemental Figure 4B).

Transendothelial Migration Assay (iTEM). The transendothelial migration assay was performed as described previously[1,13] and briefly described here. The transwell was prepared so that tumor cell transendothelial migration was in the intravasation direction (from subluminal side to luminal side of the endothelium). We measure transendothelial migration as the intravasation-directed transendothelial migration (iTEM) from the tissue to the blood side of the endothelium. To prepare the endothelial monolayer, the underside of each transwell was coated with 50 μl of Matrigel (2.5 μg/ml; Invitrogen). Approximately 100,000 HUVEC cells were plated on the Matrigel coated underside of the transwells. Transwells were then flipped into a 24-well plate containing 200 μl of EGM-2 and monolayers were formed over a 48 hours period. The integrity of the endothelium used in this assay has been validated using electrical resistance and blockade of diffusion of small molecules[13]. Macrophages and tumor cells were labeled with cell tracker dyes (CMFDA, CMPTX from Invitrogen) before the experiment. Then, 15,000 macrophages and 37,500 tumor cells were added to the upper chamber in 200 μl of DMEM supplemented with 0.5% FBS while the bottom chamber contained EGM-2 supplemented with 3000 u/ml of CSF-1. After 18 hours of transmigration, the tranwells were fixed and stained for ZO-1 as previously described. Transwells were imaged using a Leica SP5 confocal microscope using a 60 × 1.4NA objective and processed using Image J [National Institutes of Health (NIH)]. Quantitation was performed by counting the number of tumor cells that had crossed the endothelium within the same field of view (60x) and represented as normalized values from at least 3 independent experiments. The quantitation of this assay is across at least 3 independent experiments, with 12 fields counted per transwell and transwells done in duplicate for each experiment.

***In vivo* circulating tumor cells and photo-converted tumor cell dissemination assay.** All procedures involving animals were conducted in accordance with NIH regulations, and approved by the Albert Einstein College of Medicine Animal Use Committee.

MTLn3 cells (parental and Dendra2 expressing) were injected into the mammary glands of 5 to 7 well old SCID mice and allowed to grow tumors for 3 weeks, until the tumors reached approximately 0.8–1.0 cm. Circulating tumor cell count was determined as previously described[36]. Briefly, 1 ml of blood was drawn from the right ventricle of anesthetized mice and plated in α-MEM media supplemented with 20% FBS. Tumor cell were counted as plated cells.

For the *in vivo* dissemination assay, a mammary imaging window was implanted and dissemination was measured as previously described[35,36,38]. Briefly, two days after the implantation of the imaging window regions of the tumor located adjacent to blood vessels were photo-converted. Approximately 5 regions were converted per tumor. After the photo-conversion and imaging of the regions (time 0), mice were treated with 1 mg/kg control IgG or Notch1 function blocking IgG (R&D Systems). The photo-converted regions were imaged at 24 hr, 48 hr, and 72 hr post treatment to determine the number of tumor cells that remained in the photo-converted primary tumor. The number of photo-converted cells remaining were counted at each time point and represented as the percent of photo-converted cells remaining compared to time 0. It should be noted that we have previously shown in the mouse mammary tumor model used in this study that the disappearance of photo-converted cells from the primary tumor gives rise to a disseminating population of tumor cells that is observed to arrive in distant organ sites seeding new metastases[14]. Furthermore, the tumor cells that disseminate from the photo-converted site are always associated with blood vessels[38] and require functional invadopodia to disseminate[14]. In addition, the imaging method used to document the disappearance of photo-converted cells detects and counts tumor cells that simply "disperse" away from the conversion site ensuring that the disappearance of converted cells requires their dissemination from the primary tumor.

References

1. Pignatelli, J. *et al.* Invasive breast carcinoma cells from patients exhibit MenaINV- and macrophage-dependent transendothelial migration. *Sci Signal* **7,** ra112, doi: 10.1126/scisignal.2005329 (2014).
2. Harney, A. S. *et al.* Real-Time Imaging Reveals Local, Transient Vascular Permeability, and Tumor Cell Intravasation Stimulated by TIE2hi Macrophage-Derived VEGFA. *Cancer Discov*. **5,** 932–943, doi: 10.1158/2159-8290.CD-15-0012 (2015).
3. Robinson, B. D. *et al.* Tumor microenvironment of metastasis in human breast carcinoma: a potential prognostic marker linked to hematogenous dissemination. *Clin. Cancer. Res.* **15,** 2433–2441, doi: 10.1158/1078-0432.CCR-08-2179 (2009).
4. Rohan, T. E. *et al.* Tumor microenvironment of metastasis and risk of distant metastasis of breast cancer. *J. Natl. Cancer Inst*. **106,** doi: 10.1093/jnci/dju136 (2014).
5. Karagiannis, G. S., Goswami, S., Jones, J. G., Oktay, M. H. & Condeelis, J. S. Signatures of breast cancer metastasis at a glance. *J. Cell Sci.* **129,** 1751–1758, doi: 10.1242/jcs.183129 (2016).
6. Goswami, S. *et al.* Identification of invasion specific splice variants of the cytoskeletal protein Mena present in mammary tumor cells during invasion *in vivo*. *Clin. Exp. Metastasis* **26,** 153–159, doi: 10.1007/s10585-008-9225-8 (2009).
7. Gertler, F. & Condeelis, J. Metastasis: tumor cells becoming MENAcing. *Trends Cell Biol*. **21,** 81–90, doi: 10.1016/j.tcb.2010.10.001 (2011).
8. Roussos, E. T. *et al.* Mena invasive (Mena(INV)) and Mena11a isoforms play distinct roles in breast cancer cell cohesion and association with TMEM. *Clin. Exp. Metastasis* **28,** 515–527, doi: 10.1007/s10585-011-9388-6 (2011).
9. Roussos, E. T., Condeelis, J. S. & Patsialou, A. Chemotaxis in cancer. *Nat. Rev. Cancer* **11,** 573–587, doi: 10.1038/nrc3078 (2011).
10. Roussos, E. T. *et al.* Mena invasive (MenaINV) promotes multicellular streaming motility and transendothelial migration in a mouse model of breast cancer. *J. Cell Sci.* **124,** 2120–2131, doi: 10.1242/jcs.086231 (2011).
11. Shapiro, I. M. *et al.* An EMT-driven alternative splicing program occurs in human breast cancer and modulates cellular phenotype. *PLoS Genet.* **7,** e1002218, doi: 10.1371/journal.pgen.1002218 (2011).
12. Gligorijevic, B. *et al.* N-WASP-mediated invadopodium formation is involved in intravasation and lung metastasis of mammary tumors. *J. Cell Sci.* **125,** 724–734, doi: 10.1242/jcs.092726 (2012).
13. Roh-Johnson, M. *et al.* Macrophage contact induces RhoA GTPase signaling to trigger tumor cell intravasation. *Oncogene* **33,** 4203–4212, doi: 10.1038/onc.2013.377 (2014).
14. Gligorijevic, B., Bergman, A. & Condeelis, J. Multiparametric classification links tumor microenvironments with tumor cell phenotype. *PLoS Biol.* **12,** e1001995, doi: 10.1371/journal.pbio.1001995 (2014).
15. Murphy, D. A. & Courtneidge, S. A. The 'ins' and 'outs' of podosomes and invadopodia: characteristics, formation and function. *Nat. Rev. Mol. Cell Biol.* **12,** 413–426, doi: 10.1038/nrm3141 (2011).
16. Weaver, A. M. Cortactin in tumor invasiveness. *Cancer Lett.* **265,** 157–166, doi: 10.1016/j.canlet.2008.02.066 (2008).
17. Sabeh, F. *et al.* Tumor cell traffic through the extracellular matrix is controlled by the membrane-anchored collagenase MT1-MMP. *J. Cell Biol.* **167,** 769–781, doi: 10.1083/jcb.200408028 (2004).
18. Hotary, K., Li, X. Y., Allen, E., Stevens, S. L. & Weiss, S. J. A cancer cell metalloprotease triad regulates the basement membrane transmigration program. *Genes Dev.* **20,** 2673–2686, doi: 10.1101/gad.1451806 (2006).
19. Stoletov, K., Montel, V., Lester, R. D., Gonias, S. L. & Klemke, R. High-resolution imaging of the dynamic tumor cell vascular interface in transparent zebrafish. *Proc. Natl. Acad. Sci. USA* **104,** 17406–17411, doi: 10.1073/pnas.0703446104 (2007).
20. Condeelis, J. & Segall, J. E. Intravital imaging of cell movement in tumours. *Nat. Rev. Cancer* **3,** 921–930, doi: 10.1038/nrc1231 (2003).
21. Han, J., Hendzel, M. J. & Allalunis-Turner, J. Notch signaling as a therapeutic target for breast cancer treatment? *Breast Cancer Res*. **13,** 210, doi: 10.1186/bcr2875 (2011).
22. Bolos, V. *et al.* Notch activation stimulates migration of breast cancer cells and promotes tumor growth. *Breast Cancer Res*. **15,** R54, doi: 10.1186/bcr3447 (2013).
23. Reedijk, M. *et al.* High-level coexpression of JAG1 and NOTCH1 is observed in human breast cancer and is associated with poor overall survival. *Cancer Res.* **65,** 8530–8537, doi: 10.1158/0008-5472.CAN-05-1069 (2005).
24. Andrieu, G., Tran, A. H., Strissel, K. J. & Denis, G. V. BRD4 regulates breast cancer dissemination through Jagged1/Notch1 signaling. *Cancer Res.*, doi: 10.1158/0008-5472.CAN-16-0559 (2016).
25. Diaz, B., Yuen, A., Iizuka, S., Higashiyama, S. & Courtneidge, S. A. Notch increases the shedding of HB-EGF by ADAM12 to potentiate invadopodia formation in hypoxia. *J. Cell Biol.* **201,** 279–292, doi: 10.1083/jcb.201209151 (2013).
26. Andersson, E. R. & Lendahl, U. Therapeutic modulation of Notch signalling–are we there yet? *Nat. Rev. Drug Discov.* **13,** 357–378, doi: 10.1038/nrd4252 (2014).
27. Sharma, V. P. *et al.* Tks5 and SHIP2 regulate invadopodium maturation, but not initiation, in breast carcinoma cells. *Curr. Biol.* **23,** 2079–2089, doi: 10.1016/j.cub.2013.08.044 (2013).
28. Beaty, B. T. & Condeelis, J. Digging a little deeper: the stages of invadopodium formation and maturation. *Eur. J. Cell Biol.* **93,** 438–444, doi: 10.1016/j.ejcb.2014.07.003 (2014).
29. Beaty, B. T. *et al.* Talin regulates moesin-NHE-1 recruitment to invadopodia and promotes mammary tumor metastasis. *J. Cell Biol.* **205,** 737–751, doi: 10.1083/jcb.201312046 (2014).
30. Bravo-Cordero, J. J., Hodgson, L. & Condeelis, J. S. Spatial regulation of tumor cell protrusions by RhoC. *Cell Adh Migr* **8,** 263–267 (2014).
31. Bravo-Cordero, J. J. *et al.* Spatial regulation of RhoC activity defines protrusion formation in migrating cells. *J. Cell Sci.* **126,** 3356–3369, doi: 10.1242/jcs.123547 (2013).
32. Mader, C. C. *et al.* An EGFR-Src-Arg-cortactin pathway mediates functional maturation of invadopodia and breast cancer cell invasion. *Cancer Res.* **71,** 1730–1741, doi: 10.1158/0008-5472.CAN-10-1432 (2011).
33. Moshfegh, Y., Bravo-Cordero, J. J., Miskolci, V., Condeelis, J. & Hodgson, L. A Trio-Rac1-Pak1 signalling axis drives invadopodia disassembly. *Nat. Cell Biol.* **16,** 574–586, doi: 10.1038/ncb2972 (2014).
34. Philippar, U. *et al.* A Mena invasion isoform potentiates EGF-induced carcinoma cell invasion and metastasis. *Dev. Cell* **15,** 813–828, doi: 10.1016/j.devcel.2008.09.003 (2008).
35. Patsialou, A. *et al.* Intravital multiphoton imaging reveals multicellular streaming as a crucial component of *in vivo* cell migration in human breast tumors. *Intravital* **2,** e25294, doi: 10.4161/intv.25294 (2013).
36. Wyckoff, J. B. *et al.* Direct visualization of macrophage-assisted tumor cell intravasation in mammary tumors. *Cancer Res.* **67,** 2649–2656, doi: 10.1158/0008-5472.CAN-06-1823 (2007).
37. Patsialou, A. *et al.* Selective gene-expression profiling of migratory tumor cells *in vivo* predicts clinical outcome in breast cancer patients. *Breast Cancer Res.* **14,** R139, doi: 10.1186/bcr3344 (2012).
38. Kedrin, D. *et al.* Intravital imaging of metastatic behavior through a mammary imaging window. *Nat. Methods* **5,** 1019–1021, doi: 10.1038/nmeth.1269 (2008).
39. Forse, C. L. *et al.* Menacalc, a quantitative method of metastasis assessment, as a prognostic marker for axillary node-negative breast cancer. *BMC Cancer* **15,** 483, doi: 10.1186/s12885-015-1468-6 (2015).
40. Agarwal, S. *et al.* Quantitative assessment of invasive mena isoforms (Menacalc) as an independent prognostic marker in breast cancer. *Breast Cancer Res.* **14,** R124, doi: 10.1186/bcr3318 (2012).
41. Bravo-Cordero, J. J., Hodgson, L. & Condeelis, J. Directed cell invasion and migration during metastasis. *Curr. Opin. Cell Biol.* **24,** 277–283, doi: 10.1016/j.ceb.2011.12.004 (2012).

42. Yamaguchi, H. *et al.* Molecular mechanisms of invadopodium formation: the role of the N-WASP-Arp2/3 complex pathway and cofilin. *J. Cell Biol.* **168,** 441–452, doi: 10.1083/jcb.200407076 (2005).
43. Beaty, B. T. *et al.* beta1 integrin regulates Arg to promote invadopodial maturation and matrix degradation. *Mol. Biol. Cell* **24,** 1661–1675, S1661-1611, doi: 10.1091/mbc.E12-12-0908 (2013).
44. Desmarais, V. *et al.* N-WASP and cortactin are involved in invadopodium-dependent chemotaxis to EGF in breast tumor cells. *Cell Motil. Cytoskeleton* **66,** 303–316, doi: 10.1002/cm.20361 (2009).
45. Bravo-Cordero, J. J., Magalhaes, M. A., Eddy, R. J., Hodgson, L. & Condeelis, J. Functions of cofilin in cell locomotion and invasion. *Nat. Rev. Mol. Cell Biol.* **14,** 405–415, doi: 10.1038/nrm3609 (2013).
46. Weitsman, G. *et al.* Imaging tumour heterogeneity of the consequences of a PKCalpha-substrate interaction in breast cancer patients. *Biochem. Soc. Trans.* **42,** 1498–1505, doi: 10.1042/BST20140165 (2014).
47. Wang, W. *et al.* Identification and testing of a gene expression signature of invasive carcinoma cells within primary mammary tumors. *Cancer Res.* **64,** 8585–8594, doi: 10.1158/0008-5472.CAN-04-1136 (2004).
48. Patsialou, A. & Condeelis, J. S. Metastatic cells: moving onco-targets. *Oncotarget* **5,** 3424–3425, doi: 10.18632/oncotarget.2057 (2014).
49. Hughes, S. K. *et al.* PTP1B-dependent regulation of receptor tyrosine kinase signaling by the actin-binding protein Mena. *Mol. Biol. Cell* **26,** 3867–3878, doi: 10.1091/mbc.E15-06-0442 (2015).
50. Pickup, M. W. *et al.* Stromally derived lysyl oxidase promotes metastasis of transforming growth factor-beta-deficient mouse mammary carcinomas. *Cancer Res.* **73,** 5336–5346, doi: 10.1158/0008-5472.CAN-13-0012 (2013).
51. Viski, C. *et al.* Endosialin-Expressing Pericytes Promote Metastatic Dissemination. *Cancer Res.* **76,** 5313–5325, doi: 10.1158/0008-5472.CAN-16-0932 (2016).
52. Jin, F., Brockmeier, U., Otterbach, F. & Metzen, E. New insight into the SDF-1/CXCR4 axis in a breast carcinoma model: hypoxia-induced endothelial SDF-1 and tumor cell CXCR4 are required for tumor cell intravasation. *Mol. Cancer Res.* **10,** 1021–1031, doi: 10.1158/1541-7786.MCR-11-0498 (2012).
53. Boimel, P. J. *et al.* Contribution of CXCL12 secretion to invasion of breast cancer cells. *Breast Cancer Res.* **14,** R23, doi: 10.1186/bcr3108 (2012).
54. Pollard, J. W. Macrophages define the invasive microenvironment in breast cancer. *J. Leukoc. Biol.* **84,** 623–630, doi: 10.1189/jlb.1107762 (2008).
55. Oudin, M. J. *et al.* Characterization of the expression of the pro-metastatic Mena(INV) isoform during breast tumor progression. *Clin. Exp. Metastasis* **33,** 249–261, doi: 10.1007/s10585-015-9775-5 (2016).
56. Wyckoff, J. *et al.* A paracrine loop between tumor cells and macrophages is required for tumor cell migration in mammary tumors. *Cancer Res.* **64,** 7022–7029, doi: 10.1158/0008-5472.CAN-04-1449 (2004).
57. Ojalvo, L. S., Whittaker, C. A., Condeelis, J. S. & Pollard, J. W. Gene expression analysis of macrophages that facilitate tumor invasion supports a role for Wnt-signaling in mediating their activity in primary mammary tumors. *J. Immunol.* **184,** 702–712, doi: 10.4049/jimmunol.0902360 (2010).
58. Ryeom, S. W. The cautionary tale of side effects of chronic Notch1 inhibition. *J. Clin. Invest.* **121,** 508–509, doi: 10.1172/JCI45976 (2011).
59. Bravo-Cordero, J. J. *et al.* A novel spatiotemporal RhoC activation pathway locally regulates cofilin activity at invadopodia. *Curr. Biol.* **21,** 635–644, doi: 10.1016/j.cub.2011.03.039 (2011).
60. Mueller, F. *et al.* FISH-quant: automatic counting of transcripts in 3D FISH images. *Nat. Methods* **10,** 277–278, doi: 10.1038/nmeth.2406 (2013).
61. Kelly, T., Mueller, S. C., Yeh, Y. & Chen, W. T. Invadopodia promote proteolysis of a wide variety of extracellular matrix proteins. *J. Cell. Physiol.* **158,** 299–308, doi: 10.1002/jcp.1041580212 (1994).
62. Roussos, E. T. *et al.* Mena deficiency delays tumor progression and decreases metastasis in polyoma middle-T transgenic mouse mammary tumors. *Breast Cancer Res.* **12,** R101, doi: 10.1186/bcr2784 (2010).

Acknowledgements

This work was supported by grants from the NIH: (CA150344 and CA100324 to J.S.C., X.C. and R.J.E.), (CA170507–01 to M.H.O.), (F32CA159663 to M.R.J.), (R01EB13571 to R.H.S.), (CA205262 to L.H.), (K22CA196750 to J.J.B.C.) the Department of Defense Breast Cancer Research Program (W81XWH-14-1-0286 to J.P.), the TCI Young Scientist Cancer Research Award JJR Fund to J.J.B.C. and the Albert Einstein College of Medicine Integrated Imaging Program.

Author Contributions

J.P. designed the experimental approach, performed the experimental work, analyzed and interpreted the data, coordinated the project and wrote the manuscript. J.J.B.C. designed the experimental approach, performed invadopodia assays and *in vivo* work, analyzed and interpreted data and edited the manuscript. M.R.J. designed experimental approach and performed invadopodia assays. S.J.G. designed FISH probes and carried out FISH experiments and interpreted the data. Y.W. performed animal handling, *in vivo* work and associated techniques. X.C. preformed purification and testing of the Mena^{INV} specific antibody. R.J.E. designed and preformed quality control on the Mena^{INV} specific antibody. A.X. preformed tissue staining with the Mena^{INV} antibody. R.S. assisted in the development of FISH probes. L.H. contributed to data interpretation and discussion. J.S.C. and M.H.O. conceived the hypothesis, designed the experimental approach, led the project, interpreted the data and wrote the manuscript. All authors reviewed the manuscript.

Additional Information

Supplementary information accompanies this paper at http://www.nature.com/srep

Competing financial interests: J.S. Condeelis has ownership interest (including patents) in MetaStat; and is a consultant/advisory board member for Deciphera and MetaStat. No potential conflicts of interest were disclosed by the other authors.

How to cite this article: Pignatelli, J. *et al.* Macrophage-dependent tumor cell transendothelial migration is mediated by Notch1/Mena^{INV}-initiated invadopodium formation. *Sci. Rep.* **6**, 37874; doi: 10.1038/srep37874 (2016).

Macrophage-dependent tumor cell transendothelial migration is mediated by Notch1/Mena^{INV} -initiated invadopodium formation

Jeanine Pignatelli[1,2,4]#*, Jose Javier Bravo-Cordero[1,2,5]#, Minna Roh-Johnson[1,2,6], Saumil J. Gandhi[1], Yarong Wang[1,2], Xiaoming Chen[1], Robert J. Eddy[1], Alice Xue[1], Robert H. Singer[1], Louis Hodgson[1,2], Maja H. Oktay[1,3]*, and John S. Condeelis[1,2]*

[1]Department of Anatomy and Structural Biology Albert Einstein College of Medicine of Yeshiva University, Bronx, NY 10461, [2] Gruss Lipper Biophotonics Center Albert Einstein College of Medicine of Yeshiva University, Bronx, NY 10461, [3]Department of Pathology Albert Einstein College of Medicine of Yeshiva University, Bronx, NY 10461, [4]Current Address: Pfizer Oncology Targeted Therapeutics Division, 401 N Middletown Rd, Pearl River, NY 10965, [5]Current Address: Division of Hematology and Oncology, Department of Medicine, Mount Sinai School of Medicine, Tisch Cancer Institute, New York, NY, [6]Current Address: Fred Hutchinson Cancer Research Center, Basic Sciences Division, 1100 Fairview Ave N, Seattle, WA 98109

# These authors contributed equally.

*Corresponding authors

*Correspondence to jeanine.pignatelli@pfizer.com, maja.oktay@einstein.yu.edu and john.condeelis@einstein.yu.edu

Supplemental Figure 1

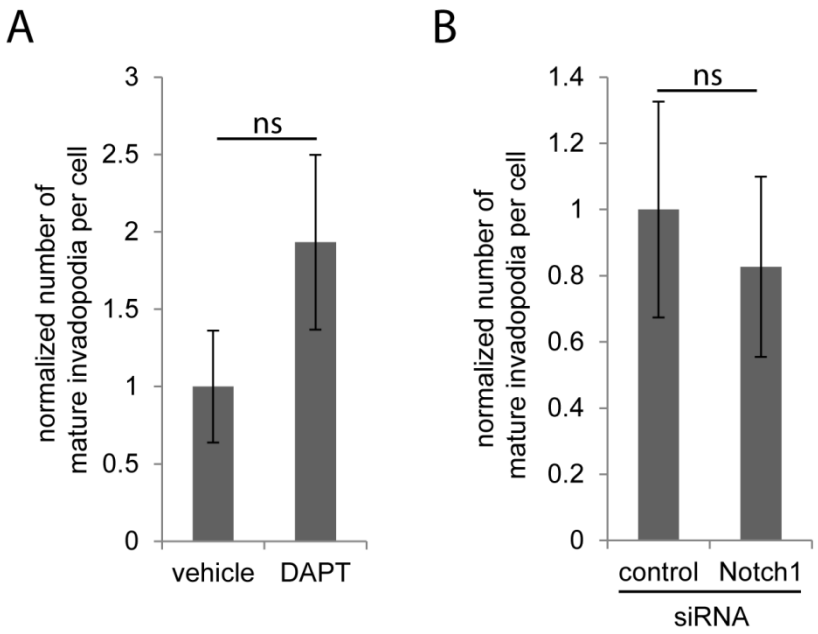

Supplemental Figure 1: Notch1 is not required for the formation of spontaneous tumor cell invadopodia in the absence of macrophages. (A) Quantitation of the number of mature invadopodia per cell in MDA-MB-231 cells plated on gelatin with the addition of vehicle or DAPT γ- secretase inhibitor. **(B)** Quantitation of the number of mature invadopodia per cell in MDA-MB-231 cells on gelatin treated with control or Notch1 siRNA. *ns = not significant*.

Supplemental Figure 2

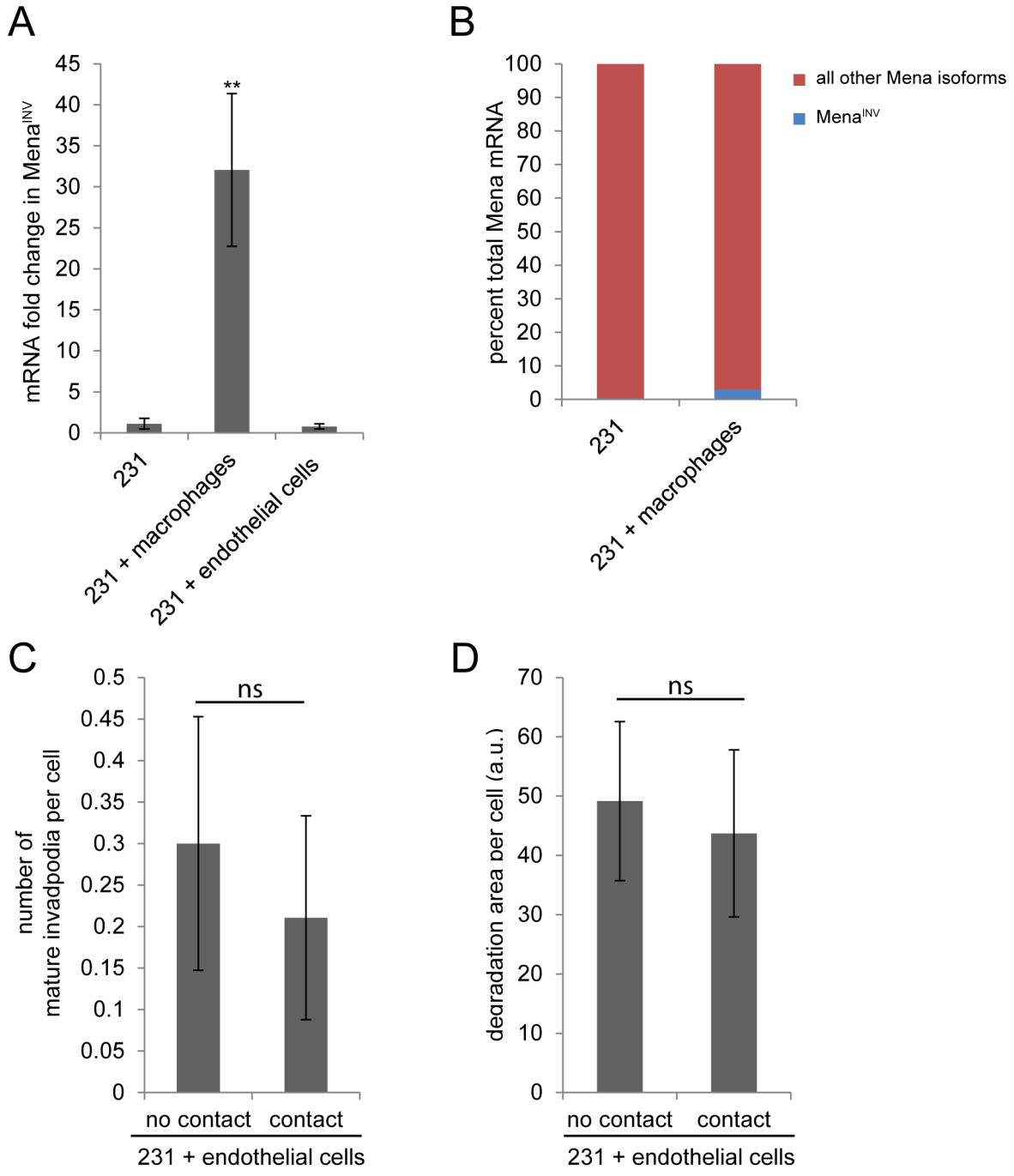

Supplemental Figure 2: Macrophages are the specific TMEM cell that induces Mena^{INV} expression in tumor cells. (A) Mena^{INV} expression occurs only in response to tumor cell contact with macrophages. mRNA fold expression change is shown in response to co-culture of tumor cells with either tumor cell (231), macrophages or endothelial cells. **(B)** Quantification of

the percent of Mena^{INV} isoform mRNA compared to the total of all Mena isoforms (panMena) in MDA-MB-231 cells plated alone or with BAC1.2F5 macrophages indicating that Mena^{INV} is present as less than 5% of panMena. **(C)** Quantitation of the number of mature invadopodia per cell in MDA-MB-231 tumor cells plated with HUVEC primary endothelial cells with the two cell types either not in contact or in contact with each other. **(D)** Quantitation of the area of matrix degradation in MDA-MB-231 cells plated with HUVEC primary endothelial cells with the two cell types either not in contact or in contact with each other. *ns* = *not significant*. $^{**}P < 0.005$

Supplemental Figure 3

A

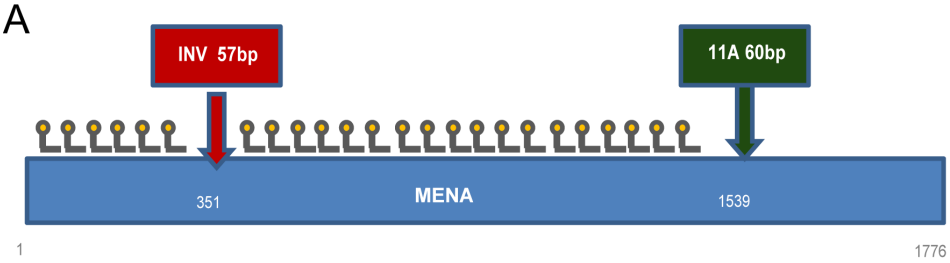

B

MENA FISH Probes

Probe (5'-> 3')	Probe Position*	Percent GC
cctgacagatactctgttca	6	45.00%
taaaccatcacagcagctct	28	45.00%
ccacttcttattggcatcat	50	40.00%
ctctgctgaatccagttgag	84	50.00%
gcctgtatggtgatagatat	107	40.00%
ccaccactctgaatgtgttg	129	50.00%
tgatggtcctgaatcttcct	151	45.00%
ggaatggcacagtttatcac	175	45.00%
ttgattgtacttcaaccctt	197	35.00%
actggtggaaggtctgtgta	219	50.00%
atacacctgtctagcatctc	242	45.00%
tctttgctgccaaagttgag	265	45.00%
acttgcgaagacattggcat	287	45.00%
acacttctaaggcatgcatc	312	45.00%
tttgtctaggcaatgttggc	351	45.00%
acttgagcaggtagttgtga	373	45.00%
ttcttgggatgggccatttt	395	45.00%
gttgtcttctttgaatttcc	420	35.00%
ttttgccgttgctgttcttg	442	45.00%
tttctctttccattctttct	489	30.00%
ctttctaacctctctctctc	514	45.00%
cgttcttgtctctctctctc	574	50.00%
tctcgttcttgtctttcttg	679	40.00%
ctttctaactgctcttgtcg	739	45.00%
acttgatattctgcgctctc	779	45.00%
agtctcaacagaggcagggg	806	60.00%
ctcccagcacagagtttaga	828	50.00%
cctggctcagaagcagaaga	850	55.00%
ctgttgggatggagtctcgg	893	60.00%
caagtggtcccaagacaatg	915	50.00%
gccaaaaagaatccagatgc	1120	45.00%
gcgattgtcttctgacatgg	1142	50.00%
cagctgcaagtccagttaaa	1164	45.00%
cactttcctaagttttgctc	1193	40.00%
cttgggaaagaggtatcctc	1222	50.00%
ggagttcacaccaatagcat	1250	45.00%
gcctgtatctgttttagatg	1274	40.00%
ctaaaggaaggggtccattt	1299	45.00%
tcttccattaaaccactacc	1321	40.00%
tttcagcaattcttctcctc	1362	40.00%
tctgtttctattgttgatcc	1384	35.00%
ttcaccttgtcctcttttt	1406	35.00%
ccttagaagttacaggctct	1431	45.00%
tcaggtgtacttgttgaaga	1453	40.00%
ttcccaaggttttcttgttg	1475	40.00%
tgccattcattgtatttgtt	1497	30.00%
ctggagataacaggtgactt	1519	45.00%
atttttccttggagaatccc	1541	40.00%

C

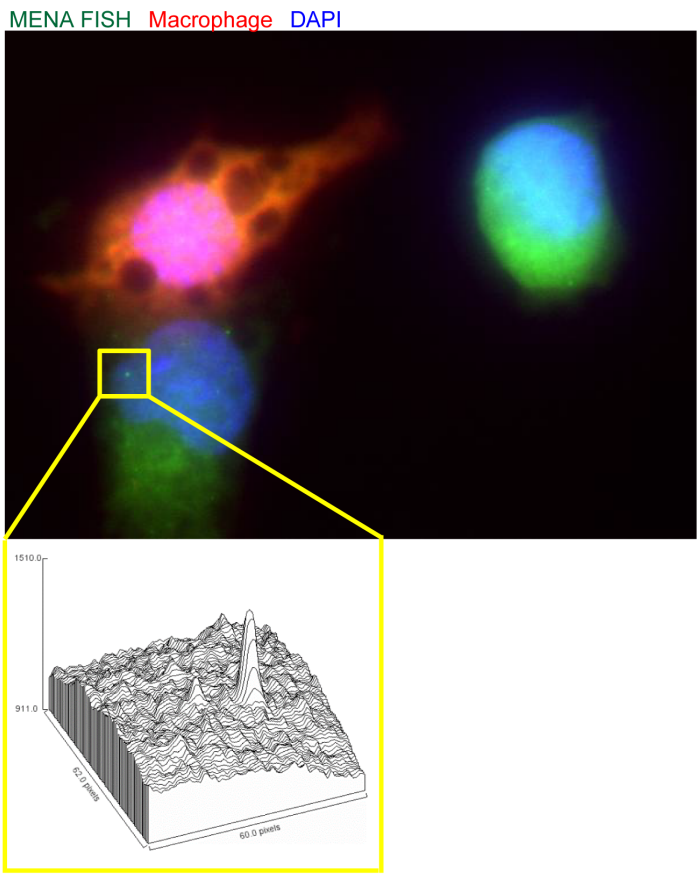

Supplemental Figure 3: Design of MENA FISH probes. (A) Schematic of FISH probes binding on MENA RNA. (B) Table of MENA FISH probes used (probe sequence, position on MENA, and percent GC). (C) MENA FISH in MDA-MB-231 cells with and without contact with macrophages (green is MENA FISH probes, macrophages are labeled with cell tracker red and blue is DAPI). Yellow box demonstrates active transcription site with florescence intensity above background.

Supplemental Figure 4

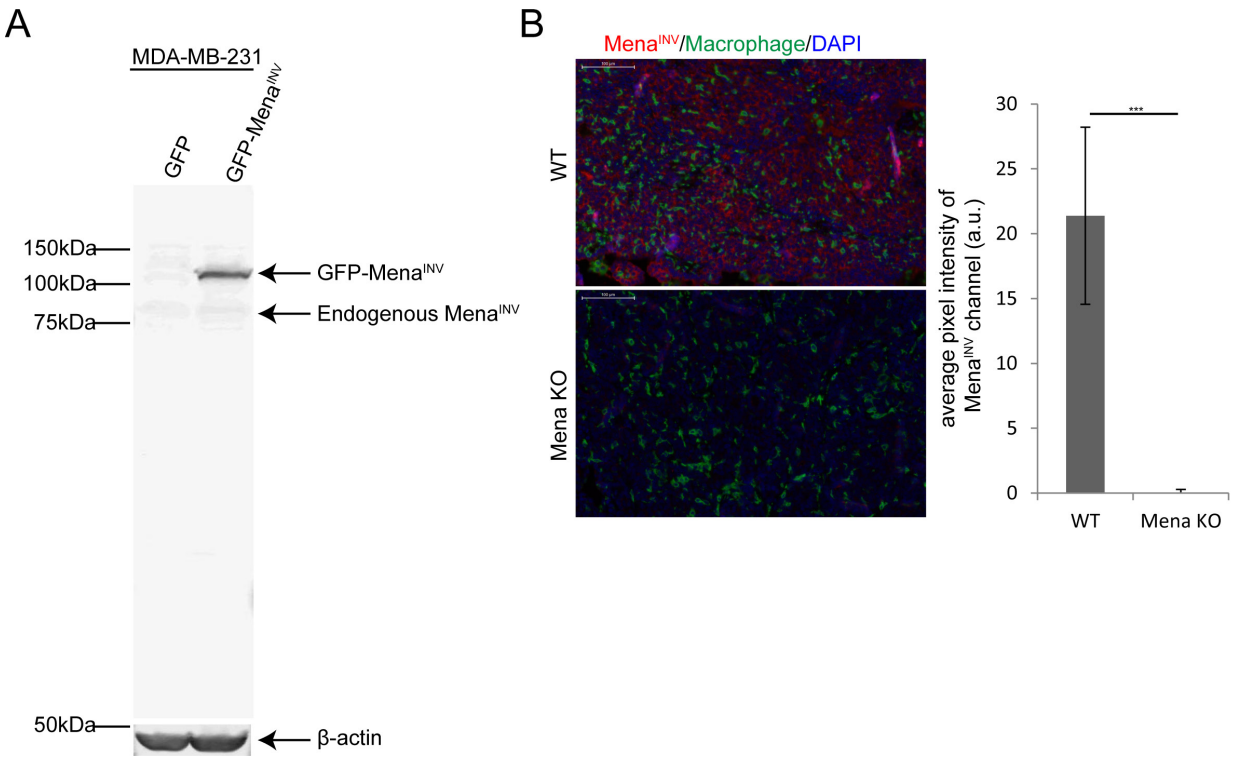

Supplemental Figure 4: Design and validation of Mena^{INV} antibody. (A) Western blot with Mena^{INV} specific antibody and β-actin of lysates from MDA-MB-231 GFP and GFP-Mena^{INV} expressing cells. **(B)** Tissue immunofluorescence (red) of sections from PyMT tumors of WT and Mena-null (MENA knock out) mice showing the presence and absence of staining, respectively. Graph quantifies the average pixel intensity of Mena^{INV} staining in PyMT tissues (background subtracted).

*P< 0.05, **P < 0.005, ***P < 0.0005

Rebastinib inhibits recruitment and function of TIE2+ macrophages in metastatic breast cancer

One sentence summary: Rebastinib is a selective TIE2 kinase inhibitor that inhibits primary tumor growth and metastasis through inhibition of infiltration of TIE2-expressing macrophages and their function in the tumor microenvironment of metastasis (TMEM), and angiopoietin/TIE2 mediated angiogenesis.

Authors: Allison S. Harney[1,2,3,4*], Jeanine Pignatelli [1,4], Bryan D. Smith[5], Ece Kadioglu[6], Scott C. Wise[5], Molly M. Hood[5], Michael D. Kaufman[5], Cynthia B. Leary[5], Wei-Ping Lu[5], Gada Al-Ani[5], Xiaoming Chen[1,4], David Entenberg[1,3,4], Maja H. Oktay[1,3,7], Yarong Wang[1,3,4], Lawrence Chun[8], Michele De Palma[6], Joan G. Jones[1,3,7,9], and Daniel L. Flynn[5*], John S. Condeelis[1,3,4*]

Affiliations: [1]Department of Anatomy & Structural Biology, Albert Einstein College of Medicine, New York, New York 10461, USA; [2]Department of Radiology, Albert Einstein College of Medicine, New York, New York 10461, USA; [3]Integrated Imaging Program, Albert Einstein College of Medicine, New York, New York 10461, USA; [4]Gruss-Lipper Biophotonics Center, Albert Einstein College of Medicine, New York, New York 10461, USA; [5] Deciphera Pharmaceuticals, LLC, 1601 Trapelo Road Waltham, MA 02451; [6] ISREC, School of Life Sciences, École Polytechnique Fédérale de Lausanne (EPFL), Lausanne, CH-1015, Switzerland; [7]Department of Pathology Albert Einstein College of Medicine, New York, New York 10461, USA; [8] Emerald Bio, 7869 NE Day Rd. W, Bainbridge Island, WA USA 98110; and [9]Department of Epidemiology & Population Health, Albert Einstein College of Medicine, New York, New York 10461, USA;

[*] These authors contributed equally to this work.

Address for Correspondence:
John Condeelis
Albert Einstein College of Medicine
1301 Morris Park Ave.

Bronx, NY 10461
Email: John.Condeelis@Einstein.yu.Edu

Daniel L. Flynn
Deciphera Pharmaceuticals, LLC
1601 Trapelo Road, Suite 152
Waltham, MA 02451
Email: dflynn@deciphera.com

Funding sources: This research was funded by Deciphera Pharmaceuticals, LLC, the Department of Defense Breast Cancer Research Program under award number (W81XWH-13-1-0010 A.S.H and W81XWH-14-1-0286 J.P), NIH CA100324, CA150344, CA013330-44S3, and the Integrated Imaging Program at Albert Einstein College of Medicine. Views and opinions of, and endorsements by, the authors do not reflect those of the US Army or the Department of Defense.

Conflict of interest: JC and MDP are Scientific Advisory Board members of Deciphera Pharmaceuticals; JC and JJ have equity in MetaStat, Inc.; BS, SW, MM, MK, CL, W-PL, GA, and DF are/were employees of Deciphera Pharmaceuticals; DF, BS, MK, SW, CL, GA-A, and W-PL have equity interests in Deciphera Pharmaceuticals.

Statement of Translational Relevance

Tumor-infiltrating myeloid cells promote tumor progression by mediating angiogenesis, tumor cell intravasation and metastasis, which can offset the effects of chemotherapy, radiation, and anti-angiogenic therapy. We show here that rebastinib, a switch control small molecule inhibitor of TIE2, is a promising therapy for blocking angiogenesis and the infiltration and function of protumoral TIE2 expressing macrophages in breast and pancreatic neuroendocrine tumors. The TIE2 inhibitory potency of rebastinib allows for intermittent dosing, and the combination of rebastinib with microtubule inhibiting chemotherapeutic agents, eribulin or paclitaxel, further reduces tumor volume and metastasis, and extends survival. By blocking multiple pathways in tumor progression, rebastinib elicits significant anti-tumor effects in mouse models of metastatic cancers. Rebastinib is a promising therapy for achieving TIE2 inhibition to block metastasis in patients.

Abstract: Tumor-infiltrating myeloid cells promote tumor progression by mediating angiogenesis, tumor cell intravasation and metastasis, which can offset the effects of chemotherapy, radiation, and anti-angiogenic therapy. Here, we show that the kinase switch control inhibitor rebastinib inhibits TIE2 activity, a tyrosine kinase receptor expressed on endothelial cells and pro-tumoral TIE2-expressing macrophages (TEMs), in mouse models of metastatic cancer. Rebastinib reduces tumor growth and metastasis in an orthotopic mouse model of metastatic mammary carcinoma through reduction of TIE2+ myeloid cell infiltration and blockade of tumor cell intravasation mediated by perivascular $TIE2^{Hi}$/$VEGFA^{Hi}$ macrophages in the tumor microenvironment of metastasis (TMEM). The anti-tumor effects of rebastinib enhance the efficacy of microtubule inhibiting chemotherapeutic agents, either eribulin or paclitaxel, by reducing tumor volume, metastasis, and improving overall survival. Rebastinib inhibition of angiopoietin/TIE2 signaling impairs multiple pathways in tumor progression mediated by pro-tumoral TEMs, including TMEM-dependent dissemination and angiopoietin/TIE2 dependent angiogenesis. Rebastinib is a promising therapy for achieving TIE2 inhibition in cancer patients.

Introduction

Anti-tumor therapies targeting the tumor vasculature by inhibiting the vascular-endothelial growth factor-A (VEGFA) signaling have been aggressively pursued to block angiogenesis and induce tumor vascular regression (1). However, anti-angiogenic treatments targeting the VEGFA pathway do not induce lasting tumor regressions, either in mouse models or patient trials (2, 3) (4). Further, some aggressive forms of anti-angiogenic therapy may promote tumor invasion and metastasis in mouse tumor models (5).

The angiopoietin (ANG)/TIE2 kinase signaling pathway is a pivotal endothelial cell angiogenic signaling axis in the tumor microenvironment and has emerged as an attractive anti-vascular target (3, 6). Clinically, elevated patient serum levels of ANG-2 have been linked with poor outcome and recurrence (7, 8). ANG/TIE2 signaling is central to the initiation of angiogenesis through vascular remodeling by disrupting endothelial-perivascular cell interactions. While ANG-1 is a TIE2 agonist and has a higher binding affinity to TIE2 than ANG-2, ANG-2 can act as a context-dependent agonist (9). By displacing ANG-1 from TIE2, ANG-2 can induce vascular plasticity and sensitize endothelial cells to other angiogenic signals, such as VEGFA (6).

In addition to expression on endothelial cells, TIE2 is expressed on a subset of pro-angiogenic macrophages (TIE2-expressing macrophages, TEMs) that areinvolved in the promotion of tumor angiogenesis, as well as cancer cell intravasation and metastasis (10-12) (13, 14). While anti-vascular agents (such as bevacizuamab and other VEGFA pathway inhibitors) have shown efficacy in decreasing tumor angiogenesis and disease burden in both preclinical and clinical settings (15, 16), one of the mechanisms of tumor resistance or recurrence after anti-angiogenic therapy has been attributed to tumor-infiltrating myeloid cells in response to cell death and hypoxia after vascular regression (17). Of note, proangiogenic tumor-infiltrating TEMs have been shown to be involved in supporting angiogenesis during anti-

angiogenic therapies (2, 3). Thus, the ANG/TIE2 axis has become an attractive target for inhibiting angiogenesis and also the pro-tumoral functions of TIE2+ myeloid cells.

Tumor-infiltrating macrophages are a source of cytokines and chemokines that support tumor growth, cancer cell survival and motility; suppress immune destruction; and promote angiogenesis, dissemination and metastasis (11, 18-22). Tumor-associated macrophages (TAMs) not only promote tumor progression, but can limit the efficacy of the tumor response to chemotherapy or radiotherapy (23-27). TEMs are a subpopulation of TAMs known to be aggressively pro-angiogenic, pro-metastatic, and immunosuppressive in the tumor microenvironment (2, 3, 21, 28). In pre-clinical studies of mammary carcinoma, ANG-2 blockade prevented up-regulation of TIE2 upon entry of myeloid cells at the tumor site and impeded the association of TEMs with the nascent tumor vasculature, thereby disabling the pro-angiogenic activity of TEMs (12). Further, ANG-2 inhibition resulted in dramatically decreased metastasis (12, 29).

In mammary carcinoma a subpopulation of perivascular TEMs compose the Tumor Microenvironment of Metastasis (TMEM), where TEMs are in direct contact with a mammalian enabled (Mena)-expressing tumor cell and an endothelial cell (30-32). TMEM are associated with breast cancer metastasis and predict distant recurrence in breast cancer patients independently of other clinical prognostic indicators (30, 31). Mechanistically, TMEM-associated TEMs locally dissolve vascular junctions through VEGFA signaling to induce local, transient vascular permeability events allowing motile tumor cells to intravasate thereby acutely increasing CTCs (11).

Biologics that inhibit ANG/TIE2 signaling have been developed, notably angiopoietin-sequestering biologics such as the dual ANG-1/ANG-2 peptibody AMG-386 (trebananib) and the ANG2-specific monoclonal antibodies MEDI3617 and LC06 (33, 34). In clinical studies, angiopoietin-sequestering biologics increase progression free survival in patients with metastatic breast cancer, ovarian cancer, and other solid cancers (35, 36). While biologics that

sequester TIE2 ligands ANG1 or ANG2 may find clinical utility, there are additional ligands, including ANG4, which activate TIE2 receptors and escape sequestration by ANG1/ANG2 sequestering biologics (37, 38). Additionally, the extracellular matrix (ECM) can activate TIE2 via association with integrins, especially alpha□beta1, and fibronectin/$\alpha 5\beta 1$ (39) and the ECM cross-linking enzyme lysyl oxidase, which regulates TIE2 signaling through low-density lipoprotein receptor–related protein (LRP)5 (40). Furthermore, internalized TIE2 mediates intracellular events such as nuclear translocation to activate DNA damage response (41). A selective small molecule inhibitor of TIE2 kinase would be capable of intercepting all of the above activating mechanisms, including those not blocked by ANG-sequestering biologics.

Herein we report that rebastinib is a potent and selective picomolar inhibitor of the TIE2 receptor tyrosine kinase that inhibits kinase activity by an allosteric “switch control” mechanism. The goals of this study were to evaluate the cellular effects of rebastinib on both endothelial and macrophage cell populations, its efficacy, both as a single agent and in combination with chemotherapy, in cancer models characterized by TEM involvement, and to further characterize its *in vivo* effects on myeloid cell composition and vascularization in the tumor microenvironment. Given its high TIE2 inhibitory potency, we evaluated rebastinib’s effects on TMEM-mediated tumor cell dissemination and metastasis, and further defined its mechanism of action for inhibiting TMEM function. Consented rebastinib-treated patients were also evaluated for clinical biomarker targeting of the ANG/TIE2 axis. The results of this study suggest that targeting the ANG/TIE2 signaling axis with rebastinib has significant inhibitory effects on TEM-mediated tumor progression.

Materials and Methods

TIE2 kinase assay and determination of inhibitor potency

Kinase activity was determined by following the production of ADP from the kinase reaction through coupling with the pyruvate kinase/lactate dehydrogenase system as detailed in supplementary data.. Percent inhibition values were obtained by comparison of reaction rates with DMSO controls. IC_{50} values were calculated from a series of percent inhibition values determined at a range of inhibitor concentrations using Prism software (GraphPad, San Diego, CA). Using the pyruvate kinase/lactate dehydrogenase assay from above, various concentrations of rebastinib were added to an assay mixture. The dissociation rate constant, k_{off}, were calculated as detailed in Supplementary data.

Crystallization, Data Collection and Structure Refinement of rebastinib with TIE2

Purified TIE2 (808-1124) crystals were grown as detailed in Supplementary data. Diffraction data of TIE2-rebastinib crystals were collected at the Advanced Light Source (ALS) Beamline 5.0.1 at a wavelength of 0.9774Å using an ADSC Q310r detector. Data were reduced with XDS and scaled to 2.05Å resolution using XSCALE (55). TIE2-rebastinib crystallizes in space group P4(1) with unit cell dimensions a=b=63.81Å, c=177.45, α=β=γ=90° with two molecules in the asymmetric unit. The structure was solved using PHASER (56) and the PDB entry 2oo8 (57) as the search model. The model was completed with COOT (58) and refined with REFMAC5 (59) using ligand restraint generated with JLigand (60) and one TLS group per chain to Rwork=0.148 and Rfree=0.166. Data set and refinement statistics are summarized in Table S1.

Western blot assays

Cells were obtained from the American Type Culture Collection (ATCC, Manassas, VA). iBMM TIE2hi macrophages were generated by transducing mouse bone marrow macrophages with an

SFFV.TAG.WPRE lentivector as described previously (61), expressing TIE2 under control of a human PGK promoter. Western blot assays to detect total and phospho-TIE2 in HUVECs, EA.hy926, and iBMM TIE2hi cells are detailed in the Supplementary data. Antibodies against phospho-TIE2 Tyr992 (catalog #4221) and rabbit IgG (HRP-conjugated; catalog #7074), were obtained from Cell Signaling Technology (Danvers, MA). The antibody against total TIE2 (catalog #sc-324) was obtained from Santa Cruz Biotechnology, Inc. (Dallas, TX).

HUVEC transwell migration assay

Human Umbilical Vein Endothelial Cells (HUVECs) (Corning 354151) were maintained in EGM medium (Lonza CC-3124) and used within the first 6 passages for transwell assays detailed in Supplementary data.

Mice

All studies involving mice were carried out in accordance with the National Institutes of Health regulation concerning the care and use of experimental animals and with the approval of the Animal Care and Use Committee of Molecular Imaging, Inc. (Ann Arbor, MI), an AAALAC accredited facility or with the approval by the Albert Einstein College of Medicine Animal Care and Use Committee. Transgenic mice expressing the Polyoma Middle T (PyMT) oncogene under the control of the mammary tumor virus long terminal repeat (MMTV-LTR) were bred in house at the Albert Einstein College of Medicine and maintained on the FVB background.

Transgenic male C57Bl6/6J/RIP1-Tag2 mice heterozygous for the oncogene were bred with wild-type females. Pups were genotyped for the SV40 large TAg by Transnetyx (http://www.transnetyx.com). Starting from 12 weeks of age, RIP1-Tag2 mice were maintained on a sucrose-enriched diet and monitored daily. All procedures involving RIP1-Tag2 mice were performed according to protocols approved by the Veterinary Authorities of the Canton Vaud according to the Swiss Law (license 2574 and 2574/a).

PyMT syngeneic breast cancer implant model

Female FVB/NJ mice (JAXWEST:RB05) were implanted in the 4th mammary fat pad on the left side with one million cells in serum-free media that had been dissociated from tumor fragments from MMTV-PyMT donor mice. Treatments began on Day 31 when the mean tumor burden for all groups in the experiment was 843 mg or on Day 52 when the mean tumor burden for all groups in the experiment was 930 mg as detailed in figure 2 and Supplementary data. For the eribulin survival study in combination with rebastinib, treatments began on Day 42 when the mean tumor burden for all groups in the experiment was 889 mg. Primary tumors were resected on day 45 when the mean tumor burden for the vehicle group was 1,288 mg. Study progression and necropsy for all cohorts are detailed in the Supplementary data.

Quantification of the F4/80$^+$ and TIE2$^+$ percent area staining in PyMT: After F4/80 and TIE2 immunostaining, whole slides were digitized on a Pannoramic P250 Flash II digital whole slide scanner at 20x magnification. Digital slides were then analyzed in Visiomorph DP (Visiopharm) with a custom developed app specific to mammary gland morphology as detailed in the Supplementary data.

Labeling of tumor vasculature and extravasation of 155 kDa dextran-TMR and measuring CTCs in PyMT: One hour before the termination of the experiments with rebastinib, 3 micro-g of 155 kDa TMR-dextran was administered by tail vein i.v. to label sites of vascular permeability. In addition, CTCs were isolated from anesthetized mice from blood drawn from the right ventricle of the heart and scored. Both were done as described previously (11) and detailed in Supplementary data.

Immunofluorescence in PyMT: Tumor sections were prepared and stained as described previously (11) and detailed in Supplementary data. The following primary antibodies were used for immunostaining of mouse tumor tissues: rat anti-mouse CD68 (clone FA-11, Serotec), or AlexaFluor647-conjugated CD68 (eBioscience), mouse anti-Mena (NBP1–87914, Novus

Biologicals), rat anti-ZO-1 (clone R40.76, Millipore). Sections were washed with PBS-T and the primary antibodies were detected with AlexaFluor488, 555 or 647 secondary antibody conjugates (Molecular Probes/Invitrogen) and nuclei stained with 4,6-diamidino-2-phenylindole (DAPI).

TMEM immunohistochemistry: Tumor sections were prepared, stained and quantified as previously described (30).

RIP1-Tag2 transgenic mouse model

11.5- to 12.5-week-old male RIP1-Tag2 mice were treated daily by gavage with rebastinib at 10 mg/kg or vehicle control 0.4% HPMC for 4 weeks. Before euthanasia, the mice were retro-orbitally injected with FITC-labeled lectin (to reveal perfused blood vessels). Pancreata and livers were harvested at necropsy for analysis. Immunofluorescence staining, lectin labeling of vasculature imaging and quantification of the RIP1-Tag2 (PNET) model is detailed in the Supplementary data.

To quantify liver micrometastases in PNET bearing mice livers were harvested and fixed overnight in 4% PFA solution at 4°C. The left lobe of each liver was dissected, processed and embedded in O.T.C., as described for pancreata. Analysis of cryosections is detailed in the Supplementary data.

In vitro intravasation (iTEM) assay

The iTEM assay was performed as described previously (50, 51) and detailed in the Supplementary data. Transwells were imaged using a Leica SP5 confocal microscope using a 60× 1.4 numerical aperture objective and processed using ImageJ [National Institutes of Health (NIH)] and IMARIS programs. Quantitation was performed by counting the number of tumor cells that had crossed the endothelium within the same field of view (60×, 10 random fields).

Plasma ANG2 levels in rebastinib treated patients

Post-dose (Cmax) and pre-dose trough plasma samples on Cycle 1 Day 8 and pre-dose trough plasma samples on Cycle 1 Day 22 were analyzed for levels of ANG2 and rebastinib concentration detailed in the Supplementary data.

Statistical analysis

Individual animals in each cohort are presented as individual points on a dot plot. A horizontal line indicates the mean value and the error bars represent the standard error of the mean. Statistical significance was determined by the comparison of the means of two groups using an unpaired, two-sided *t*-test using Prism (Graph Pad Inc.). Data sets were checked for normality (D'Agostino & Pearson omnibus normality test or Shapiro-Wilk normality test) and unequal variance using Prism (Graph Pad Inc.). Welch's correction was applied to *t*-tests as needed. *P* values of less than 0.05 were deemed significant.

Results

XRay co-crystal structure of rebastinib with TIE2 kinase exhibits unique attributes of Type II switch control binding

A co-crystal structure of rebastinib was obtained in complex with the human TIE2 kinase domain (residues K808 through A1124) at 2.05 Å resolution (Table S1). Analysis revealed a Type II binding mode in which rebastinib induces TIE2 into a DFG-out inactive enzymatic conformation, making key interactions with regions of the activation loop conformation-controlling *switch* (yellow ribbon, Figure 1), regions of TIE2 which serve as the *cognate switch pocket* (dashed red oval, Figure 1), and the ATP hinge region.

For TIE2 activation, the switch is required to bind into its cognate switch pocket. Rebastinib out-competes the switch for binding into this pocket. Thus, in Figure 1A and B, rebastinib occupies the TIE2 switch pocket (dashed red oval), and the activating switch (yellow) is displaced into an inactive conformation, precluding the ability of TIE2 to activate. Rebastinib binding out-competes the switch by the inhibitor t-butyl moiety (**A**) displacing switch residue Phe983 (labeled as **1**). The fluoro-phenyl ring of the inhibitor (**B**) additionally stabilizes Phe983 in this inactive state through π-stacking interactions. Inhibitor urea moiety (**D**) forms hydrogen bonds with both the conserved catalytic salt bridge Glu872 (**9**)/Lys855 (**10**) and the switch residue Asp982 (**6**). This binding modality further nucleates a hydrogen bonding network comprising residues His962, Asp964, Arg968, Asn969, Asp982, and Gly984 (residues **2-7**), collapsing these residues into an inactive conformational state incompatible with enzymatic shuttling of phosphate from ATP to a protein substrate. A unique electrostatic π-stacking interaction is formed between switch residue Arg987 (**8**), the inhibitor quinolinyl ring (**C**) and Glu872 (**9**). In composite, rebastinib directly forms 5 hydrogen bonds with TIE2, with overall binding further nucleating an additional 25 hydrogen bonds inducing the switch, switch pocket, and catalytic residues into an inactive state. The hydrogen bond network additionally is

consistent with stabilizing the C-terminal inhibitory motif (green) in position for occluding the substrate binding pocket of TIE2. This conformational state of TIE2 induced by rebastinib is incapable of loading a protein substrate or ATP cofactor, and provides structural determinants of the picomolar potency of rebastinib (Figure 1C). Biophysical thermal melt studies also confirmed potent binding of rebastinib to TIE2, resulting in a ΔTM of 14.9C versus apo-TIE2 (Figure S1).

Biochemical inhibition of TIE2 and prolonged off-rate

In biochemical assays, rebastinib demonstrated sub-nanomolar potency as an inhibitor of recombinant human TIE2 kinase (IC_{50} = 0.63 nM, Figure 1C). This IC_{50} exceeded the limit of further titration based on the concentration of TIE2 required for the assay. Rebastinib retained sub-nanomolar potency at adenosine triphosphate (ATP) concentrations as high as 4 mM (Figure 1D). Rebastinib was found to slowly dissociate from TIE2, yielding a dissociation rate constant (k_{off}) value of 0.0012 $minutes^{-1}$ (Figure 1C, E). The $t_{1/2}$ value associated with this k_{off} value for recovery of kinase activity was approximately 10 h for unphosphorylated TIE2 (Figure 1C).

In assays with a more complex cellular environment using human umbilical vascular endothelial cells (HUVECs) or EA.hy926 cells, which express TIE2, rebastinib inhibited ANG1-stimulated TIE2 kinase activity with IC_{50} values of 0.058 and 0.091 nM, respectively (Figure 1C). In bone marrow-derived murine macrophages transduced to express TIE2 kinase (IBMM $TIE2^{hi}$), rebastinib inhibited TIE2 phosphorylation with an IC_{50} value of 0.26 nM (Figure 1C). In a functional chemoxtaxis assay, rebastinib inhibited ANG1-mediated migration of HUVECs with an IC_{50} of 0.022 nM (Figure 1C and Figure S2). In transiently transfected Chinese Hamster Ovary (CHO) cells overexpressing constitutively phosphorylated TIE2, rebastinib inhibited TIE2 activity with an IC_{50} value of 2.0 nM (Figure 1C). Rebastinib demonstrated a prolonged off-rate (> 24 hr) against TIE2 kinase in transfected CHO cells after inhibitor washout (Figure 1F).

Rebastinib was evaluated in a panel of 300 human kinases, confirming its selectivity as a TIE2 inhibitor (Table S2). TRKA was identified as the nearest neighbor kinase inhibited by rebastinib (Figure 1G). The cellular IC_{50} for inhibition of TRKA phosphorylation by rebastinib is 0.13 nM, which is 3 fold higher than the IC_{50} of TIE2. Related kinases TRKB and TRKC exhibited IC_{50} values of 0.42 nM and 2.74 nM, respectively, showing lesser inhibition by rebastinib. BCR-ABL and FLT3 inhibition by rebastinib are even less potent with IC_{50} values 62- and 71-fold that for TIE2, respectively. Rebastinib has been previously shown to inhibit the BCR-ABL fusion oncoprotein (42). Since rebastinib is approximately 62 fold more selective in binding to TIE2 than BCR-ABL, the effect of rebastinib as a selective TIE2 inhibitor has been further examined in mammary carcinoma and pancreatic neuroendocrine tumors (PNETs).

Rebastinib inhibits mammary carcinoma growth and extends mouse survival

To examine rebastinib inhibition of TIE2 signaling in vivo, we used the orthotopic mouse mammary cancer implant model in which the polyoma middle T antigen is under the control of the mouse mammary tumor virus long terminal repeat (MMTV-PyMT) (43, 44). PyMT tumors exhibit histology similar to human luminal breast cancer, and progress to metastasis (45). Further, PyMT tumors assemble perivascular TMEM, the microenvironmental structures associated with tumor cell intravasation and dissemination in mouse mammary tumors and human breast cancer patients, which contain $TIE2^{Hi}$/$VEGFA^{Hi}$ macrophages (11, 30, 31, 46).

Rebastinib significantly reduced primary tumor growth by 75%in the PyMT model and rebastinib inhibition with tumor growth was additive with paclitaxel and reduced tumor growth by 90% of control, in combination (Figure 2A). Eribulin, like paclitaxel, is an inhibitor of microtubules and is approved for the treatment of relapse of refractory metastatic breast cancer. Rebastinib was evaluated in a post-surgical (adjuvant) setting in the PyMT model in combination with eribulin after primary mammary tumor resection. In the absence of the primary tumor the duration of animal survival is a result of overall systemic tumor burden (primarily lung

metastases). Eribulin single agent afforded a median survival of 54 days post tumor resection (red curve), less than median survival of 84 days in the vehicle cohort (black curve). Eribulin in combination with rebastinib extended survival of mice to between 196 to 200 days, depending on the rebastinib dosing schedule (Figure 2B). Together these data demonstrate that rebastinib treatment in PyMT mammary tumors, either daily or intermittent dosing of rebastinib, alone or in combination with a chemotherapy agent, reduces primary tumor volume and extends survival time.

Rebastinib reduces lung metastases in mammary carcinoma and liver metastasis in pancreatic neuroendocrine tumors

TEMs are known to support tumor cell dissemination and metastasis in mammary carcinomas (11, 12, 47). Inhibition of TEM-mediated dissemination by rebastinib was hypothesized to reduce tumor cell metastasis to the lung. Indeed, in orthotopic PyMT tumor, rebastinib was found to reduce the formation of lung metastases alone by 72% and in combination with paclitaxel by 93% (Figure 2C and D)

Given the efficacy of intermittent dosing of rebastinib in extending survival and reducing lung metastases, the effect of rebastinib in combination with paclitaxel therapy was evaluated in the PyMT model for the effect on metastasis. Combination of paclitaxel with rebastinib dosed once weekly at 10 mg/kg afforded inhibition of average number and volume (72% and 95%, respectively) of lung nodules as measured by microCT (Figure 2E and F). Combination with rebastinib dosed twice weekly at 10 mg/kg afforded even greater inhibition of number and volume (93% and 98%, respectively) of lung nodules, while lower doses inhibited lung metastasis but with decreased efficacy (Figure 2E and F).

Unlike PyMT mammary carcinoma, daily oral dosing of rebastinib at 10 mg/kg for 4 weeks did not detectably inhibit the growth of pancreatic insulinomas in the transgenic RIP1-Tag2 model of pancreatic neuroendocrine tumor (PNET) (48) (Figure S3). However, we

evaluated rebastinib for inhibition of liver metastases. According to a late treatment protocol targeting established PNETs, 11-12-week-old male RIP1-Tag2 mice were treated for 4 weeks with rebastinib and liver micrometastasis quantified at termination. Rebastinib inhibited liver metastases by 75% compared to vehicle control (Figure 2G).

Rebastinib reduces TIE2^{Hi} macrophages and microvessel density in mammary carcinoma and pancreatic neuroendocrine tumors

TEMs have been associated with tumor angiogenesis, tumor cell dissemination and metastasis (10-12). Since treatment with rebastinib reduced metastasis to the lungs in the PyMT mammary carcinoma and metastasis in the PNET model, we sought to investigate TEM infiltration in the primary tumors. In the mammary carcinoma PyMT mice, rebastinib decreased TIE2 macrophages and decreased the number of infiltrating F4/80+ macrophages (Figure 3A-C), whereas in the PNET model, rebastinib did not affect the total macrophage infiltrate (F4/80+ area), but significantly decreased intratumoral TIE2 macrophages (Figure 3D, E-F). Rebastinib treatment also led to a decrease in protumoral MRC1+ F4/80+ macrophages at the tumor invasion front in the PNET model (Figure 3G and H).

Taxane-based chemotherapies, such as paclitaxel, mobilize bone marrow-derived mesenchymal and endothelial progenitors, and CD11b+ myeloid cells, including TIE2-expressing monocytes, into the primary tumor microenvironment (49-57). TIE2+ monocyte progenitors are known to transform into TIE2+ macrophages, which associate with newly constructed tumor blood vessels and promote tumor regrowth (20, 58, 59). The effect of paclitaxel on microvessel density and the presence of TIE2+ macrophages was examined in PyMT tumors, either untreated or treated with rebastinib (Figures 3, 4 and S4). Rebastinib, in combination with paclitaxel, decreased both total macrophage infiltration and TIE2+ macrophage infiltration (Figure 3A-C, S4). When CD31+ microvessel density was measured,

treatment with paclitaxel alone increased microvessel density (MVD) over HPMC control-treated animals (Figure 4A). When treated with rebastinib in combination with chemotherapy MVD was reduced to significantly below HPMC control levels, which is similar to MVD of rebastinib treatment alone (Figure 4A). These results indicate that paclitaxel increases both microvessel density and TIE2+ staining and macrophages in PyMT tumors while rebastinib inhibits the paclitaxel induced increases. In addition, rebastinib ablated vascular TIE2 expression in the RIP1-Tag2 PNET model and reduced the density of perfused (i.e., functional) blood vessels (Figure 4B and C), thus showing anti-angiogenic effects in two mouse tumor models.

TIE2 inhibition with rebastinib disrupts TMEM-mediated vascular permeability and tumor cell intravasation in mammary carcinoma

Since rebastinib exhibited efficacy in reduction of primary tumor burden (Figure 2), reduced TIE2+ macrophages in primary tumors (Figure 3) and lung metastases after administration of intermittent doses (Figure 2), we investigated if rebastinib inhibits $TIE2^{Hi}$ macrophage function in TMEM structures, the sites of tumor cell intravasation and dissemination in mammary tumors using a 10 mg/kg twice weekly intermittent dosing regimen.

TMEM density was not affected by TIE2 inhibition with rebastinib (Figures 5A and B). However, inhibition of TIE2 signaling with rebastinib reduced TMEM-mediated changes in vascular permeability and the number of CTCs as compared to vehicle control (Figures 5C-E). Staining of vascular ZO-1 increased and extravascular dextran (vascular permeability) decreased after administration of rebastinib indicating that vascular junctions were stabilized, reducing vascular permeability (Figure 5C and F). Although total TMEM density was not affected (Figure 5A and B), TMEM function was impaired as quantified by the ratio of extravascular dextran to vascular ZO-1 (Fig. 5G), consistent with a decrease in $TIE2^{Hi}$ macrophage function in TMEM.

The association of pericytes with tumor blood vessels promotes vascular maturation and decreases vascular permeability and metastasis (49). Rebastinib increased vascular maturation in the PNET model, as shown by the higher proportion of pericyte-covered, $NG2^{+}$ blood vessels (Figure S4). Thus, in both mammary carcinomas and PNETs, rebastinib induced vascular phenotypes that were consistent with decreases in permeability, cancer cell dissemination, and metastasis.

Rebastinib inhibits macrophage-dependent transendothelial migration in vitro

Due to the role of $TIE2^{Hi}$ macrophages in the TMEM functions of vascular permeability, and tumor cell transendothelial migration leading to intravasation at TMEM *in vivo* (Figure 6A) (11), we studied whether inhibition of TIE2 with rebastinib would impair TMEM–mediated tumor cell transendothelial migration in vitro. We studied this by using the previously established *in vitro* TMEM-dependent subluminal-to-luminal transendothelial migration (iTEM) assay (Figure 6B) (50, 51). We found that rebastinib significantly inhibits macrophage-dependent transendothelial migration of breast cancer cells in the intravasation direction to background levels (observed in the absence of macrophages) at concentrations as low as 100 pM and with complete ablation at 500 pm (Figure 6C left). The inhibitory effect of rebastinib caused a reduction of intravasation to background levels seen when macrophages were absent from the assay system (Figure 6C).

To determine if the $TIE2^{Hi}$ macrophages are the cells inhibited by rebastinib in this assay, the iTEM assay was conducted using the complete dose response evaluation of rebastinib but in the absence of macrophages. When the TIE2+ macrophages were selectively excluded from the iTEM assay, rebastinib had no effect on tumor cell intravasation at any concentration (Figure 6C right). That TIE2 expression on the macrophages is required for TMEM-mediated transendothelial tumor cell migration was demonstrated by using murine macrophages in the iTEM assay that expressed either low or high levels of TIE2 (Figure S5).

As shown in Figure 6D, using macrophages expressing high levels of TIE2 resulted in a robust 4-fold increase in tumor cell transendothelial migration compared to background, whereas using macrophages expressing low levels of TIE2 (control) did not support as large an increase. Rebastinib treatment ablated transendothelial migration induced by the macrophages expressing high levels of TIE2 (Figure 6D). Collectively, these data indicate that TIE2 signaling in the macrophages of the TMEM is required for tumor cell transendothelial migration. These data also demonstrate that inhibition of TIE2 in the iTEM assay selectively impairs $TIE2^{Hi}$ macrophages and does not impair the endothelial monolayer integrity or tumor cell transendothelial migration behavior.

Furthermore, inhibition of TRKA, the nearest neighbor kinase inhibited by rebastinib (Figure 1G), using the selective TRK inhibitor entrectinib (IC_{50} = 130 pM), had no effect on tumor cell transendothelial migration in either the presence or absence of macrophages indicating that the inhibition seen with rebastinib was not due to off target effects involving TRKA (Figure 6E). Additionally, rebastinib had no effect on tumor cell proliferation at the concentrations used in these studies, ruling out a direct effect of rebastinib on tumor cells in the iTEM assay (Figure S6).

Rebastinib therapy results in an ANG2 biomarker readout in human patients

In order to clinically evaluate TIE2 inhibition, ANG2 levels were examined in 20 consented patients from a Phase 1 CML and AML study (NCT 00827138) before and after treatment with 100 or 150 mg twice weekly rebastinib. Clinically, compensatory elevations in circulating growth factor ligands is observed upon inhibition of their cognate receptor tyrosine kinases, including VEGF/VEGFR2, CSF1/CSF1R, and others (52, 53). Thus, the effect of rebastinib on compensatory increases in circulating angiopoietin levels secondary to TIE2 inhibition was evaluated. On day 22 after starting rebastinib treatment, increases in ANG2 were observed in 19/20 patients, no change was observed in one patient, and a >2-fold increase in

ANG2 plasma levels was observed in 14/20 (70%) patients. The average fold increase for all 20 patients was 2.6 ± 1.2 SD (Figure 6F). To assess whether changes in plasma levels of ANG2 were correlated with plasma levels of rebastinib, data were fit to linear regression models. Both C_{max} (Figure S7) and trough exposures of rebastinib on Day 8 (Figure S7) significantly correlated with increased levels of plasma ANG2. Increased plasma ANG2 levels also correlated with trough rebastinib exposures on Day 22 (Figure S7).

Discussion

Here we report that rebastinib is a novel switch control inhibitor of TIE2 tyrosine kinase with picomolar potency for blocking TIE2 enzymatic and cellular activity in endothelial cells and TEMs, and exhibits efficacy in malignant mammary carcinoma and pancreatic neuroendocrine tumors. TIE2 blockade by rebastinib results in inhibition of tumor growth, invasion and metastasis. Examination of the effects of rebastinib at the cellular level demonstrates that rebastinib reduced tumor vascular density, TIE2 macrophages, and macrophage infiltration in the PyMT mammary tumor model. Intratumoral TIE2 macrophages were also reduced in the transgenic mouse model of PNET, RIP1-Tag2. In PyMT tumors, although TMEM density on the vasculature was not decreased by rebastinib, TMEM function was dramatically impaired by rebastinib effects on $TIE2^{+}$ macrophages, as evidenced by decreased vascular permeability, circulating tumor cells, and metastasis in vivo and transendothelial migration in vitro. The effects of rebastinib are further elevated when combined with paclitaxel or eribulin treatment in mice.

Rebastinib is a potent picomolar inhibitor of TIE2 kinase that inhibits by an allosteric "switch control pocket" mechanism. Analysis of the co-crystal structure of rebastinib with TIE2 revealed a Type II binding mode in which rebastinib induces TIE2 into a DFG-out inactive enzymatic conformation, making key interactions with regions of the conformation-controlling *switch,* with regions of TIE2 which serve as the *cognate switch pocket,* and with the kinase hinge region. This binding mode engenders picomolar potency for rebastinib inhibition of TIE2 biochemically and in cellular macrophage and endothelial assays. The TIE2 kinase binding mode of rebastinib results in a long-dissociation off rate ($t_{1/2}$ = 10 h).

TEMs are a subset of highly skewed pro-tumoral macrophages in the tumor microenvironment that are elevated following treatment with chemotherapy, anti-angiogenic agents, or vascular disrupting agents that render tumors hypoxic (2, 10, 12, 13). TEM recruitment contributes to evasive revascularization and invasion in these hypoxic tumors (54).

Perivascular TEMs have been shown to participate in defined structures called TMEM, which mediate tumor cell intravasation from primary tumors (11, 30, 31, 51). Administration of rebastinib to orthotopic models of mammary carcinoma and pancreatic neuroendocrine tumors resulted inreduced vascular density, reduced TIE2+ macrophages, and, as a consequence, TMEM function. In addition to efficacy as an anti-vascular agent, rebastinib reduces the pro-angiogenic TEM population in the tumor microenvironment, limiting revascularization and tumor growth. In contrast to other anti-vascular agents, rebastinib has the potential to not only decrease tumor volume in combination with chemotherapy, but may also prevent TEM-mediated tumor regrowth and increased TMEM function leading to metastasis. This is further supported by the evidence that rebastinib reduces tumor cell invasion, dissemination and metastasis in both the PyMT and RIP1-Tag2 models of invasive and metastatic cancers, and reverses paclitaxel-induced increased intra-tumoral macrophages and eribulin-induced reduction in survival secondary to lung metastases in the PyMT model.

Mechanistically, tumor cell dissemination in mammary carcinoma occurs exclusively at $TIE2^{Hi}$/$VEGFA^{Hi}$ TMEM sites. Motile tumor cells cross the endothelium when $TIE2^{Hi}$/$VEGFA^{Hi}$ macrophages in TMEM locally dissolve vascular junctions through VEGFA signaling (11). Rebastinib impaired TMEM function in vivo, resulting in reduced vascular permeability and tumor cell intravasation, and a corresponding dramatic decrease in CTCs. Decreased tumor cell intravasation from the primary tumor prevented tumor cell metastasis, explaining the decrease in metastatic lung nodules with rebastinib treatment and further supporting the potential impact of rebastinib in preventing TEM-mediated tumormetastasis. It is also noted that the effects of rebastinib *in vivo* for inhibiting TMEM function phenocopy macrophage ablation in the MaFIA mouse and selective ablation of VEGF in $TIE2^{Hi}$ perivascular macrophages (11). The role of TEMs in TMEM-mediated tumor cell intravasation has been further confirmed in the *in vitro* assay replicating transendothelial tumor cell migration at TMEM. In the presence of 0.5 nM rebastinib, tumor cell intravasation was reduced to the very low background levels of tumor cell

intravasation measured in the absence of macrophages, indicating that TIE2 signaling in macrophages is essential for tumor cell transendothelial cell migration in this assay. In the absence of macrophages in the iTEM assay, rebastinib did not affect tumor cell intravasation. Furthermore, we demonstrated that incorporation of TIE2-overexpressing macrophages into the iTEM assay led to the most robust tumor cell transendothelial migration. Rebastinib reversed the enhanced tumor cell migration induced by TIE2-overexpressing macrophages. Collectively, these results support the role of $TIE2^{Hi}$ macrophages in transendothelial migration and demonstrate that blocking $TIE2^{Hi}$ macrophages with rebastinib impairs an essential mechanism in tumor cell intravasation and metastasis in mammary carcinoma.

Finally, clinical effects of rebastinib on ANG2 plasma levels in patients were correlated with exposure levels of rebastinib indicating that circulating levels of ANG2 may provide a circulating biomarker of TIE2 target engagement. Rebastinib is currently in Phase 1b for treatment of solid tumors characterized by a significant contribution from the TEM microenvironment.

Taken together, these data demonstrate that rebastinib, a switch control small molecule inhibitor of TIE2, is a promising therapy for blocking angiogenesis and the infiltration and function of protumoral TEMs in the tumor microenvironment. Rebastinib inhibition of TIE2 reduces tumor volume and dissemination of metastatic mammary carcinoma cells by impairing TIE2 in the tumor microenvironment and specifically also impairing macrophage TIE2 function in TMEM structures. The TIE2 inhibitory potency of rebastinib allows for intermittent dosing, and the combination of rebastinib with microtubule inhibiting chemotherapeutic agents, eribulin or paclitaxel, further reduces tumor volume and metastasis, and extends survival. By blocking multiple pathways in tumor progression, rebastinib elicits significant anti-tumor effects in mouse models of metastatic breast cancer. Rebastinib is a promising therapy for achieving TIE2 inhibition in patients.

References

1. Shojaei F. (2012). Anti-angiogenesis therapy in cancer: current challenges and future perspectives. **Cancer Lett**. 320(2):130-7. PMID: 22425960.
2. Welford AF, Biziato D, Coffelt SB, Nucera S, Fisher M, Pucci F, Di Serio C, Naldini L, De Palma M, Tozer GM, Lewis CE. (2011). TIE2-expressing macrophages limit the therapeutic efficacy of the vascular-disrupting agent combretastatin A4 phosphate in mice. **J Clin Invest**. 121(5):1969-73. PMID: 21490397 / PMCID: PMC3083764.
3. Rigamonti N, Kadioglu E, Keklikoglou I, Wyser Rmili C, Leow CC, De Palma M. (2014). Role of angiopoietin-2 in adaptive tumor resistance to VEGF signaling blockade. **Cell Rep**. 8(3):696-706. PMID: 25088418.
4. Sennino B, Ishiguro-Oonuma T, Wei Y, Naylor RM, Williamson CW, Bhagwandin V, Tabruyn SP, You WK, Chapman HA, Christensen JG, Aftab DT, McDonald DM. (2012). Suppression of tumor invasion and metastasis by concurrent inhibition of c-Met and VEGF signaling in pancreatic neuroendocrine tumors. **Cancer Discov**. 2(3):270-87. PMID: 22585997 / PMCID: PMC3354652.
5. O'Connell JT, Sugimoto H, Cooke VG, MacDonald BA, Mehta AI, LeBleu VS, Dewar R, Rocha RM, Brentani RR, Resnick MB, Neilson EG, Zeisberg M, Kalluri R. (2011). VEGF-A and Tenascin-C produced by S100A4+ stromal cells are important for metastatic colonization. **Proc Natl Acad Sci U S A**. 108(38):16002-7. PMID: 21911392 / PMCID: PMC3179047.
6. Saharinen P, Eklund L, Pulkki K, Bono P, Alitalo K. (2011). VEGF and angiopoietin signaling in tumor angiogenesis and metastasis. **Trends Mol Med**. 17(7):347-62. PMID: 21481637.
7. Eroglu Z, Stein CA, Pal SK. (2013). Targeting angiopoietin-2 signaling in cancer therapy. **Expert Opin Investig Drugs**. 22(7):813-25. PMID: 23621441.
8. Sfiligoi C, de Luca A, Cascone I, Sorbello V, Fuso L, Ponzone R, Biglia N, Audero E, Arisio R, Bussolino F, Sismondi P, De Bortoli M. (2003). Angiopoietin-2 expression in breast cancer correlates with lymph node invasion and short survival. **Int J Cancer**. 103(4):466-74. PMID: 12478661.
9. Maisonpierre PC, Suri C, Jones PF, Bartunkova S, Wiegand S, Radziejewski C, Compton D, McClain J, Aldrich TH, Papadopoulos N, Daly TJ, Davis S, Sato TN, Yancopoulos GD. (1997). Angiopoietin-2, a natural antagonist for Tie2 that disrupts in vivo angiogenesis. **Science**. 277(5322):55-60. PMID: WOS:A1997XJ41800036.
10. Gabrusiewicz K, Liu D, Cortes-Santiago N, Hossain MB, Conrad CA, Aldape KD, Fuller GN, Marini FC, Alonso MM, Idoate MA, Gilbert MR, Fueyo J, Gomez-Manzano C. (2014). Anti-vascular endothelial growth factor therapy-induced glioma invasion is associated with accumulation of Tie2-expressing monocytes. **Oncotarget**. 5(8):2208-20. PMID: 24809734 / PMCID: PMC4039157.
11. Harney AS, Arwert EN, Entenberg D, Wang Y, Guo P, Qian BZ, Oktay MH, Pollard JW, Jones JG, Condeelis JS. (2015). Real-Time Imaging Reveals Local, Transient Vascular Permeability, and Tumor Cell Intravasation Stimulated by TIE2hi Macrophage-Derived VEGFA. **Cancer Discov**. 5(9):932-43. PMID: 26269515 / PMCID: PMC4560669.
12. Mazzieri R, Pucci F, Moi D, Zonari E, Ranghetti A, Berti A, Politi LS, Gentner B, Brown JL, Naldini L, De Palma M. (2011). Targeting the ANG2/TIE2 axis inhibits tumor growth and metastasis by impairing angiogenesis and disabling rebounds of proangiogenic myeloid cells. **Cancer Cell**. 19(4):512-26. PMID: 21481792.
13. Hughes R, Qian BZ, Rowan C, Muthana M, Keklikoglou I, Olson OC, Tazzyman S, Danson S, Addison C, Clemons M, Gonzalez-Angulo AM, Joyce JA, De Palma M, Pollard JW, Lewis CE. (2015). Perivascular M2 Macrophages Stimulate Tumor Relapse after Chemotherapy. **Cancer Res**. 75(17):3479-91. PMID: 26269531.

14. Piao Y, Park SY, Henry V, Smith BD, Tiao N, Flynn DL, de Groot JF. (2016). Novel MET/TIE2/VEGFR2 inhibitor altiratinib inhibits tumor growth and invasiveness in bevacizumab-resistant glioblastoma mouse models. **Neuro Oncol**. 18(9):1230-41. PMID: 26965451 / PMCID: PMC4998992.
15. Ferrara N. (2016). VEGF and Intraocular Neovascularization: From Discovery to Therapy. **Transl Vis Sci Technol**. 5(2):10. PMID: 26981332 / PMCID: PMC4790412.
16. Jayson GC, Kerbel R, Ellis LM, Harris AL. (2016). Antiangiogenic therapy in oncology: current status and future directions. **Lancet**. 388(10043):518-29. PMID: 26853587.
17. Bergers G, Hanahan D. (2008). Modes of resistance to anti-angiogenic therapy. **Nat Rev Cancer**. 8(8):592-603. PMID: 18650835 / PMCID: PMC2874834.
18. Wyckoff J, Wang W, Lin EY, Wang Y, Pixley F, Stanley ER, Graf T, Pollard JW, Segall J, Condeelis J. (2004). A paracrine loop between tumor cells and macrophages is required for tumor cell migration in mammary tumors. **Cancer Res**. 64(19):7022-9. PMID: 15466195.
19. Wyckoff JB, Wang Y, Lin EY, Li JF, Goswami S, Stanley ER, Segall JE, Pollard JW, Condeelis J. (2007). Direct visualization of macrophage-assisted tumor cell intravasation in mammary tumors. **Cancer Res**. 67(6):2649-56. PMID: 17363585.
20. De Palma M, Venneri MA, Galli R, Sergi Sergi L, Politi LS, Sampaolesi M, Naldini L. (2005). Tie2 identifies a hematopoietic lineage of proangiogenic monocytes required for tumor vessel formation and a mesenchymal population of pericyte progenitors. **Cancer Cell**. 8(3):211-26. PMID: 16169466.
21. Coffelt SB, Chen YY, Muthana M, Welford AF, Tal AO, Scholz A, Plate KH, Reiss Y, Murdoch C, De Palma M, Lewis CE. (2011). Angiopoietin 2 stimulates TIE2-expressing monocytes to suppress T cell activation and to promote regulatory T cell expansion. **J Immunol**. 186(7):4183-90. PMID: 21368233.
22. Liu L, Cash TP, Jones RG, Keith B, Thompson CB, Simon MC. (2006). Hypoxia-induced energy stress regulates mRNA translation and cell growth. **Mol Cell**. 21(4):521-31. PMID: 16483933 / PMCID: PMC3153113.
23. Shiao SL, Ruffell B, DeNardo DG, Faddegon BA, Park CC, Coussens LM. (2015). TH2-Polarized CD4(+) T Cells and Macrophages Limit Efficacy of Radiotherapy. **Cancer Immunol Res**. 3(5):518-25. PMID: 25716473 / PMCID: PMC4420686.
24. Shree T, Olson OC, Elie BT, Kester JC, Garfall AL, Simpson K, Bell-McGuinn KM, Zabor EC, Brogi E, Joyce JA. (2011). Macrophages and cathepsin proteases blunt chemotherapeutic response in breast cancer. **Genes Dev**. 25(23):2465-79. PMID: 22156207 / PMCID: PMC3243057.
25. Nakasone ES, Askautrud HA, Kees T, Park JH, Plaks V, Ewald AJ, Fein M, Rasch MG, Tan YX, Qiu J, Park J, Sinha P, Bissell MJ, Frengen E, Werb Z, Egeblad M. (2012). Imaging tumor-stroma interactions during chemotherapy reveals contributions of the microenvironment to resistance. **Cancer Cell**. 21(4):488-503. PMID: 22516258 / PMCID: PMC3332002.
26. DeNardo DG, Brennan DJ, Rexhepaj E, Ruffell B, Shiao SL, Madden SF, Gallagher WM, Wadhwani N, Keil SD, Junaid SA, Rugo HS, Hwang ES, Jirstrom K, West BL, Coussens LM. (2011). Leukocyte complexity predicts breast cancer survival and functionally regulates response to chemotherapy. **Cancer Discov**. 1(1):54-67. PMID: 22039576 / PMCID: PMC3203524.
27. Escamilla J, Schokrpur S, Liu C, Priceman SJ, Moughon D, Jiang Z, Pouliot F, Magyar C, Sung JL, Xu J, Deng G, West BL, Bollag G, Fradet Y, Lacombe L, Jung ME, Huang J, Wu L. (2015). CSF1 receptor targeting in prostate cancer reverses macrophage-mediated resistance to androgen blockade therapy. **Cancer Res**. 75(6):950-62. PMID: 25736687 / PMCID: PMC4359956.
28. Ibberson M, Bron S, Guex N, Faes-van't Hull E, Ifticene-Treboux A, Henry L, Lehr HA, Delaloye JF, Coukos G, Xenarios I, Doucey MA. (2013). TIE-2 and VEGFR kinase activities drive immunosuppressive function of TIE-2-expressing monocytes in human breast tumors. **Clin Cancer Res**. 19(13):3439-49. PMID: 23649001.
29. Dvorak HF, Orenstein NS, Carvalho AC, Churchill WH, Dvorak AM, Galli SJ, Feder J, Bitzer AM, Rypysc J, Giovinco P. (1979). Induction of a fibrin-gel investment: an early event in line 10

hepatocarcinoma growth mediated by tumor-secreted products. **J Immunol**. 122(1):166-74. PMID: 762415.
30. Robinson BD, Sica GL, Liu YF, Rohan TE, Gertler FB, Condeelis JS, Jones JG. (2009). Tumor microenvironment of metastasis in human breast carcinoma: a potential prognostic marker linked to hematogenous dissemination. **Clin Cancer Res**. 15(7):2433-41. PMID: 19318480 / PMCID: PMC3156570.
31. Rohan TE, Xue X, Lin HM, D'Alfonso TM, Ginter PS, Oktay MH, Robinson BD, Ginsberg M, Gertler FB, Glass AG, Sparano JA, Condeelis JS, Jones JG. (2014). Tumor microenvironment of metastasis and risk of distant metastasis of breast cancer. **J Natl Cancer Inst**. 106(8). PMID: 24895374 / PMCID: PMC4133559.
32. Harney AS, Wang Y, Condeelis JS, Entenberg D. (2016). Extended Time-lapse Intravital Imaging of Real-time Multicellular Dynamics in the Tumor Microenvironment. **J Vis Exp**. (112):e54042. PMID: 27341448 / PMCID: PMC4927790.
33. Oliner J, Min H, Leal J, Yu D, Rao S, You E, Tang X, Kim H, Meyer S, Han SJ, Hawkins N, Rosenfeld R, Davy E, Graham K, Jacobsen F, Stevenson S, Ho J, Chen Q, Hartmann T, Michaels M, Kelley M, Li L, Sitney K, Martin F, Sun JR, Zhang N, Lu J, Estrada J, Kumar R, Coxon A, Kaufman S, Pretorius J, Scully S, Cattley R, Payton M, Coats S, Nguyen L, Desilva B, Ndifor A, Hayward I, Radinsky R, Boone T, Kendall R. (2004). Suppression of angiogenesis and tumor growth by selective inhibition of angiopoietin-2. **Cancer Cell**. 6(5):507-16. PMID: 15542434.
34. Leow CC, Coffman K, Inigo I, Breen S, Czapiga M, Soukharev S, Gingles N, Peterson N, Fazenbaker C, Woods R, Jallal B, Ricketts SA, Lavallee T, Coats S, Chang Y. (2012). MEDI3617, a human anti-angiopoietin 2 monoclonal antibody, inhibits angiogenesis and tumor growth in human tumor xenograft models. **Int J Oncol**. 40(5):1321-30. PMID: 22327175.
35. McConachie A, Newman D, Tucci M, Puckett A, Tsao A, Hughes J, Benghuzzi H. (1999). The effect on bioadhesive polymers either freely in solution or covalently attached to a support on human macrophages. **Biomed Sci Instrum**. 35:45-50. PMID: 11143390.
36. Monk BJ, Poveda A, Vergote I, Raspagliesi F, Fujiwara K, Bae DS, Oaknin A, Ray-Coquard I, Provencher DM, Karlan BY, Lhomme C, Richardson G, Rincon DG, Coleman RL, Herzog TJ, Marth C, Brize A, Fabbro M, Redondo A, Bamias A, Tassoudji M, Navale L, Warner DJ, Oza AM. (2014). Anti-angiopoietin therapy with trebananib for recurrent ovarian cancer (TRINOVA-1): a randomised, multicentre, double-blind, placebo-controlled phase 3 trial. **Lancet Oncol**. 15(8):799-808. PMID: 24950985.
37. Brunckhorst MK, Wang H, Lu R, Yu Q. (2010). Angiopoietin-4 promotes glioblastoma progression by enhancing tumor cell viability and angiogenesis. **Cancer Res**. 70(18):7283-93. PMID: 20823154 / PMCID: PMC2940950.
38. Valenzuela DM, Griffiths JA, Rojas J, Aldrich TH, Jones PF, Zhou H, McClain J, Copeland NG, Gilbert DJ, Jenkins NA, Huang T, Papadopoulos N, Maisonpierre PC, Davis S, Yancopoulos GD. (1999). Angiopoietins 3 and 4: diverging gene counterparts in mice and humans. **Proc Natl Acad Sci U S A**. 96(5):1904-9. PMID: 10051567 / PMCID: PMC26709.
39. Cascone I, Napione L, Maniero F, Serini G, Bussolino F. (2005). Stable interaction between alpha5beta1 integrin and Tie2 tyrosine kinase receptor regulates endothelial cell response to Ang-1. **J Cell Biol**. 170(6):993-1004. PMID: 16157706 / PMCID: PMC2171441.
40. Mammoto T, Jiang E, Jiang A, Mammoto A. (2013). Extracellular matrix structure and tissue stiffness control postnatal lung development through the lipoprotein receptor-related protein 5/Tie2 signaling system. **Am J Respir Cell Mol Biol**. 49(6):1009-18. PMID: 23841513.
41. Hossain MB, Shifat R, Johnson DG, Bedford MT, Gabrusiewicz KR, Cortes-Santiago N, Luo XM, Lu ZM, Ezhilarasan R, Sulman EP, Jiang H, Li SSC, Lang FF, Tyler J, Hung MC, Fueyo J, Gomez-Manzano C. (2016). TIE2-mediated tyrosine phosphorylation of H4 regulates DNA damage response by recruiting ABL1. **Science Advances**. 2(4). PMID: WOS:000380072100014.

42. Chan WW, Wise SC, Kaufman MD, Ahn YM, Ensinger CL, Haack T, Hood MM, Jones J, Lord JW, Lu WP, Miller D, Patt WC, Smith BD, Petillo PA, Rutkoski TJ, Telikepalli H, Vogeti L, Yao T, Chun L, Clark R, Evangelista P, Gavrilescu LC, Lazarides K, Zaleskas VM, Stewart LJ, Van Etten RA, Flynn DL. (2011). Conformational control inhibition of the BCR-ABL1 tyrosine kinase, including the gatekeeper T315I mutant, by the switch-control inhibitor DCC-2036. **Cancer Cell**. 19(4):556-68. PMID: 21481795 / PMCID: PMC3077923.
43. Lin EY, Jones JG, Li P, Zhu L, Whitney KD, Muller WJ, Pollard JW. (2003). Progression to malignancy in the polyoma middle T oncoprotein mouse breast cancer model provides a reliable model for human diseases. **Am J Pathol**. 163(5):2113-26. PMID: 14578209 / PMCID: PMC1892434.
44. Roussos ET, Wang Y, Wyckoff JB, Sellers RS, Wang W, Li J, Pollard JW, Gertler FB, Condeelis JS. (2010). Mena deficiency delays tumor progression and decreases metastasis in polyoma middle-T transgenic mouse mammary tumors. **Breast Cancer Res**. 12(6):R101. PMID: 21108830 / PMCID: PMC3046446.
45. Lin EY, Nguyen AV, Russell RG, Pollard JW. (2001). Colony-stimulating factor 1 promotes progression of mammary tumors to malignancy. **J Exp Med**. 193(6):727-40. PMID: 11257139.
46. Newman AC, Hughes CC. (2012). Macrophages and angiogenesis: a role for Wnt signaling. **Vasc Cell**. 4(1):13. PMID: 22938389 / PMCID: PMC3479425.
47. De Palma M, Mazzieri R, Politi LS, Pucci F, Zonari E, Sitia G, Mazzoleni S, Moi D, Venneri MA, Indraccolo S, Falini A, Guidotti LG, Galli R, Naldini L. (2008). Tumor-targeted interferon-alpha delivery by Tie2-expressing monocytes inhibits tumor growth and metastasis. **Cancer Cell**. 14(4):299-311. PMID: 18835032.
48. Hanahan D. (1985). Heritable formation of pancreatic beta-cell tumours in transgenic mice expressing recombinant insulin/simian virus 40 oncogenes. **Nature**. 315(6015):115-22. PMID: 2986015.
49. Keskin D, Kim J, Cooke VG, Wu CC, Sugimoto H, Gu C, De Palma M, Kalluri R, LeBleu VS. (2015). Targeting vascular pericytes in hypoxic tumors increases lung metastasis via angiopoietin-2. **Cell Rep**. 10(7):1066-81. PMID: 25704811 / PMCID: PMC4342328.
50. Pignatelli J, Goswami S, Jones JG, Rohan TE, Pieri E, Chen X, Adler E, Cox D, Maleki S, Bresnick A, Gertler FB, Condeelis JS, Oktay MH. (2014). Invasive breast carcinoma cells from patients exhibit MenaINV- and macrophage-dependent transendothelial migration. **Sci Signal**. 7(353):ra112. PMID: 25429076 / PMCID: PMC4266931.
51. Roh-Johnson M, Bravo-Cordero JJ, Patsialou A, Sharma VP, Guo P, Liu H, Hodgson L, Condeelis J. (2014). Macrophage contact induces RhoA GTPase signaling to trigger tumor cell intravasation. **Oncogene**. 33(33):4203-12. PMID: 24056963 / PMCID: PMC3962803.
52. Schmitz V, Vilanueva H, Raskopf E, Hilbert T, Barajas M, Dzienisowicz C, Gorschluter M, Strehl J, Rabe C, Sauerbruch T, Prieto J, Caselmann WH, Qian C. (2006). Increased VEGF levels induced by anti-VEGF treatment are independent of tumor burden in colorectal carcinomas in mice. **Gene Ther**. 13(16):1198-205. PMID: 16617302.
53. Ries CH, Cannarile MA, Hoves S, Benz J, Wartha K, Runza V, Rey-Giraud F, Pradel LP, Feuerhake F, Klaman I, Jones T, Jucknischke U, Scheiblich S, Kaluza K, Gorr IH, Walz A, Abiraj K, Cassier PA, Sica A, Gomez-Roca C, de Visser KE, Italiano A, Le Tourneau C, Delord JP, Levitsky H, Blay JY, Ruttinger D. (2014). Targeting tumor-associated macrophages with anti-CSF-1R antibody reveals a strategy for cancer therapy. **Cancer Cell**. 25(6):846-59. PMID: 24898549.
54. Cortes-Santiago N, Hossain MB, Gabrusiewicz K, Fan X, Gumin J, Marini FC, Alonso MM, Lang F, Yung WK, Fueyo J, Gomez-Manzano C. (2016). Soluble Tie2 overrides the heightened invasion induced by anti-angiogenesis therapies in gliomas. **Oncotarget**. 7(13):16146-57. PMID: 26910374 / PMCID: PMC4941303.
55. Kabsch W. (2010). Xds. **Acta Crystallogr D Biol Crystallogr**. 66(Pt 2):125-32. PMID: 20124692 / PMCID: PMC2815665.

56. McCoy AJ, Grosse-Kunstleve RW, Adams PD, Winn MD, Storoni LC, Read RJ. (2007). Phaser crystallographic software. **Journal of applied crystallography**. 40(Pt 4):658-74. PMID: 19461840 / PMCID: PMC2483472.
57. Hodous BL, Geuns-Meyer SD, Hughes PE, Albrecht BK, Bellon S, Caenepeel S, Cee VJ, Chaffee SC, Emery M, Fretland J, Gallant P, Gu Y, Johnson RE, Kim JL, Long AM, Morrison M, Olivieri PR, Patel VF, Polverino A, Rose P, Wang L, Zhao H. (2007). Synthesis, structural analysis, and SAR studies of triazine derivatives as potent, selective Tie-2 inhibitors. **Bioorg Med Chem Lett**. 17(10):2886-9. PMID: 17350837.
58. Emsley P, Lohkamp B, Scott WG, Cowtan K. (2010). Features and development of Coot. **Acta Crystallogr D Biol Crystallogr**. 66(Pt 4):486-501. PMID: 20383002 / PMCID: PMC2852313.
59. Murshudov GN, Skubak P, Lebedev AA, Pannu NS, Steiner RA, Nicholls RA, Winn MD, Long F, Vagin AA. (2011). REFMAC5 for the refinement of macromolecular crystal structures. **Acta Crystallogr D Biol Crystallogr**. 67(Pt 4):355-67. PMID: 21460454 / PMCID: PMC3069751.
60. Lebedev AA, Young P, Isupov MN, Moroz OV, Vagin AA, Murshudov GN. (2012). JLigand: a graphical tool for the CCP4 template-restraint library. **Acta Crystallogr D Biol Crystallogr**. 68(Pt 4):431-40. PMID: 22505263 / PMCID: PMC3322602.
61. Squadrito ML, Baer C, Burdet F, Maderna C, Gilfillan GD, Lyle R, Ibberson M, De Palma M. (2014). Endogenous RNAs modulate microRNA sorting to exosomes and transfer to acceptor cells. **Cell Rep**. 8(5):1432-46. PMID: 25159140.

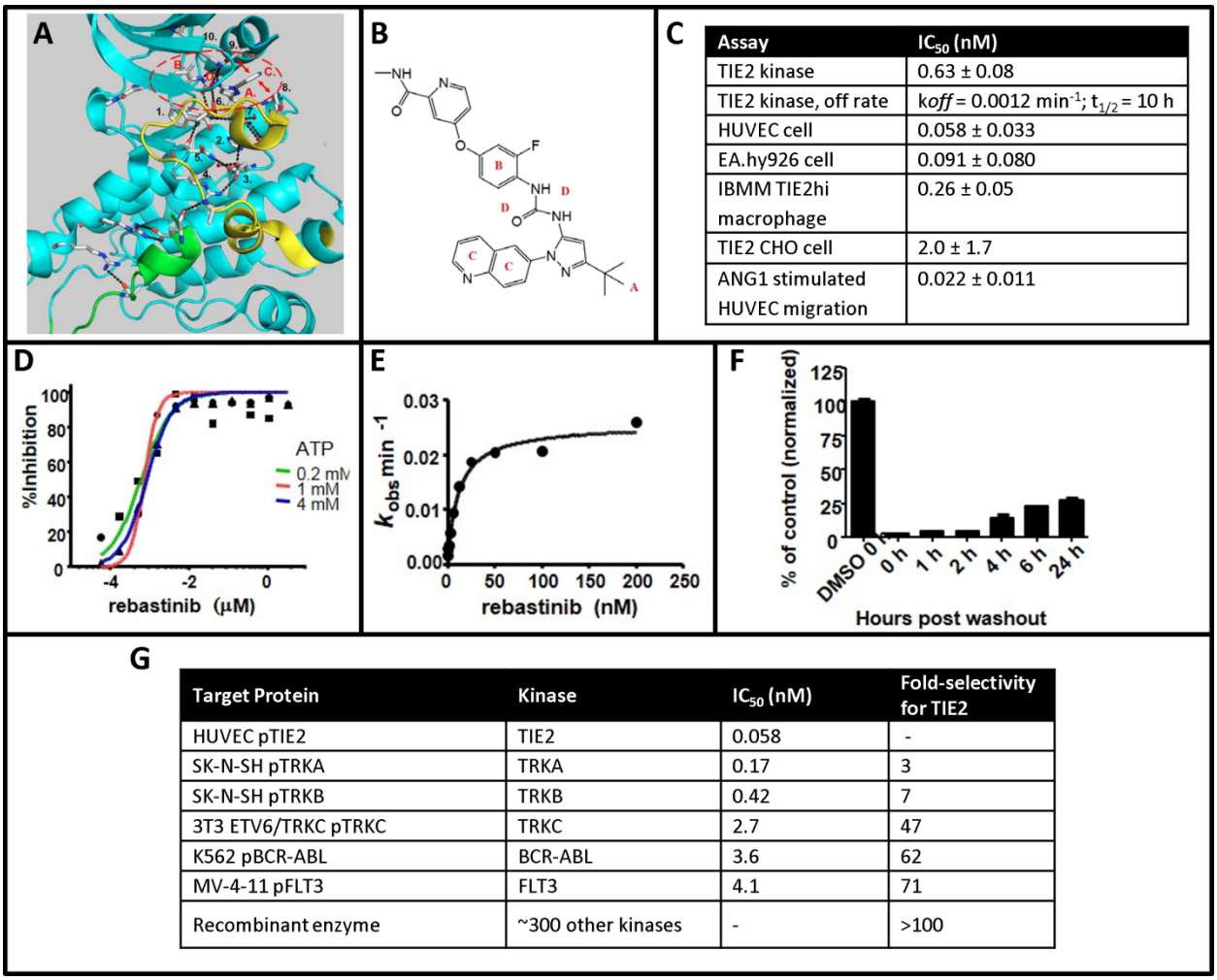

Assay	IC_{50} (nM)
TIE2 kinase	0.63 ± 0.08
TIE2 kinase, off rate	*koff* = 0.0012 min^{-1}; $t_{1/2}$ = 10 h
HUVEC cell	0.058 ± 0.033
EA.hy926 cell	0.091 ± 0.080
IBMM TIE2hi macrophage	0.26 ± 0.05
TIE2 CHO cell	2.0 ± 1.7
ANG1 stimulated HUVEC migration	0.022 ± 0.011

Target Protein	Kinase	IC_{50} (nM)	Fold-selectivity for TIE2
HUVEC pTIE2	TIE2	0.058	-
SK-N-SH pTRKA	TRKA	0.17	3
SK-N-SH pTRKB	TRKB	0.42	7
3T3 ETV6/TRKC pTRKC	TRKC	2.7	47
K562 pBCR-ABL	BCR-ABL	3.6	62
MV-4-11 pFLT3	FLT3	4.1	71
Recombinant enzyme	~300 other kinases	-	>100

Figure 1: Rebastinib selectively inhibits the receptor tyrosine kinase TIE2. (A) Co-crystal structure of rebastinib bound to TIE2 kinase domain. **(B)** Chemical structure of rebastinib. **(C)** Inhibition of TIE2 kinase activity with rebastinib in biochemical and cellular assays where k_{off} is the kinetic constant for rebastinib dissociation from TIE2, $t_{1/2}$ is the half-life of the rebastinib-TIE2 complex. **(D)** Dose response inhibition of TIE2 ATP-dependent kinase activity with rebastinib at indicated concentrations of ATP. **(E)** Forward kinetic analysis of rebastinib inhibition of TIE2 activity, where k_{obs} is the rate constant for achieving equilibrium inhibition. **(F)** Sustained inhibition of TIE2 phosphorylation in CHO cells by rebastinib (1 μM) at indicated time after removal of rebastinib. **(G)** Table of nearest kinases inhibited with rebastinib

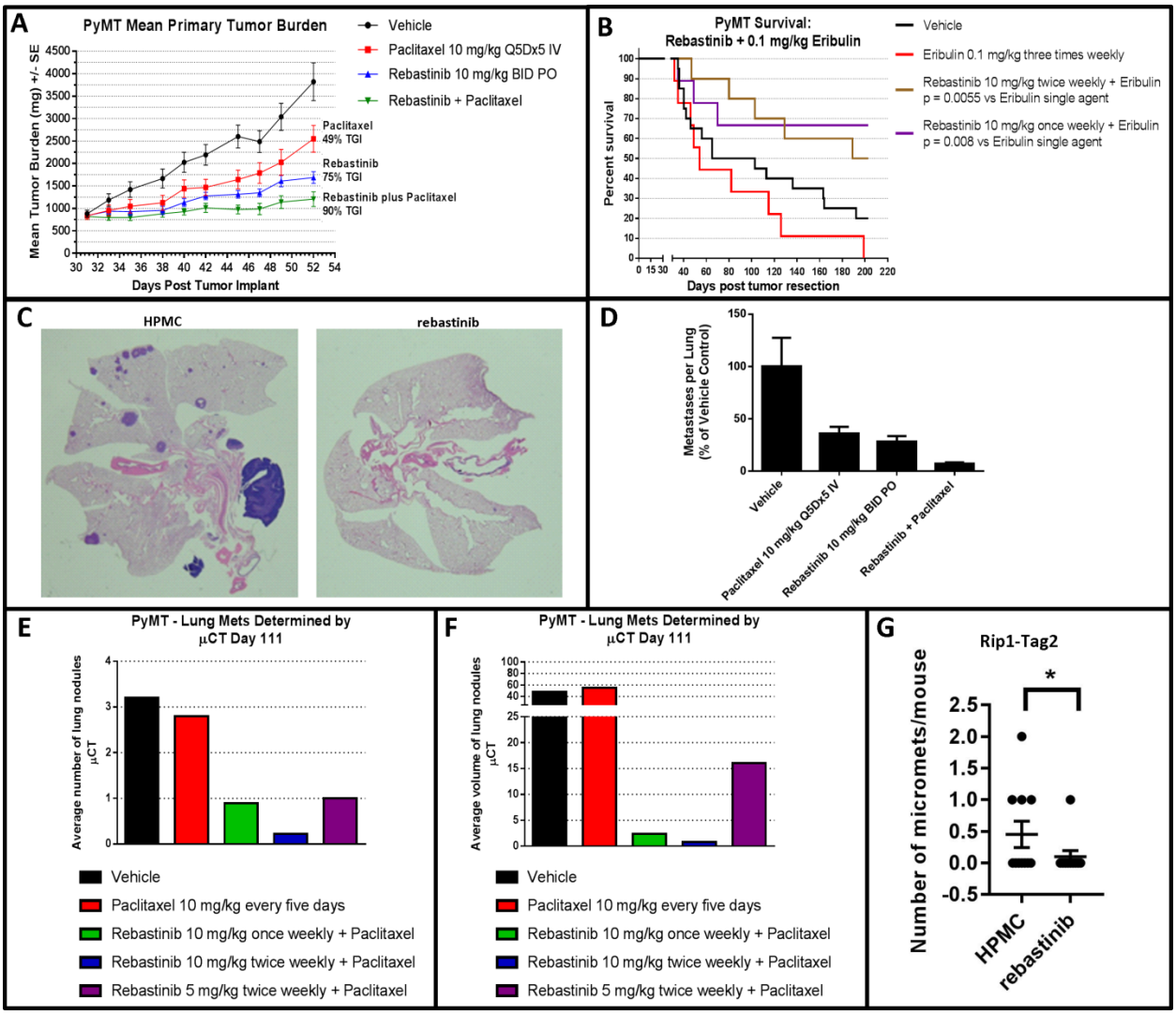

Figure 2: Rebastinib blocks primary tumor growth, inhibits metastatic growth and extends survival alone and in combination with chemotherapy. (A) Mean tumor burden in mice implanted PyMT tumors in the mammary fat pad administered vehicle control (black line), paclitaxel alone (red line), rebastinib alone (blue line) or rebastinib and paclitaxel in combination (green line). **(B)** Intermittent treatment of PyMT tumor-bearing mice with rebastinib extends overall survival in combination with eribulin. Primary mammary tumors were resected on day 42 and treatment was begun on day 45. Dosing was continued for 27 weeks and animals followed for survival. **(C)** H&E staining of lung tissue from PyMT-bearing mice for lung metastases (vehicle treated, left panel; rebastinib + paclitaxel treated, right panel). **(D)** Quantification of volume of metastatic nodules by H&E in the lungs of animals as compared to the vehicle control for the indicated treatments after 3 weeks of treatment. $P < 0.05$ for all relative to vehicle control. **(E)** Average number and **(F)** average volume of lung metastases (nodules) determined by µCT in mice at 9 weeks of treatment. **(G)** Rebastinib decreases PNET metastasis to liver**.** HPMC n=11, rebastinib n=10. * = 0.05.

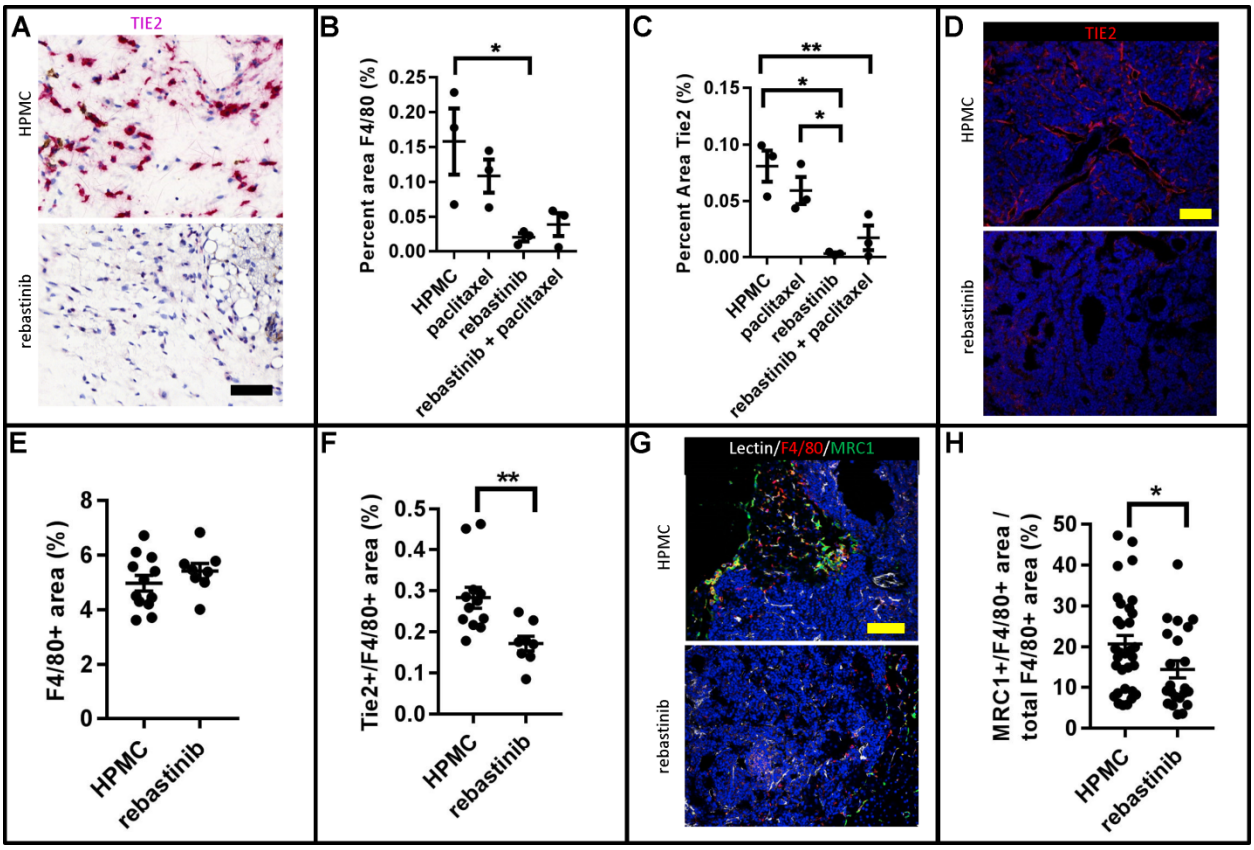

Figure 3: Rebastinib reduces TIE2^{Hi} macrophages in mammary carcinoma and PNET. (A) Immunofluorescence staining of TIE2^{Hi} macrophages in PyMT tumor tissue treated with vehicle control (HPMC) and rebastinib. TIE2 is in pink, and hematoxylin in blue. Bar = 100 μm. **(B)** Quantification of F4/80+ macrophages in PyMT tumor tissue from control, rebastinib and paclitaxel treated mice in combinations shown. One-way ANOVA determined significant difference between HPMC and rebastinib treatments. *p < 0.05. **(C)** Quantification of TIE2 staining in tumor tissue from as in (B). One-way ANOVA determined significant differences between HPMC and the treatments indicated. *P < 0.05; ** P < 0.005. **(D)** Immuno fluorescence staining of TIE2 in Rip1-Tag2 PNET in animals treated with HPMC or rebastinib. TIE2 is red, DAPI to stain nuclei is blue. Bar = 100μm. **(E)** Quantification of total F4/80+ macrophages in PNET tumors treated with rebastinib or vehicle control. No statistical significance. **(F)** Quantification of F4/80+/TIE2+ macrophages in PNET tumor tissue as percentage of tissue area. Vehicle n=12, rebastinib n=8 for E and F. P = 0.0051. **(G)** Immunofluorescence microscopy of PNET tumor sections stained for blood vessels (lectin, gray), macrophages (F4/80, red) and MRC1 (green). Bar = 150 μm. **(H)** Quantification of MRC1+/F4/80+ macrophages at invasive front of PNET tumor sections from (G) in animals treated with HPMC control or rebastinib. Each dot represents one image acquired at 200x magnification. HPMC n=9, rebastinib n=7. Statistical analysis by unpaired Student's t test. *P < 0.05

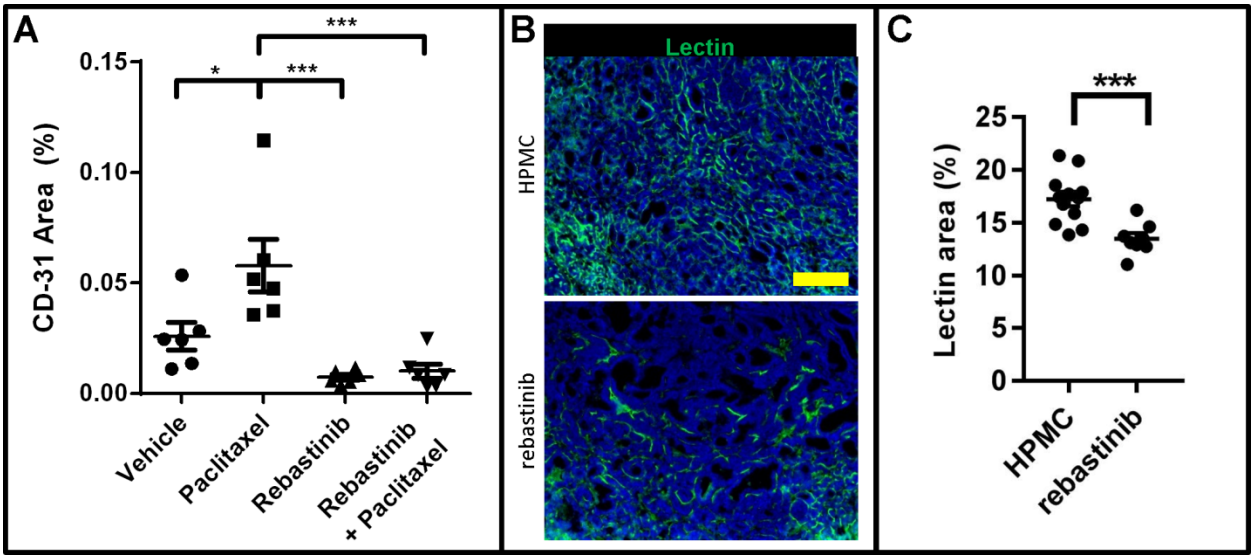

Figure 4: Rebastinib reduces microvessel density in mammary carcinoma and PNET. (A) Quantification of microvessel density from CD31 staining in PyMT tumors. *P < 0.05, ***P < 0.0005. **(B)** Immuno-fluorescence staining of vasculature with lectin (green) in PNET tumors treated with vehicle control or rebastinib. Bar = 100µm. **(C)** Quantification of microvessel density as % of lectin area from tumor tissue stained in (B) showing that rebastinib significantly reduces vascular density in PNETs. Each dot is a mouse in which multiple tumors were analyzed. HPMC n=12, rebastinib n=8. P = 0.0008.

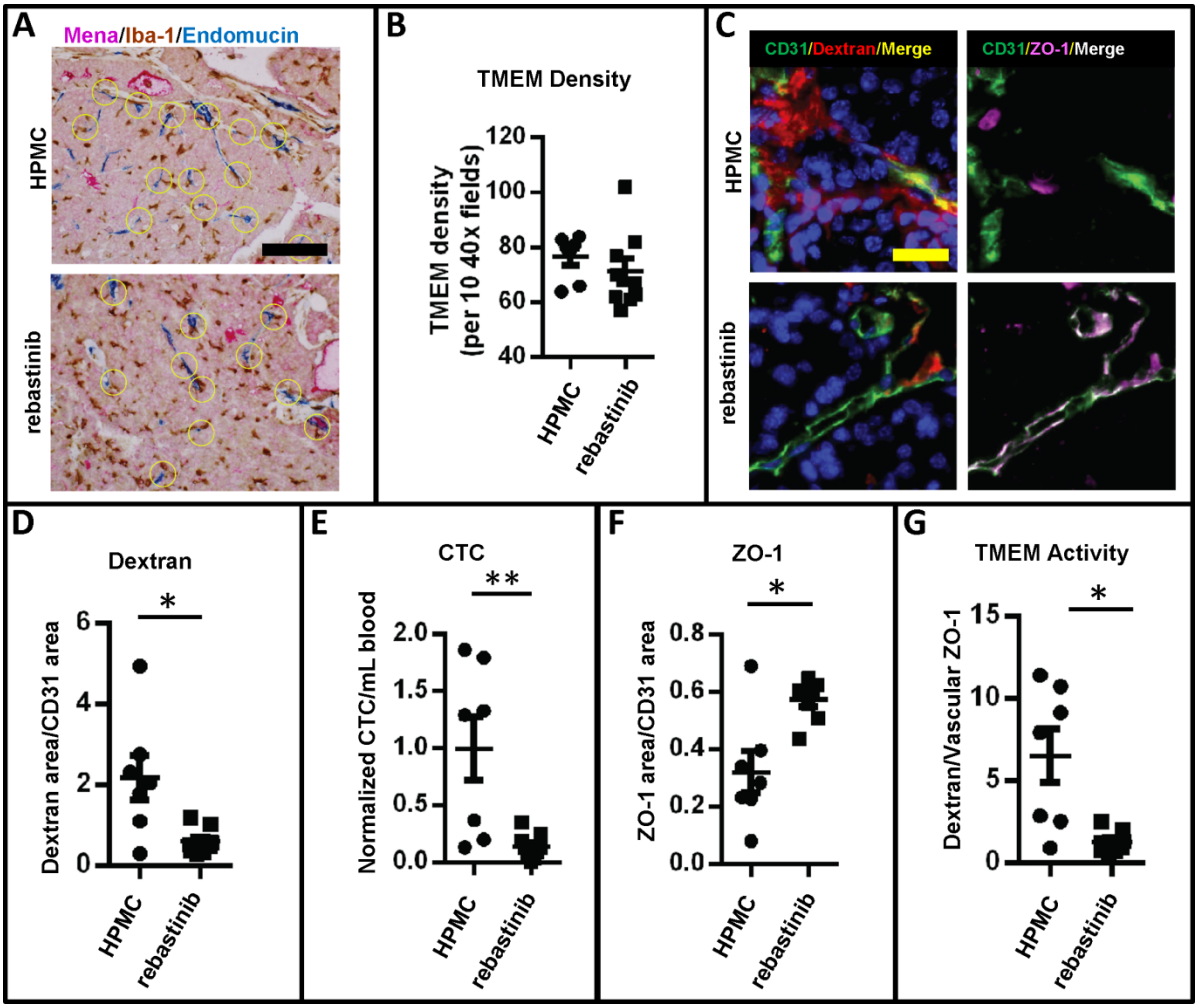

Figure 5: Inhibition of TIE2 with rebastinib impairs mechanisms of TMEM function and tumor cell dissemination. (A) IHC staining of tumors for TMEM before and after treatment with rebastinib. Vasculature (endomucin, blue), tumor cells (Mena, pink) and macrophages (Iba-1, brown). TMEM are circled. Bar = 100 μm. **(B)** Quantification of TMEM density in 10, 40X fields (no significant difference). **(C)** Immunfluorescence imaging of tumor sections. Tumors are stained for blood vessel endothelial cells (CD31, green), vascular perfusion/leakage (155 kDa dextran-TMR, red), cell nuclei (DAPI, blue), or endothelial junctions (ZO-1, magenta). Panels D-G show HPMC vehicle control or treatment with rebastinib both for twice weekly for 3 weeks. **(D)** Extravascular 155 kDa dextran-TMR (n = 7 and 9; * P = 0.042). Bar = 30 μm. **(E)** Normalized quantification of circulating tumor cells (** P = 0.004). **(E)** Vascular ZO-1 staining intensity relative to CD31 staining (*P = 0.0124). **(G)** Quantification of TMEM activity as extravascular dextran relative to ZO-1 staining intensity (n = 7 and 9; * P = 0.0177).

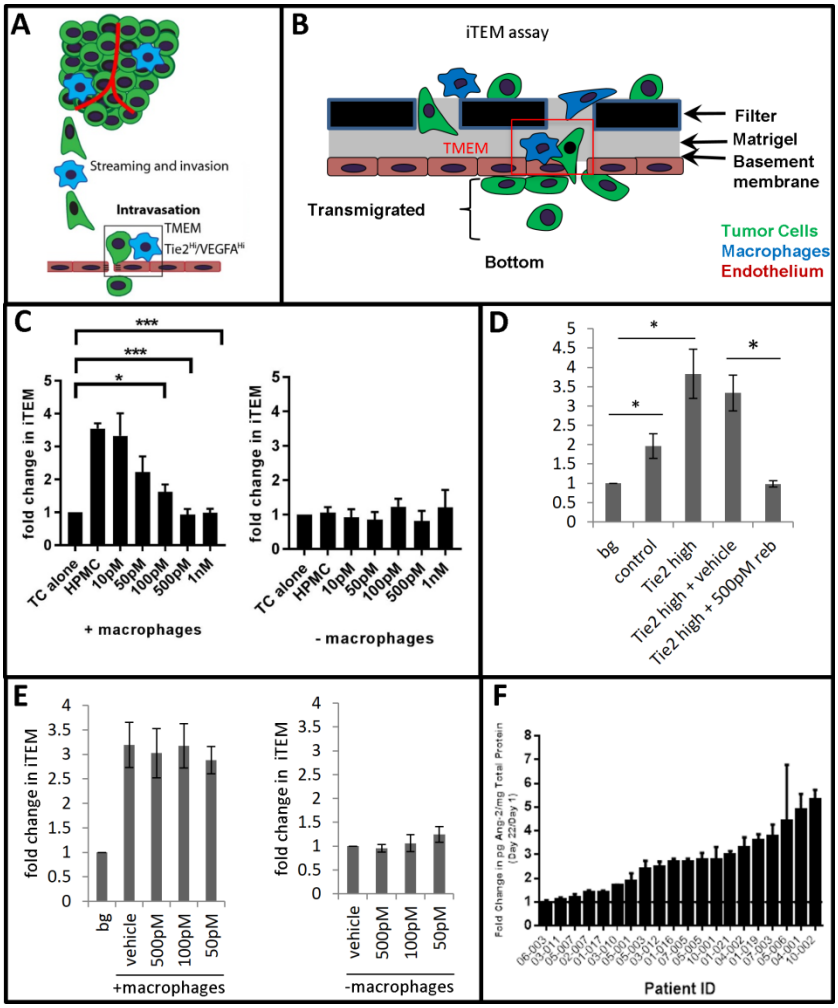

Figure 6: Rebastinib inhibits macrophage-mediated tumor cell intravasation in vitro. **(A)** Schematic diagram of TMEM-mediated tumor cell intravasation in breast tumors. Tumor cells (green) and macrophages (blue) co-migrate (called streaming) to TMEM where tumor cells cross the endothelium (pink). **(B)** The in vitro iTEM assay drawn approximately to scale where the bottom of a transwell is coated with Matrigel and a sealed HUVEC endothelial monolayer is allowed to mature so that it is impermeable to dextran diffusion and has high electrical resistance. Tumor cells (green) and macrophages (blue) are added to the top of the transwell (the luminal side). The dimensions of the iTEM assay were determined using optical sectioning with a confocal microscope. Dimensions in the cartoon can be estimated using the 10μm diameter of the blue macrophages. Tumor cells undergo transendothelial migration at sites of endothelium associated macrophages. **(C)** (Left) Fold change in the number of tumor cells that transmigrate the HUVEC monolayer in the presence of macrophages (vehicle control and with increasing concentrations of rebastinib); bg = background, tumor cells without macrophages. (Right) same as left except all in absence of macrophages. Note that rebastinib has no effect on background levels of tumor cell transendothelial migration in the absence of macrophages. **(D)** Fold change in the number of tumor cells that transmigrate the HUVEC monolayer in the presence of control GFP (spontaneous endogenous Tie2 expression) or Tie2 overexpressing iBMMs (see Figure S6 for relative expression levels) and in the presence of Tie2 overexpressing iBMMs treated with vehicle or 500 pM rebastinib (bg = background, tumor cells alone). **(E)** TrkA inhibition with entrectinib has no effect on tumor cell intravasation in vitro. Fold change in the number of tumor cells that transmigrate the HUVEC monolayer in the iTEM assay in the presence of macrophages (left graph: control and with increasing concentrations of entrectinib; bg = background, tumor cells alone) and absence of macrophages (right graph). n.s. = none significant. **(F)** For subjects who signed appropriate informed consent documents, Cmax and trough plasma levels of rebastinib on Cycle 1 Day 8 and trough plasma samples on Cycle 1 Day 22 were correlated with levels of ANG-2 determined on the same day as the PK sampling, where available. Fold change in individual patient ANG-2 plasma levels at Day 22 versus baseline pretreatment ANG2 value at Day 1. The average fold increase for all 20 patients was 2.6 ± 1.2 SD.